Universidade de São Paulo
Instituto de Física

Estudo da Hadronização de quarks pesados em um plasma de quarks e glúons em expansão hidrodinâmica para os sistemas PbPb, XeXe, ArAr e OO

Lucas Vieira Teixeira

Orientador(a): Prof.(a) Dr.(a) Alexandre Alarcon do Passo Suaide

Dissertação de mestrado apresentada ao Instituto de Física da Universidade de São Paulo, como requisito parcial para a obtenção do título de Mestre em Ciências.

Banca Examinadora:
Prof(a). Dr(a). Alexandre Alarcon do Passo Suaide - (Universidade de São Paulo)
Prof(a). Dr(a). Matthew William Luzum (Universidade de São Paulo)
Prof(a). Dr(a). Mauro Rogério Cosentino (Universidade Federal do ABC)

São Paulo
2020

University of Sao Paulo
Physics Institute

STUDY OF HADRONIZATION OF HEAVY QUARKS IN A PLASMA OF QUARKS AND GLUONS IN HYDRODYNAMIC EXPANSION FOR PbPb, XeXe, ArAr, AND OO SYSTEMS

Lucas Vieira Teixeira

Advisor: Prof.(a) Dr.(a) Alexandre Alarcon do Passo Suaide

Dissertation submitted to the Physics Institute of the University of Sao Paulo in partial fulfillment of the requirements for the degree of Master of Science.

Examining Committee:
Prof(a). Dr(a). Alexandre Alarcon do Passo Suaide - (University of Sao Paulo)
Prof(a). Dr(a). Matthew William Luzum (University of Sao Paulo)
Prof(a). Dr(a). Mauro Rogério Cosentino (University Federal pf ABC)

São Paulo
2020

FICHA CATALOGRÁFICA
Preparada pelo Serviço de Biblioteca e Informação
do Instituto de Física da Universidade de São Paulo

Teixeira, Lucas Vieira

Estudo da hadronização de quarks pesados em um plasma de quarks e glúons em expansão hidrodinâmica para os sistemas PbPb, XeXe, ArAr e OO. São Paulo, 2020.

Dissertação (Mestrado) – Universidade de São Paulo. Instituto de Física. Depto. de Física Nuclear

Orientador: Prof. Dr. Alexandre Alarcon do Passo Suaide

Área de Concentração: Física de Altas Energias

Unitermos: 1. Física de alta energia; 2. Física nuclear; 3. Hádrons; 4. Física de partículas.

USP/IF/SBI-030/2020

A Gerusa, Luciano, Bruno, Felipe, Sandra, Sirleda, João, Marta e Ozana.

Agradecimentos

Assumindo o discurso epidítico expresso aqui meus agradecimentos sinceros

À minha família e meus amigos, cujos nomes não caberiam nesta página, os quais das mais diferentes formas concedem-me o apoio para seguir em frente.

À Gerusa, ao Luciano, ao Bruno e ao Felipe por me mostrarem os caminhos bons que eu poderia seguir, por se sacrificarem para que eu pudesse ter uma boa educação e por me mostrarem o significado de perseverança.

À Sandra, minha outra mãe , a quem eu também devo minha educação. Quando estava redigindo este documento pensei em todo o apoio que me foi dado por ela.

Ao João, à Marta e à Sirleda pelo exemplo primoroso como professores e por todas as ajudas que eu recebi deles. Que algum dia eu possa transformar a vida das pessoas como vocês transformam a dos seus alunos.

Ao meu orientador, professor Dr. Alexandre pela compreensão, exemplo e pelo apoio no desenvolvimento deste trabalho. Ao professor Dr. Marcelo Munhoz, pelas conversas virtuosas e pelas críticas, que ajudaram no desenvolvimento desse trabalho.

Aos professores com os quais cursei disciplinas ao longo do Mestrado, Professor Dr. José Éboli, Professor Dr. Matthew Luzum e Professor Dr. Gabriel Teixeira Landi.

Ao Roland Katz pela amizade e ajuda indispensável neste trabalho.

Aos professores Drs. Jorge e Jacquelyn Noronha-Hostler pelas contribuições dadas para esse trabalho.

Ao Caio Prado também pelas contribuições essenciais para esse trabalho.

À Ozana, pelo exemplo, pelo apoio e presença neste Mestrado.

Aos meus colegas Fabio Canedo, Geovane e Henrique. A amizade de vocês e o apoio

nesta dissertação foram de grande ajuda, principalmente com os códigos.

Agradeço ao instituto de Física pelo apoio financeiro e estrutura para o desenvolvimento desse trabalho de pesquisa. Agradeço ao auxílio financeiro cedido pela UNIVESP que engrandeceu minha experiência com o ensino superior e ensino à distância.

Por fim, não agradeço aos desincentivos cedidos pelo nosso governo para a ciência e os jovens cientistas.

"Meu duvidar é da realidade sensível aparente
— talvez só um escamoteio de percepções. Porém, procuro cumprir.
Deveres de fundamento a vida, empírico modo, ensina: disciplina e paciência.

Meu duvidar é uma petição de mais certeza"

(Guimarães Rosa)

Resumo

O plasma de Quarks e Gluons tem valiosas informações que podem ser providas através dos quarks pesados, partículas produzidas em colisões de íons pesados. No cenário atual, há disponíveis vários modelos que se empenham para decifrar e entender melhor as propriedades do meio. Cada modelo tem ferramentas que conseguem prover informações sobre o plasma de quarks e gluons, porém ainda temos situações que permanecem sem resolução. Ademais, há propostas de colisões com sistemas pequenos nos experimentos do LHC para o RUN-3. A presente proposta traz consigo perguntas sobre a permanência de propriedades atribuídas ao QGP permanecerem em sistemas pequenos. As Partículas pesadas são essenciais nesse cenário, pois são geradas nos instantes iniciais da colisão e suas propriedades permitem que elas tragam consigo informações das interações ao longo de toda a evolução do sistema. Contudo, a análise e comparção entre os dados experimentais e predições teóricas ou fenomenológicas na área de partículas pesadas não são capazes de explicar completamente o acoplamento de quarks pesados com o meio e os processos ulteriores. Este trabalho apresenta um estudo dos efeitos do plasma interagindo com quarks pesados, sendo eles o bottom e charm. Neste trabalho analisamos como a adição de um novo ingrediente, um processo estocástico chamado coalescência afetará os nossos resultados. O programa DABMOD (STATE-OF-ART) é utilizado para gerar eventos (2d+1) event-by-event de quarks pesados atravessando um meio hidrodinâmico para os sistemas simétricos, porém com diferentes geometrias. Os quarks pesados interagem com o meio e essa interação é realizada através de parametrizações de modelos de perda de energia. Os espectros finais de partículas são obtidos após a hadronização destes quarks e ulteriores decaimento dos mésons pesados. A simulação fornece resultados de observáveis R_{AA}, $v_2\{2\}$ e $v_3\{2\}$ apresentando consistência e dentro das barras de erros com os dados disponíveis na literatura. Neste trabalho, fazemos comparações de condições iniciais com os modelos de perda de energia para PbPb $\sqrt{s_{NN}}$ =5.02 TeV e para XeXe $\sqrt{s_{NN}}$ =5.44 TeV, além de realizar predições para os sistemas ArAr $\sqrt{s_{NN}}$ =5.85 TeV, e OO $\sqrt{s_{NN}}$ =6.02 TeV. Neste trabalho, também é apresentada a razão $v_2\{4\}/v_2\{2\}$, uma ferramenta utilizada para análise das condições iniciais e o setor de quarks leves. Também investigamos as correlações entre as anisotropias de mésons pesados e todas as partículas carregadas para entender melhor como os quarks pesados se acoplam ao plasma de quarks e glúons em expansão hidrodinâmica.

Palavras-chaves: Física de alta energia. hadrons. quarks.

Abstract

Quark Gluon Plasma has valuable information that can be provided through heavy quarks, particles produced in heavy ion collisions. In the current scenario, several models are available that strive to decipher and better understand the properties of the medium. Each model has tools that can provide information about the plasma of quarks and gluons, but we still have situations that remain unresolved. In addition, there are proposals for collisions with small systems in the LHC experiment for RUN-3. This proposal brings with it questions about the permanence of properties attributed to the QGP to remain in small systems. Heavy particles are essential in this scenario, as they are generated in initial moments of the collision and its properties allow them to bring with them information about interactions throughout the evolution of the system. However, the analysis and comparison between experimental data and theoretical or phenomenological predictions in the area of heavy particles are not able to fully explain the coupling of heavy quarks with the medium and subsequent processes. This work presents a study of the effects of plasma interacting with heavy quarks, which are the bottom and charm. In this work we analyze how the addition of a new ingredient, a stochastic process called coalescence will affect our results. The DABMOD program (STATE-OF-ART) is used to generate events (2d + 1) event-by-event of heavy quarks crossing a hydrodynamic medium for symmetric systems, but with different geometries. Heavy quarks interact with the environment and this interaction is performed through parameterization of energy loss models. The final particle spectra are obtained after the hadronization of these quarks and further decay of heavy mesons. The simulation provides results of observables R_{AA}, $v_2\{2\}$ and $v_3\{2\}$ showing consistency and within the bars of errors with the data available in the literature. In this work, we make comparisons of initial conditions with the energy loss models for PbPb $\sqrt{s_{NN}} = 5.02$ TeV and for XeXe $\sqrt{s_{NN}}$ =5.44 TeV, in addition to making predictions for the ArAr $\sqrt{s_{NN}}$ =5.85 TeV, and OO $\sqrt{s_{NN}}$ =6.02 TeV systems. This work also presents the reason $v_2\{4\}/v_2\{2\}$, a tool used to analyze the initial conditions and the light quarks sector. We also investigated the correlations between heavy meson anisotropies and all charged particles to better understand how heavy quarks attach to hydrodynamically expanding quarks and gluons plasma.

Keywords: High Energy physics. Hadrons. quarks.

List of Figures

List of Tables

Contents

Chapter

1 INTRODUCTION

Particle Physics has the goal to search for the fundamental constituents of matter and understanding of their interactions. The Greek philosopher Demokritos 460-370 B.C. (22) postulated that everything is built from forms, the so-called, *atoms*, from the Greek word ἄτομος, that means indivisible.

All the knowledge acquired through the Standard Model (23, 24, 25) describes several of the measurements made by the particle accelerators. However, there are still several questions to be answered. We can list some of these questions. For example: How to include gravity in the standard model, the origin of dark matter and dark energy found in astrophysical observations, the confinement of quarks and gluons within the atomic nuclei. In order to understand and try to answer some of these questions, one of the tools used is the collision of particles. The collision of particles with relativistic speeds and the study of the consequences of this collision have been the most used means to understand the unknown behavior of elementary particles. This physics area, ultra-collisions of relativistic heavy ions, aims to help to understand this scenario. The Large Hadron Collider (LHC) in Geneva, from the European Research Center (CERN-*Conselil Européen pour la Recherche Nucléaire*) is currently the principal and most large experimental program that has been built to study collisions and the properties of the nuclear physics and elementary particles. Currently, several scientific groups around the world with several collaborations join forces to build experiments that test those questions and explore the universe's properties. We have experiments like Relativistic Heavy Ion Collider (RHIC), in Brookhaven. We also have FAIR, at Schwerionenforschung - Germany. We also have Belle-2, experiment at Japan and others around the world.

The motivation of this work is to study the effects of $(2+1)d$ event-by-event fluctuating relativistic hydrodynamic backgrounds on the nuclear modification factor and momentum anisotropies, with some correlations for hard and soft v_n of heavy-flavor

mesons for tiny systems with a new ingredient, the coalescence, a stochastic process. The properties of the smallest systems have been studied although polarized beams (26) and ultracentral deformed ion-ion collisions (27). This twain may distinguish between different scenarios in these light nuclei collisions. The structure and properties of strong interaction could be the key to understand more deeply the Quantum Chromodynamics (QCD). One of the questions about the scenario is that quarks and gluons seem to be confined inside the hadrons. This is widely accepted from an experimental point of view and calculations of lattice QCD, but its formal proof in a rigorous mathematical way is still unsolved. One way to study this question is through a form hot and dense matter that resembles the first moments of the universe. This environment has quarks and gluons deconfined. This state of matter is called Quark-Gluon Plasma (QGP). We can access this stage of matter through relativistic heavy-ion collisions in particle accelerators. There are also ways to identify meaningful indications of the Quark-Gluon-Plasma such as collective flow (28, 29), strangeness enhancement, and suppression of hard probes. The study of the QGP can help to understand important open questions of the QCD such as confinement, jets, and hadronization. According to the called "hard probes", like jet quenching (30), particle production ratios, Fourier Coefficients of the Azimuthal distribution, we can quantify, and learn more about this big small system.

The text is structured as follows: First, an introduction about Quantum Chromodynamics, a brief description of the Quark Gluon Plasma and global properties; after this, the second Chapter is about basic tools that support the phenomenological and theoretical development on high energy physics; Chapter 3 describes a discussion about small systems; Chapter 4 continues describing the evolution of the heavy quark; Chapter 5 describe how was developed of the simulation program. Finally, the results obtained from the simulation are presented and discussed in Chapter 6.

1.1 Quantum Chromodynamics

The knowledge about the constituents of the matter was only three (protons, neutrons, and electrons) until a few decades before the early 20th century(23) and after. The discovery of several particles increased enormously when particle accelerators to began to be used as a tool in Particle Physics in the 1950s. In order to understand the new particles, Gell-Mann (31) and Zweig (32) proposed independently a geometrical scheme, which is established on the quantum numbers of charge and strangeness of baryons and mesons(23). In 1964, Oscar W. Greenberg[1] (24) introduced a new charge that could have three different values, usually called color[2] degrees of freedom. The scheme of the quark

[1] See (33) for more basic details about Lie Groups.

[2] This proposal explained the inconsistency wiht the Pauli principle observed in the $\Delta^{++}(1232)$ barion. In this notation, the number denotes the mass in MeV, i. e., 1232MeV, while Δ^{++} denotes the quark

model that classifies particles according to elementary constituents, which are called *quarks* (23, 25, 35, 36).

The current theories that describe elementary particles and their interactions save gravity are arranged into *Standard Model* (23, 24, 25). According to this theory, the elementary particles are composed of quark, leptons, and mediators. Quarks have degrees of freedom called (up, down, strange, charm, bottom, and top). See in Fig. 1.

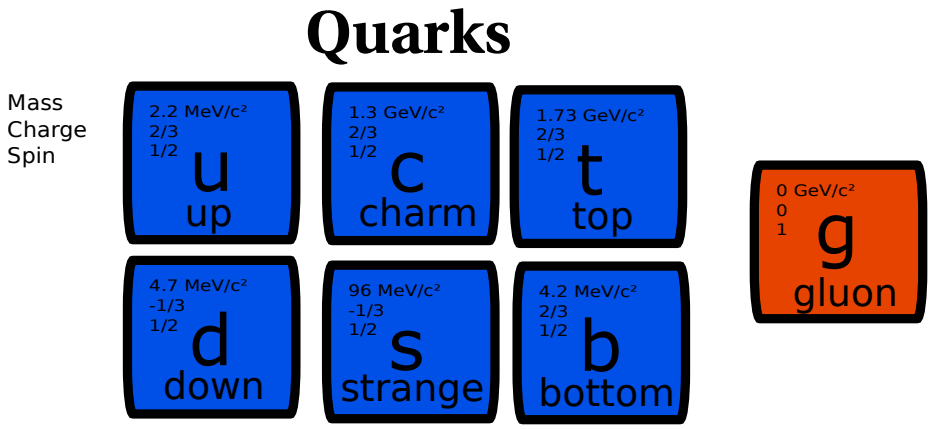

Figure 1 – Particles from the Standard Model that interact through the strong force (QCD). Data of the mass and other properties are taken from Ref.(1).

They carry fractional electric charges in addition to a quantum number named color (red, blue, and green). The Table 1.1 is a qualitative picture of the fundamental forces with the relative strength evaluated for Q=1 GeV.

Interaction	Approx. potential	Parameter Values	Relative strength
Strong	$\frac{12\pi/23}{Q^2 ln(Q^2/\Lambda^2)}$	$\Lambda \approx 0.2 GeV$	1
electromagnetic	$\frac{\alpha_{em}}{Q^2}$	$\alpha_{em} \approx 1/37$	1.4×10^{-2}
Weak	$\frac{\alpha_{em}}{Q^2 - M_W^2}$	$M_W^2 \approx 80 GeV/c^2$	2.2×10^{-6}
Gravity	$\frac{G_N m_1 m_2}{Q^2}$	$G_N \approx \frac{6.7 \times 10^{-39}}{GeV^2}$	1.2×10^{-38}

Tab. 1 – Qualitative picture of the fundamental forces with the relative strengths evaluated for $Q = 1 GeV$. This table was taken from (21).

and isospin content of the state, which in this case corresponds to a baryon of isospin 3/2 with charge +2 (34).

The gauge theory of color was first proposed in 1965 and introduced the gluons (37, 38) like an octet in a $SU(3)$ symmetry group theory as mediators of the strong force between the quark particles. The gluon field is the mediator and the color is the strong interaction (39). The existence of the quarks was first observed at the Stanford Linear Accelerator Center (SLAC) (40, 41) in inelastic scattering of electrons into protons and neutron targets. Two results contributed to the interpretation of the proton structure observed at SLAC. The first proposal to understand properties of hadron interaction is the parton model (36, 25, 23, 21), proposed by Feynman, in which the goal is to describe any particle within a hadron, describe cross sections of collisions in order to understand the behavior of quarks, and finally understand better The Strong Interaction. The word *parton* is a generic term for one of the constituents under the conditions in which it participates in the short-distance range of a collision[3]. The Deep Inelastic Scattering (DIS) led to different theoretical interpretations that constitute the basis for the parton model. There is a study proposed by Bjorken (42). He showed that the structure that describes the cross section of electron-proton collisions can be written in terms of a fraction of the momentum carried by quarks inside the nucleon in collisions at high energy. The *scaling* property predicted by Bjorken (42) is defined as:

$$x = \frac{-q^2}{2M\nu}, \tag{1.1}$$

which q is the momentum transfer from the electron to the hadrons, ν is the energy transfer in the rest frame of the hadron and M is the mass of the target hadron. This interpretation of x was understood as the fraction of the hadron momentum carried by a given parton, a point-like constituent inside the hadrons (43).

The Quantum Chromodynamics (QCD) was developed from the color gauge theory and the Yang-Mills theory, in 1973 (39, 44). This theory has a local gauge symmetry $SU(3)$. The Lagrangian is:

$$\mathcal{L} = -\frac{1}{4}G^a_{\mu\nu}G^{a,\mu\nu} + \bar{\Psi}(i\gamma_\mu D^\mu - m)\Psi, \tag{1.2}$$

in which:

- Ψ is the field to fermionic particle;
- $G^a_{\mu\nu}$ is the gauge invariant gluon field strength tensor given by $G^a_{\mu\nu} = \partial_\mu A^a_\nu - \partial_\nu A^a_\nu + gw^{abc}A^b_\mu A^c_\nu$, in which w^{abc} are the structure constants of $SU(3)$;
- D^μ is the covariant derivate $D^\mu = \partial_\mu - igt^a A^a_\mu$, which g is gauge coupling, and t^a is the generators of Lie group which defines the gauge symmetry;

[3] See (21, ch. 6), for more details about Parton Model.

- A^a_ν is the gluon field;
- a is the index of the generators of the SU(3);
- m is the quark mass. This theory has more than one quark, so you should sum the last term over all the different quarks.

We have important properties from QCD. First, we have the asymptotic freedom. These properties is well understood when we look look at the Perturbative Quantum Chromodynamics (pQCD), in which are obtained calculations that the coupling constant α_s play significant rules. In general, corrections needed to be done for scatterings $2 \to 2$. The asymptotic freedom of QCD was discovered by David Gross and Frank Wilczek (45). The correction is done through renormalization and regularization methods (23, 46). The first-order solution of the renormalization group equation for the QCD is:

$$\alpha_S(Q) = \frac{\alpha_S}{1 + (\alpha_S b_0/2\pi)\log(Q/M)}, \tag{1.3}$$

which Q is the energy scale, $b_0 = 11 - 2/3n_f$ and n_f is the number of fermions. Usually, is common to define a scale (Λ_{QCD}) that satisfies the Eq. 1.4:

$$1 = g^2 \frac{b_0}{8\pi^2} \log(M/\Lambda_{QCD}), \tag{1.4}$$

If we combine the Eq. 1.3 with Eq. 1.4, we can obtain Eq.1.5. When we analyze the Eq. 1.5, we can see for values of $Q(Q/\Lambda_{QCD} >> 1)$ the interaction becomes weaker. For the limit $Q/\Lambda_{QCD} \to \infty$ the coupling constant vanishes $\alpha_S \to 0$. This behavior making quarks and gluons roughly free particles. This limit corresponds to very high energy.

$$\alpha_S(Q) = \frac{2\pi}{b_0 \log(Q/\Lambda_{QCD})}. \tag{1.5}$$

This is the regime in which perturbative QCD is valid. See plot in Fig. 1.1

The second property is the color confinement. This behavior can be understood following the scheme:

- The QCD potential is approximately linear for large distances.
- If the distance increases the interaction grows.
- If we increase the distance, we need more energy to separate the two particles.
- The energy required to separate the particles is large so that it becomes incredibly favorable to produce a new pair $q\bar{q}$.

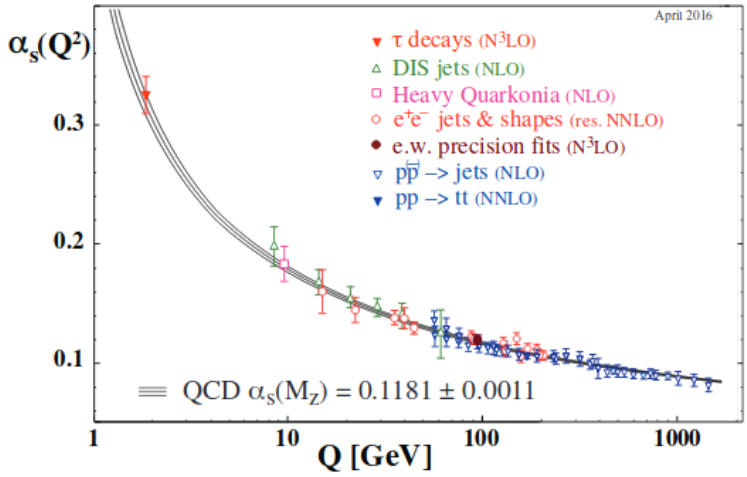

Figure 2 – Evolution of the running coupling constant of QCD as function of the energy scale (Q). The degree of perturbation theory used is indicated in brackets. The Figure was taken from Ref. (1).

The confinement is not yet fully understood. Currently, this problem is one the Millennium Problems from the Clay Mathematics Institute (47).

There is another approach to study the confinement towards examining this scenario is the lattice gauge theory, i.e., lattice QCD or just (lQCD). This theory exists since the 1970s (48). The conclusion for the first studies was that confinement is strictly a low-temperature phenomenon (48). This approach addresses solutions in non-perturbative regimes.

1.2 Creation of Quark Gluon Plasma(QGP): Collision and Phase transitions

The Quark Gluon Plasma is expected to be created in conditions of high temperature or pressure, such as the first moments of the Universe. The Primordial matter at these temperatures is not made of hadrons. When the matter (into experimental acellerators) achieves these temperatures, we have, for a short moment, a soup of quarks and gluons. Understanding the properties of the phases of QCD will teach us about the phase diagram of hot QCD matter, as a function of temperature and baryon chemical potential (Fig. 3). This sketch illustrates the current understanding of the expected features of the phase diagram of QCD. The transition from QGP to hadrons is a crossover near the vertical axis. Currently, we can understand this crossover from lattice QCD calculations (49, 48).

Understanding of the thermodynamic properties of QGP can be measured through the equation of state, current conservation, and energy-momentum. First-order transition or second-order transition studies are not required, but are not excluded from QGP

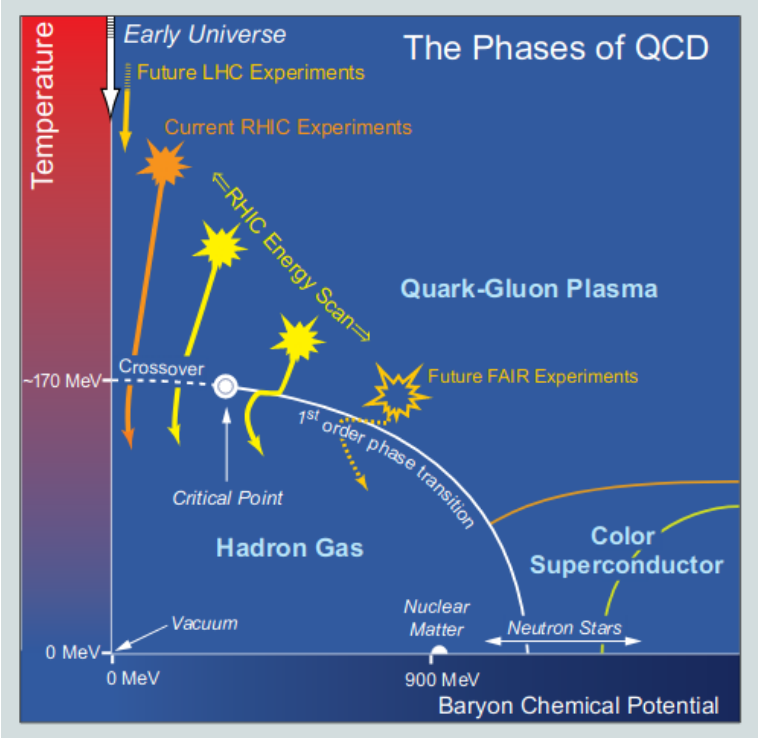

Figure 3 – Schematic QCD phase diagram for nuclear matter. The Figure was taken from Ref. (2).

discoveries (50).

The equation of state of an ideal gas of massless quarks and gluons is predicted by theoretical calculations for degrees of freedom and your determination(51):

$$[h]\frac{\epsilon_{SB}}{3T^4} = \frac{p_{SB}}{T^4} = [2(n_c - 1) + \frac{7}{2}n_c n_f]\frac{\pi^2}{90}, \tag{1.6}$$

In order to explore the properties of the phase diagram and understand the QGP, it is necessary to recreate extreme conditions of density and temperature. Usually it is used lead, gold, and xeon nuclei in particles accelerators. Once created, the environment is not static, The environment evolves with time. The time lapse in Fig. 4 illustrates the stages of the system evolution after the collision. This collision generates a very high temperature due to the energy of the collisions and a higher density. The setup for collisions under direct control are: which two nuclei collinding and with some energie[4]. However, the impact parameter b (the transverse distance between the center of masses of two participant nuclei) is unknown. Neither the location and motion of the nucleons in the nuclei. The quarks and gluons location in the nucleons are not measurable. They have to be inferred, as best as possible or as needed, event by event, from the observed outcome of the collision.

After the collision of two nuclei, the system undergoes a series of stages. We can set it into the following stages:

[4] Usually use $\sqrt{S_{NN}}$, energy of center of mass.

- Pre-Equilibrium: After the collision. Partons with large momentum ($p_T >> 2GeV/c$) and mass (b,c and t quarks) are produced in this stage.
- Quark-Gluon-Plasma (QGP): This stage is the moment where quarks and gluons are no longer confined inside the hadrons. Tha particles cross the medium and loose energy in radiative emission (gluons) or due to collisions. This stage remains until the temperature reaches a critical temperature T_C where we have the initial of the freeze-out.
- Mixed- phase: at this stage, the QGP can coexist with another state of the nuclear matter, some hadronic matter.
- Hadronization: at this stage, the partons will be confined in hadrons. The hadronization can happen with two different mechanisms: fragmentation and coalescence.
- Chemical freeze-out: The particles are fixed.
- Hadron gas: in this stage, the medium is still expanding. We don't have free quarks and gluons.
- Freeze-out: this part the density becomes low due to the expansion. The particles will now travel in the detector. They might decay or not. These particles will be measured by sensitive detectors.

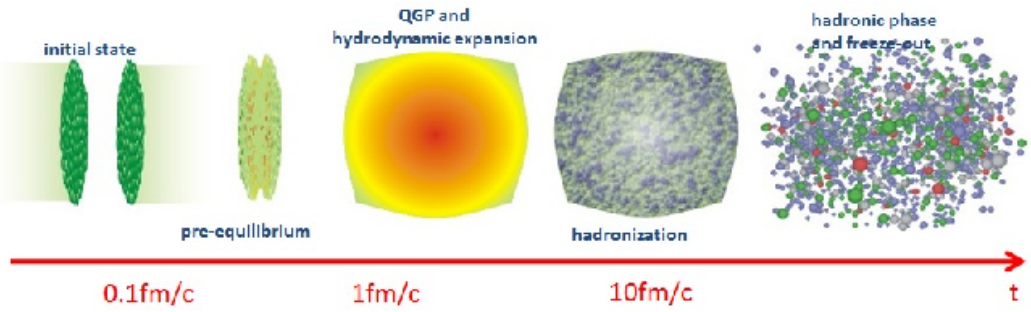

Figure 4 – Scheme of the matter created in relativistic heavy ion collision time-by-time. This figure was taken from Ref.(3)

1.3 Quark Gluon Plasma: Global properties

We can learn about QGP once we have the right tools to understand this big scenario. We need to know some physics aspects to understand well this field. As I commented before, The Quantum Chromodynamics is widely accepted as the fundamental theory describing the behavior of hadrons. Once we need to recreate matter at the corresponding high energy

density, *id est*, colliding heavy nuclei (also called "heavy ions") at ultrarelativistic energies, it is important to use and understand the best tool and model for describing this scenario.

In relativistic collisions, usually, we use kinematic variables that take simple forms under Lorentz transformations for the change of frame of reference. Usually, space-time rapidity is used to understand t and z projection of the collision. The space-time rapidity is defined as:

$$\eta_s = \frac{1}{2} ln(\frac{t+z}{t-z}), \tag{1.7}$$

which t is the proper time of the collision and z, regularly, is called longitudinal. For (x-y) it is called perpendicular. So now, we can define "y" rapidity as:

$$y = \frac{1}{2} ln(\frac{E+p_z}{E-p_z}), \tag{1.8}$$

This quantity is related to the ratio of the forward light cone to backward light-cone momentum. The Lorentz boost can give an illustrative representation:

$$\begin{bmatrix} ct\prime \\ x \end{bmatrix} = \begin{bmatrix} \cosh y & \sinh y \\ \sinh y & \cosh y \end{bmatrix} \begin{bmatrix} ct \\ x \end{bmatrix} \tag{1.9}$$

The advantage of rapidity variable is that the shape of the rapidity distribution remains unchanged under a longitudinal Lorentz boost. We can define rapidity in beam perspective like:

$$y = \sinh^{-1}(\frac{p_z}{m_b}), \tag{1.10}$$

which m_b is the mass of the nucleon (See A.1 for more details).

When we assume that a particle is emitted at an angle θ relative to the beam axis. So, we can write rapidity as

$$\eta = -ln(\tan\frac{\theta}{2}), \tag{1.11}$$

which η is called the pseudorapidity. We also can write η in terms of the momentum as

$$\eta = \frac{1}{2} ln(\frac{|\mathbf{p}|+p_z}{|\mathbf{p}|-p_z}), \tag{1.12}$$

which p_z is longitudinal momentum. Here, θ is the only quantity to be measured for the determination of pseudorapidity, independent of any particle identification mechanism.

We can write 1.12 in this way:

$$e^{\eta} = \sqrt{\frac{|\mathbf{p}| + p_z}{|\mathbf{p}| - p_z}}, \tag{1.13}$$

$$e^{-\eta} = \sqrt{\frac{|\mathbf{p}| - p_z}{|\mathbf{p}| + p_z}} \tag{1.14}$$

So, adding both of the equations, the result is:

$$|\mathbf{p}| = p_T \cosh \eta. \tag{1.15}$$

So, we can write in this form:

$$p_T = \sqrt{|\mathbf{p}|^2 - p_z^2}, \tag{1.16}$$

and now,

$$p_z = p_T \sinh \eta, \tag{1.17}$$

In this way, Thus, it is possible and appropriate to use rapidity and transverse momentum to analyze the experiments with heavy ion collisions.

Chapter

2 Quark Gluon Plasma: Evolution

In order to study the main aspects of QGP as a configuration, it is necessary, as commented before, to analyze changes over time. Since thermalization of the medium is assumed to be a fairly rapid process until the next step, the hadronization, the QGP can be described using a hydrodynamic model, which must consider the fluctuations of the initial conditions generated by the collision. Therefore, one of the main configuration steps of this study is the choice of the initial conditional model.

This configuration step is added to the algorithm. The relationship between the large degrees of collectivity evidenced by the Fourier harmonics and the strongly-coupled medium with small shear-viscosity η/s[1] are considered in the calculations. One can describe central collisions with increased elliptic flow through ideal hydrodynamics.

The next section will describe the equation of the motion, the hydrodynamic model of the medium that is one of the most widely used, the smoothed-particle hydrodynamics, usually, to describe the flow of high energy, and entropy with the low baryon number density fluid. Together, the initial conditions model and the Cooper-Frye prescription will be described.

2.1 Equations of motion

The ideal hydrodynamics is defined as a special case dissipative hydrodynamics, where we have conditions for transport coefficient. This theory was derived by Eckart and Landau-Lifshitz (52, 53). Relativistic hydrodynamics introduces the flow $u^{\mu}(x)$ which is

[1] η is described as being shear viscosity and s is entropy.

defined as a 4-velocity, i.e., $u^\mu = \gamma(1, v_x, v_y, v_z)$ which γ is Lorentz dilation factor:

$$\gamma = \frac{1}{\sqrt{1 - v_x^2 - v_y^2 - v_z^2}}. \tag{2.1}$$

This flow is normalized as $u^\mu u_\mu = 1$. The system is fundamentally described by the energy-momentum tensor $T^{\mu\nu}$, conserved charge current N^μ, and the entropy current S^μ (54, 55, 56).

$$\partial_\mu N^\mu = 0, \tag{2.2}$$

$$\partial_\mu T^{\mu\nu} = 0, \tag{2.3}$$

and finally the 2nd law of thermodynamics:

$$\partial_\mu S^\mu \geq 0. \tag{2.4}$$

The energy-momentum tensor is expressed as the Eq. 2.5, where the spatial projection operator $\Delta^{\mu\nu} = g^{\mu\nu} - u^\mu u^\nu$ is defined with Minkowski metric $g^{\mu\nu} = diag(+, -, -, -)$.

$$\partial_\mu T^{\mu\nu} = \epsilon u^\mu u^\nu - P\Delta^{\mu\nu}, \tag{2.5}$$

which ϵ and P are energy density and pressure.

The other densities variables can be obtained as:

$$N^\mu_{eq} = nu^\mu, \tag{2.6}$$

$$S^\mu_{eq} = su^\mu. \tag{2.7}$$

The orthogonality for the Eq. 2.5 is satisfied with $\Delta^{\mu\nu} u_\nu = 0$. For equilibrium state is assumed when is fully specified by $(n, \epsilon, \mathbf{u})$ or with the thermal potential $\alpha = \mu/T$ and the inverse 4-temperature $\beta^\mu = u^\mu/T$, in which the quantity μ is the chemical potential. The pressure p can be obtained from (54, 55, 56):

$$S^\mu = p\beta^\mu - \alpha dN^\mu_{eq} + \beta_\lambda dT^{\mu\nu}_{eq}. \tag{2.8}$$

Based on the above by using the Gibbs-Duhem equation $d(p\beta^\mu) = N^\mu_{eq} d\alpha - T^{\mu\nu}_{eq} d\beta_\lambda$, the entropy current rate can be expressed as (54, 55, 56):

$$dS^\mu_{eq} = -\alpha dN^\mu_{eq} + \beta_\lambda dT^{\mu\nu}_{eq}. \tag{2.9}$$

Once that the system is not in equilibrium, the particle current, entropy current, and energy-momentum current rate can be expressed as:

$$N^{\mu} = N^{\mu}_{eq} + \delta N^{\mu} = nu^{\mu} + V^{\mu}, \tag{2.10}$$

$$S^{\mu} = S^{\mu}_{eq} + \delta S^{\mu} = su^{\mu} + \Phi^{\mu}, \tag{2.11}$$

$$T^{\mu\nu} = T^{\mu}_{eq} + \delta T^{\mu} = [\epsilon u^{\mu}u^{\nu} - p\Delta^{\mu\nu}] + \Pi\Delta^{\mu\nu} + \pi^{\mu\nu} + (W^{\mu}u^{\nu} + W^{\nu}u^{\mu}), \tag{2.12}$$

which V^{μ} describe the net flow of charge, Φ^{μ} is the entropy flow, and W^{μ} the energy flow. In the Eq. 2.12 $\Pi = -\frac{1}{3}\Delta_{\mu\nu}T^{\mu\nu} - p$ is the bulk viscous pressure, and $\pi^{\mu\nu} = [(1/2)(\Delta^{\mu\sigma}\Delta^{\nu\tau}+\Delta^{\nu\sigma}\Delta^{\mu\tau}-(1/3)\Delta^{\mu\nu}\Delta^{\sigma\tau})]T_{\sigma\tau}$ is the shear stress tensor. It's important to take a note about the Landau Frame (u^{μ}) whose is the eigenvector of energy-momentum tensor. For the rest frame, usually is used as:

$$u_{\nu}T^{\mu\nu} = \epsilon u^{\mu}. \tag{2.13}$$

For the Eq. 2.9, equilibrium relation is made an assumption. He is valid near equilibrium state so that it can be generalized as:

$$dS^{\mu} = -\delta N^{\mu}\partial_{\mu}\alpha + \delta T^{\mu\nu}\partial_{\mu}\beta_{\nu} + \partial_{\mu}Q^{\mu}, \tag{2.14}$$

in which the term Q^{μ} is the deviation of the particle current, and energy-momentum tensor. Usually, is needed to choose the value for Q^{μ} for obtaining first order theories or second order theories[2]. For Israel-Stewart theory, the most general form of Q^{μ} can be written as:

$$Q^{\mu} = -(\beta_0\Pi^2 - \beta_1 q^{\nu}q_{\nu} + \beta_2\pi_{\nu\lambda}\pi^{\nu\lambda})\frac{u^{\mu}}{2T} - \frac{\alpha_0\Pi q^{\mu}}{T} + \frac{\alpha_1\pi^{\mu\nu}q_{\nu}}{T}, \tag{2.15}$$

in which the term β_i and α_i are thermodynamics coefficients, and q^{μ} is the heat flow.

The entropy production rate can be expressed, after generalization to the near equilibrium state, as (54, 55, 56):

$$T\partial_{\mu}S^{\mu} = \Pi X - q^{\mu}X_{\mu} + q^{\mu\nu}X_{\mu\nu}, \tag{2.16}$$

[2] $Q^{\mu} = 0$ is to first order theory.

in which the thermodynamics forces are defined as: $X = -\nabla \cdot u$, $X^{\mu} = \nabla^{\mu}\mu/T - u^{\nu}\partial_{\nu}u^{\mu}$, and $X^{\mu\nu} = \nabla^{\langle\nu\mu\rangle}u$[3].

Postulating a linear relation between the dissipative flows and thermodynamic forces the second law $\partial_{\mu}S^{\mu} \geq 0$ is satisfied. Based on the Eq. 2.16, we can define as:

$$\Pi = -\zeta\theta, \tag{2.18}$$

$$q^{\mu} = -\lambda\frac{nT^2}{\epsilon + p}\nabla^{\mu}(\frac{\mu}{T}), \tag{2.19}$$

$$\pi^{\mu\nu} = 2\eta\nabla^{\langle\mu\nu\rangle}u, \tag{2.20}$$

in which, ζ, λ, η are the positive transport coefficients, bulk viscosity, heat conductivity, and shear viscosity, respectively.

Several studies use first order theory (57, 58, 59), but causality is violated. So, it's important to know about the theoretical limits.

2.2 FORMULATION OF THE SMOOTHED PARTICLE HYDRODYNAMICS

In order to increase knowledge about the hydrodynamic behavior of QGP, Smoothed Particle Hydrodynamics (SPH) was used. This approach fits perfectly with variational formalism. Once we have relativistic nuclear collisions, where an extremely compressed and high-temperature hadronic matter expands within a very large space region, The SPH is widely used because of your fixed conserved quantity and changes of geometry. The SPH parametrizes the matter flow in terms of discrete Lagrangian coordinates attached to some conserved quantity. For the use of this method in the study of Heavy-ion Collisions, it is interesting to use hyperbolic coordinates to use this tool. We can define the coordinates as:

$$\tau = \sqrt{t^2 + z^2}, \tag{2.21}$$

$$\eta = \frac{1}{2}\tanh\frac{t + z}{t - z}. \tag{2.22}$$

[3] This indicates the symmetric involving trace-free projection. The symmetric trace-free projection is the traceless part of the spatial projection defined as:

$$A_{\langle\alpha\beta\rangle} = (\Delta^{\lambda}_{\alpha}\Delta^{\mu}_{\beta} - \frac{1}{3}\Delta_{\alpha\beta}\Delta^{\lambda\mu})A_{\lambda\mu} \tag{2.17}$$

The metric tensor for this coordinate system is:

$$\mathbf{g} = \begin{pmatrix} 1 & 0 & 0 & 0 \\ 0 & -1 & 0 & 0 \\ 0 & 0 & -1 & 0 \\ 0 & 0 & 0 & -\tau^2 \end{pmatrix},$$

with $\sqrt{-g} = \tau$.

Once the metric is independent of space, the parametrization can be defined as[4]:

$$\tau\gamma_i s_i = \sum_{j=1}^{n} v_j W(q_{ij}). \tag{2.23}$$

The use of SPH determines an amount to be conserved. Once defined, one can write:

$$\tau\gamma_i s_i \rightarrow s^* = \sum_{j=1}^{n} v_j W(\vec{r} - \vec{r}', h), \tag{2.24}$$

in which $s^*(\vec{r}, t) = \gamma s$, W being positive represents a function called Kernel whose normalization is given by:

$$\int W(\vec{r} - \vec{r}', h) d\vec{r} = 1, \tag{2.25}$$

where h is defined as the kernel size. The choice of smoothing kernel is an important one. The role of W is to introduce a sort of short-wavelength cut in the Fourier representation of the density variable. This means that will we have a continuous and well defined first derivative and we are replacing the continuous fluid by a collection of SPH particles (60) (61). Within the limit of $h \rightarrow 0$, we will have:

$$\lim_{h \to 0} W(\vec{r} - \vec{r'}, h) = \delta(\vec{r} - \vec{r'}), \tag{2.26}$$

A is defined as an extensive thermodynamic quantity, so we had $s = dA/dV$, where dV is an infinitesimal volume element.

$$A = \int d^3\vec{r} s^*(\vec{r}, t). \tag{2.27}$$

The longitudinal motion is presupposed to be uniform, so that velocity of all particles in the medium is given by:

$$u_i = (\sqrt{1 + u_x^2 + u_y^2}, u_x^2, u_y^2, 0). \tag{2.28}$$

[4] The i and j index represent the index position of variables into the general definition of the SPH particles. In relativistic hydrodynamics, this index can be related to the position of some extensive quantity.

For the SPH method, the associated current can be defined as (62):

$$J^* = \sigma u^\mu, \tag{2.29}$$

which σ can be defined as a sum of small piece-wise distributions.

$$j(\mathbf{r},\tau)^* = \sum_{\alpha=1}^{N} v_\alpha \frac{d\mathbf{r}_\alpha(\tau)}{d\tau} W[\mathbf{r}-\mathbf{r}_\alpha; h]. \tag{2.30}$$

For the SPH method, the relation between σ and σ^* can be written as:

$$\sigma^*(\mathbf{r}_\alpha(\tau)) = \gamma\sigma(\mathbf{r}_\alpha(\tau)), \tag{2.31}$$

so, the "*specific volume*" associated with the particle α can be defined as (60):

$$V_\alpha = \frac{v_\alpha}{\sigma(\mathbf{r}(\tau))} = \frac{\gamma_\alpha v_\alpha}{\sigma^*\mathbf{r}(\tau)}. \tag{2.32}$$

These ingredients are sufficient to make a relation between the new density and the reference density. The definition can be related as (60, 27):

$$a^*(\mathbf{r},\tau) = \sum_{\alpha=1}^{N_{SPH}} = a(\mathbf{r}(\tau))\frac{v_\alpha}{\sigma(\mathbf{r}(\tau))}. \tag{2.33}$$

For the case of Ideal Hydrodynamics (27), the lagrangian in the case of the Minkowski metric is given by the action:

$$I = \int L dt = -\int \epsilon d^4x \tag{2.34}$$

in which ϵ is the proper energy density of the fluid, and can be regarded as the Lagrangian density. The SPH parametrization of this density can be defined as:

$$I_{SPH} = -\int \sum_a \frac{v_\alpha \epsilon_\alpha}{\gamma_\alpha \sigma_\alpha} dt = \int \sum_\alpha (\frac{E}{\gamma})_\alpha dt \tag{2.35}$$

in which $(v\epsilon/\sigma)_\alpha$ is the rest energy of the particle α. This formulation is written in the local frame using 2.31.

After using SPH and compute the evolution of the medium, it is necessary to address the decoupling of the medium. Usually, it is implemented The Copper-Frye method to this medium freeze-out.

2.3 COOPER FRYE METHOD

After beginning the hydrodynamic evolution of the system, there will be a tendency for inelastic collisions to decrease and hadrons to remain more prevalent in the final

processes of the system. The Cooper-Frye (63) method can assist the study of QGP through the freeze-out process mentioned above. Once there is expansion it can be expected to increase free-path until the medium is no longer considered a liquid. Thus, the descriptions so far associated with a local thermal equilibrium will no longer apply.

The Cooper Frye prescription definition uses some thermodynamics constraint along with a hypersurface. The definition of this constraint is associated with the Eq. 2.36:

$$dn = f(x,p)d^3\mathbf{p}, \tag{2.36}$$

in which p is the particle four-momentum and $f(x,p)$ is the one-body distribution function. In ideal hydrodynamics, it can be written as:

$$f(x,p) = \frac{g}{(2\pi)^3}\frac{1}{exp[\beta(u_\mu p^\mu - \mu)] \pm 1}, \tag{2.37}$$

in which g is the degeneracy factor of the particle, μ is the chemical potential and β is $1/T$. The $\pm$ is to fermions and bosons respectively.

One can now formalize the current j^μ associated with the density n as:

$$j^\mu = \int \frac{p^\mu}{E} dn = \int f(x,p)\frac{p^\mu}{E} d^3\mathbf{p}. \tag{2.38}$$

By integrating the above equation over the hypersurface the total number of particles is obtained:

$$N = \int j^\mu d\sigma_\mu. \tag{2.39}$$

The invariant distribution follows as:

$$E\frac{dN}{d^3p} = \int \frac{p^\mu d\sigma_\mu}{\exp[\beta(u_\mu p^\mu - \mu)] \pm 1}. \tag{2.40}$$

The Eq. 2.40 is the invariant distribution Cooper Frye equation.

2.4 EQUATION OF STATE

In the study of the hydrodynamics of heavy ion collision physics, the fundamental parameters for relating thermodynamics and energy density, pressure, fluid particle number is the equation of state (EOS). This equation of state can explicitly relate phase transition to study effects and properties on the QGP and particle interactions with the medium (56). In order to calculate EOS the lattice QCD is usually used (48, 50, 49, 64). There are combinations of Lattice QCD with other models that try to describe systems like tetraquarks (65).

The equation of state can be defined as (56):

$$\frac{\epsilon = 3P}{T^4} = \frac{d_2}{T^2} + \frac{d_4}{T^4} + \frac{c_1}{T^{n_1}} + \frac{c^2}{T^{n_2}}, \tag{2.41}$$

in which d_i,c_i, and n_i are parameters, T is the temperature, P is the pressure and ϵ is the energy density. The equation of state is the $sp95p - v1$ and $sp95n - v1$ in which this label means fractions of the ideal entropy.

In this work the equation $sp95n - v1$ is used with parameters $d_2 = 0.2654GeV$, $d_4 = 6.563\times10^{-3}\text{GeV}^4$, $c_1 = -4.370\times10^{-5}\text{GeV}^8$,$n_1 = 8$, $n_2 = 9$, and $c_2 = 5.774\times10^{-6}\text{GeV}^9$.

2.5 INITIAL CONDITIONS

In general, Initial conditions generate energy profiles or entropy at QGP with thermalization time to involve fluid dynamics. Usually, these models are employed in two ways: dynamic models, in which they explicitly simulate the start state and the pre-equilibrium evolution of the collision (66, 67, 68) and a non-dynamic simplistic model, in which it is neglected. The pre-equilibrium evolution and in which static profiles are built along with a thermalization time.

2.5.1 TRENTO

In this work, we use IP-GLASMA (67), so-called Reduced Event-by-event Thickness Nuclear Topology (TRENTO). IP-GLASMA uses weakly-coupled color-glass condensate (CGC) effective field theory (69) in which Classical Yang-Mills evolution is also used to describe the event-by-event data for higher order flow and other observables. At first, the TRENTO is used to generate the initial conditions for proton-proton, proton-nucleus, and nucleus-nucleus. The basis of its principle starts from the function $T_{A,B}(x, y)$. This one represents two projectiles colliding along the z axis. Projectiles are represented by the function Thickness:

$$T_{A,B}(x, y) = \int dz \rho^{part}_{A,B}(x, y, z), \tag{2.42}$$

in which ρ is nuclear matter density. In this model, there is a scalar field defined as $f(T_A, T_B)$, where it is proportional to the entropy created at mid-rapidity and at the hydrodynamic thermalization time. This function has been optimized so that we can define it as:

$$f = T_R(p, A, B) = (\frac{T^p_A + T^p_B}{2})^2, \tag{2.43}$$

where p is an adjustment parameter for an interpolated shape between the values of the two projectiles. From the configuration of function f it is possible to execute and calculate multiplicity distributions. The Fig. 5 shows these results. The p parameter is defined as a tool to transform the function T_R. This mean that p interpolates among qualitatively different physical mechanisms for entropy production. Each value of p means that for a pair of nucleon participants we can set this entropy associated a some mechanism. $p = 1$ (called arithmetic) the reduced thickness is equivalent to a Monte Carlo wounded nucleon model and deposits a blob of entropy for each nucleon. For $p = 0$ (called geometric) there is a single roughly symmetric blob at the mid-point of the collision and $p = -1$ means a suppression of entropy along the direction of the impact parameter.

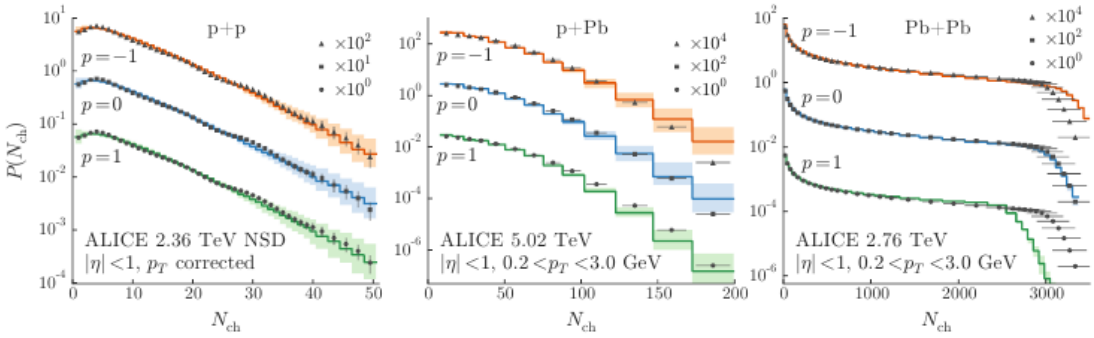

Figure 5 – Multiplicity distributions for proton-proton, proton-lead, and lead-lead collisions. These graphics were taken from (4). The p is dimensionless parameter that can simplify the thickness function for certain values. Data points (triangles, squares, circles) are experimental distributions from ALICE (5, 6).

The new thickness functions can be calculated by:

$$T_A = \sum_{i=1}^{N_{part}} w_i \int dz \rho(x - x_i, y - y_i, z - z_i), \tag{2.44}$$

in which w_i and $(x-x_i, y-y_i, z-z_i)$ are the normalization and position of the participating projectiles within the nucleus. After the Hydrodynamic evolution, the average charged-particle multiplicity $\langle N_{ch} \rangle$ is a good approximation to the total entropy (Eq. 2.46) and can be written as (70):

$$\langle N_{ch} \rangle \approx \int dx dx T_R \tag{2.45}$$

$$dS/dy|_{\tau=\tau_0} \approx T_R(p; T_A; T_B). \tag{2.46}$$

After this approach, the final number of charged particles is Poisson distribution, i.e. $P(N_{ch}) = Poisson(\langle N_{ch} \rangle)$ (71).

2.6 COALESCENCE

In this project, we had as one of our goals, to investigate the influence of the process of coalescence in the QGP hadronization stage (72). To formulate this process, we worked with the use of hybrid coalescence plus the fragmentation process. This process widely used as an "*instant approach*" of Coalescence (73, 74). This approach, the probability distribution whose meson of momentum $P_{coal}[q, Q \to M]$ is formed by the coalescence of a quark related with momentum $\mathbf{p}_M$, the heavy meson of momentum, is given by:

$$P_{coal}[q, Q \to M](\mathbf{p}_q, \mathbf{u}) = N \int d^3\mathbf{p}_q f_M(\mathbf{p}_q, \mathbf{p}_Q) n_q(\mathbf{p}_q, \mathbf{u}, T_d) \delta(\mathbf{p}_M - \mathbf{p}_q - \mathbf{p}_Q), \tag{2.47}$$

where N is a normalization factor. n_q is a momentum distribution of light quarks at the hadronization time, and f_M is the probability density that there are two quarks within a meson state. To realize the differences of the mesons that obtained from the projection of the two quark states onto the meson state, a basic harmonic oscillator model is used. The quarks being relativistic, the projection is performed in their center-of-mass frame following a Lorentz boost of their phase space coordinates from the global frame to the center-of-mass frame. This setup is assuming that the light quarks have a uniform spatial distribution in the medium cell where the heavy quark is located. one can average the probability density over the spatial coordinates as follows:

$$f(\mathbf{p}_q, \mathbf{p}_Q) = g_M h_M \frac{(2\sqrt{\pi}\sigma)^3}{(2\pi)^3} e^{-\mathbf{p}_{rel}^2 \sigma^2}, \tag{2.48}$$

in which g_M is color-spin-isospin statistical factor for the two spin 1/2 quarks and h_M are a new "*thermal*" factor. The width $\sigma = \frac{1}{\sqrt{\mu\omega}}$ is given by the angular frequency of the harmonic oscillator ω and the reduced mass of the two quark system $\mu = m_q m_Q/(m_q + m_Q)$.

We define $\mathbf{p}_{rel}$ as:

$$\mathbf{p}_{rel} = \frac{m_q \mathbf{p}'_Q - m_Q \mathbf{p}'_q}{m_q + m_Q}, \tag{2.49}$$

in which the right side of the Eq. 2.49 is based in momenta in center-of-mass frame[5].

The momentum density distribution of the light quarks n_q is defined as:

$$n_q = \frac{g_q}{e^{\sqrt{(p_q^{cell2} + m_q^2/T_d)}} + 1} = \frac{g_q}{e^{p_q \cdot u/T_d} + 1}, \tag{2.50}$$

where p_q^{cell} is the light quark momentum in the local rest frame of the medium cell, $g_q = 6$. g_q is the degeneracy-spin factor of light quarks, $p_q \cdot u$ is the four-product

[5] The momenta is denoted with primed coordinates.

between the four-momentum of the light quarks in the global frame, and $u = (\gamma_u, \gamma_u \mathbf{u})$ with $\gamma = \frac{1}{\sqrt{1-\mathbf{u}^2}}$. Once there is a dependence on the speed of the fluid concerning n_q, the derived coalescence probabilities will depend not only on the heavy quark momentum but also on the angle between them and on the local flow.

This approach is also performed for the bottom $P_{coal}[q_1, q_2, Q \to B]$ in which the heavy baryon of momentum p_B is formed by coalescence of a heavy quark with momentum p_Q and two light quarks of momenta p_{q1} and p_{q2} is given by:

$$\begin{aligned} P_{coal}[q_1, q_2, Q \to B](\mathbf{p}_q, \mathbf{u}) =& N \int d^3\mathbf{p}_{q1} d^3\mathbf{p}_{q2} f_B(\mathbf{p}_{q1}, \mathbf{p}_{q2}, \mathbf{p}_Q) n_{q1}(\mathbf{p}_{q1}, \mathbf{u}, T_d) \times \\ & n_{q2}(\mathbf{p}_{q2}, \mathbf{u}, T_d) \delta(\mathbf{p}_B - \mathbf{p}_{q1} - \mathbf{p}_{q2} - \mathbf{p}_Q), \end{aligned} \tag{2.51}$$

in which N is the global normalization factor, f_B is the probability density obtained by combining the two light quarks first and then using their center of mass to merged with the heavy quark. The Eq. 2.51 is given by:

$$f_B(p_{q1}, p_{q2}, p_Q) = g_B h_B \frac{2\sqrt{\pi}^6 (\sigma_1 \sigma_2)^3}{(2\pi)^6} e^{-p_{rel}^2 \sigma_1^2 - p_{rel2} \sigma_2^2}, \tag{2.52}$$

in which and h_B are the "*thermal*" factor included, and g_B is the usual color-spin-isospin degeneracy factor. This term inspired by the thermal model of hadronization (74) has been included. The $h_{H=H,B} = \exp[-(m_H - m_{H_0})/T_d]$ in which H is the hadron state for which we want to compute P_{coal}, m_H is the mass, and m_{H0} Is the mass of the corresponding ground state H_0.

In order to assist in the calibration of the coalescence model, the reference of low and intermediate p_T enhancement of the Λ_c^+/D^0 ratio is considered. These data tend to confirm the presence of heavy-light quarks coalescence in heavy ion collisions for lower p_T. The ratio for the prompt D^+/D^0 and D^{*+}/D^0 are built with the basic coalescence model [6]. They are only based on the color-spin-isospin degeneracy factors, the rest of the probabilities canceling out. The ratio is given by:

$$\frac{D^+_{prompt}}{D^0_{prompt}} = \frac{D^+_{prompt} + D^{+*}_{prompt}(D^{*+}_{prompt} \to D^+)}{D^0_{prompt} + D^{+*}_{dir}(D^{+*}_{prompt} \to D^0) + D^0_{dir.}(D^{0*}_{dir.} \to D^0)} \tag{2.53}$$

in which "*prompt*" means including feed-downs from excited states and "dir." means the direct production (without feed-downs) that we obtain from the coalescence model.

[6] i.e. without the thermal factors.

Chapter

3 SMALL SYSTEMS

After the first steps of the study of heavy ion collisions, one of the results was the understanding that relativistic hydrodynamics plays an important role in the QGP behavior. We can list some species of collisions made in the second half of the last century that had an important influence on the properties of QGP and heavy quarks. Collisions as p+Au, d+Au, and He+Au are examples of these collisions (75, 76). In this century there are some questions about Quark Gluon Plasma for small systems[1] that remain unclear. One of them is about the existence of the QGP for small systems, as O+O, e Ar+Ar. Some studies use theories already known, Glauber, to represent the mix of possible collisions (77), being these collisions with p+O, O+O, He+Au, and Be+Au. In this work mentioned above, it is used to generate the nuclei an Argonne V18 (78), and Ubarna (79). The hydrodynamic part is performed using the program SONIC (80, 81). A good indication of the QGP would be the positive contribution of v_2 (82).

3.1 p-Pb Collisions Xe, Ar, and O collisions

As mentioned earlier, observables are corresponding to the QGP that can be tested on small systems. Observable as v_2 is possible to be measured in configurations with measurements of long-range, near-side angular correlation by the CMS collaboration in pp collisions at different energies (83). In 2013 the three heavy-ion LHC experiments that measure collective flow (29, 84, 85, 86, 87) and this asymmetric collisions indicate signatures of collective flow. The PHENIX collaboration at RHIC also reanalyzed data

[1] It can be understood as being elements with atomic mass less than that observed in Lead, an essential element for the study of the QGP and widely used. These types of elements (systems) directly affect the characteristics of the nucleon in collisions.

from d+Au collisions and confirmed the LHC discovery (88, 89) with certain caveats[2] (eccentric protons for the initial conditions) (90). The collision p+A one becomes sensitive to the assumed proton shape and its fluctuations, while in X(A,He,..)+A collisions spatial eccentricities are dominated by nucleon size scale fluctuations.

At the LHC, Xe^{129} collisions were to study for analyzing small systems, which had quite the unexpected result of measuring a deformed Xe^{129} in ultracentral collisions (91, 92, 93). The most theoretical predictions for this system it appears that quantitatively hold up to experimental data (94, 95) such that is well understood. The proposal is to study the hydrodynamic in small symmetric ion collisions through DAB-MOD (96). These results arise from a rather non-trivial interplay between the shrinking path length and the enhancement of eccentricities in small systems at high multiplicity. There are theoretical predictions for these systems (7).

For the studied systems (Ar^{40}, O^{16}) we can take as a basis an entropy distribution (Fig. 6). It is worth noting that, for the O + O system, despite being the smallest system, entropy density predictions show a higher concentration of entropy in the central part of the system (7).

For this system O + O compared to Pb + Pb it is clear that it will produce a smaller system, it does not mean that these small droplets of the quark gluon plasma are indistinguishable. The radius calculation of the initial condition is:

$$R^2 = \frac{\int r^2 s(r,\phi) r dr d\phi}{\int s(r,\phi) r dr d\phi}, \tag{3.1}$$

which it is worth noting that the radius is not of a sphere but rather the variance from the center of mass. The radius described as a variance denotes implications for $\langle r \rangle$.

[2] Caveat, according to Cambridge dictionary is a warning to consider something before taking any more action, or a statement that limits a more general statement. For details about the proton caveats Cf. Adare(89), 2015.

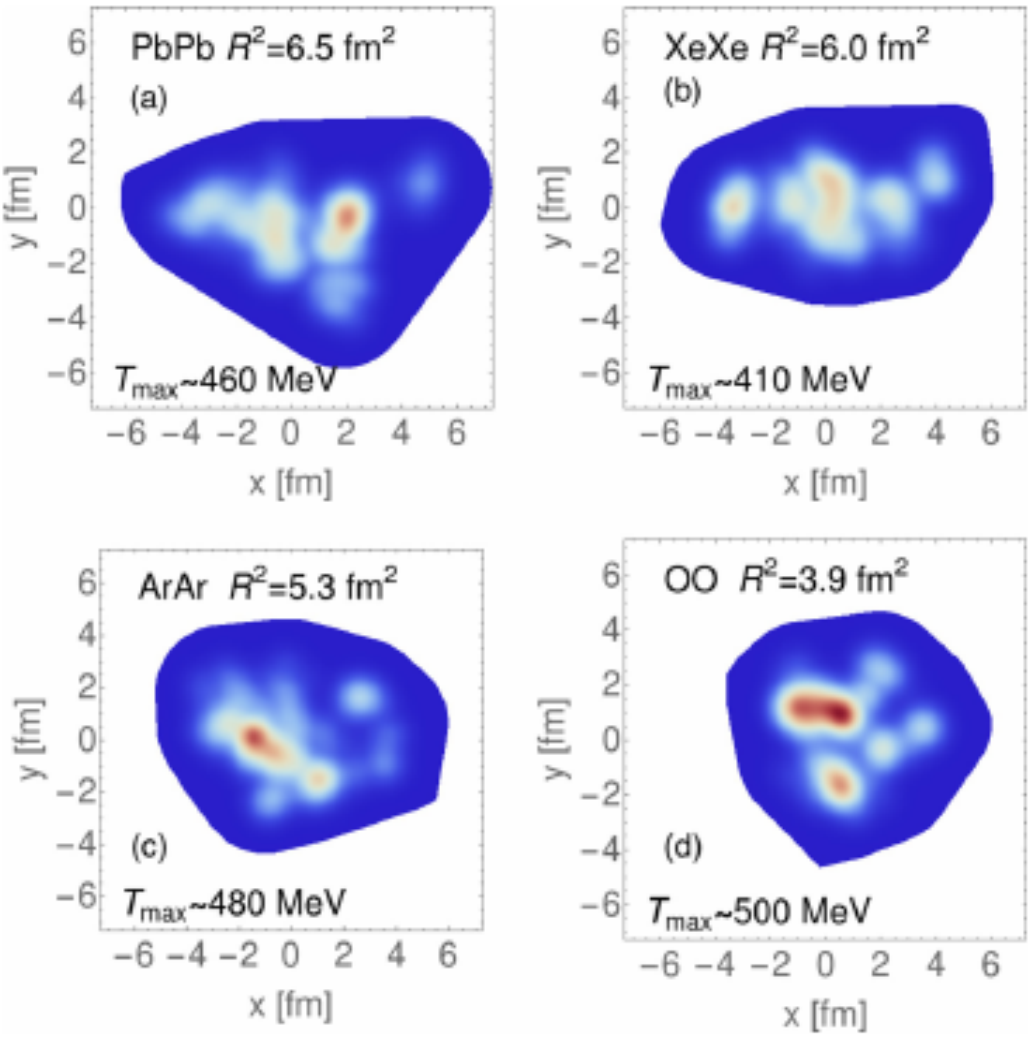

Figure 6 – Entropy density plots of four example initial conditions TRENTO. Red (light gray) indicates the largest entropy densities and blue (dark gray) indicates less entropy density. This figure was taken from (7).

Chapter

4 Heavy Quark in QGP

When we have the creation of heavy quarks inside of QGP, they interact with the medium before generating particles observed in the detector. The study of QGP has one of the main observables that give information about nuclear effects are the nuclear modification factor called R_{AA}. The R_{AA} is a measurement of the suppression factor experienced by particles inside the QGP and it is defined as the ratio between the pT spectra of the particles of interest (in this case, the heavy mesons B_0 and D_0 or leptons produced from these mesons via semi-leptonic decays), with a normalization factor N defined in terms of the number of binary collisions (97). The suppression or enhancement ($R_{AA} > 1$ or $R_{AA} < 1$) represent connections with nuclear effects from QGP.

$$R_{AA} = \frac{1}{N} \frac{dN_{AA}/dp_T}{dN_{pp}/dp_T} \tag{4.1}$$

In addition to the surprising reality that the nuclear modification factor gives us information about QGP, we can get some properties, like collective behavior between particles inside the medium. When we see the plot in Fig. 7, the experimental data can show how many models we have in the literature and how they can make representation for the data. In this work we oversample the number of heavy quarks for each hydrodynamic background, we are able to reconstruct the entire R_{AA} for each event.

The Fig. 7 represents the R_{AA} for mid-central collsions$30 - 50\%$ from D mesons. These data are compared with different theoretical predictions for this observable. However, we can observe that, although these predictions seem to describe the general behavior of the data, there are divergences in the description of R_{AA} and v_2[1] that make transport models have difficulty. For instance, the POWLANG-HTL predictions for the R_{AA} seem to describe well the result while v_2 predictions underestimate the suppression. This problem involving

[1] v_2 is the azimuthal anisotropy usually defined as an expansion of a fourier series. The section 4.4 will explain with more details about it.

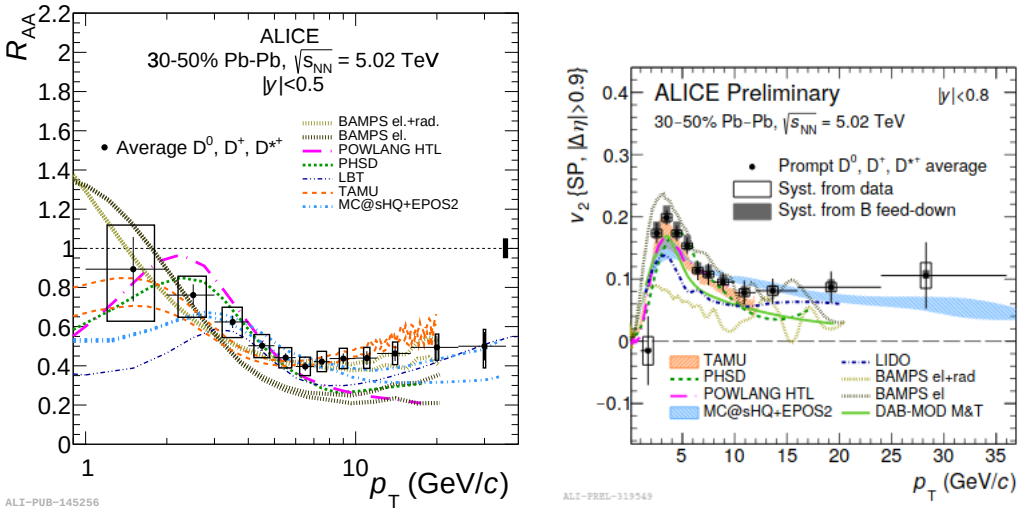

Figure 7 – Experimental measurements in PbPb collisions at $\sqrt{s_{NN}} = 5.02$TeV. Average non-strange D-meson R_{AA} in the $30-50\%$ centrality class (left) and elliptic flow v_2 in the $30-50\%$ centrality class (right) measured in Pb–Pb collisions at $\sqrt{s_{NN}} = 5.02$ TeV, compared with the Transport models (8, 9, 10, 11, 12, 13, 14, 15).

the R_{AA} and v_2 has been around for a fairly long time (100, 101). In the literature, several ingredients influence these results, such as the fluctuations of the initial conditions for the quark gluon plasma, the heavy quarks energy loss mechanisms inside the medium and the interactions among themselves. Moreover, different evaluations of the same observables may lead to different biases that could harm the correct description of these data, as is the case when analyzing some observable that is not sensitive to the initial conditions fluctuations, for instance.

In this chapter, the interactions of the heavy quarks inside the QGP is discussed, since its initial production until the decays to electrons. Also, the flow harmonics analysis is described for different approaches in order to obtain an estimation method that leads to unbiased results.

4.1 Heavy Quark Production

In the previous chapters and sections, the heavy quarks created inside the QGP are not directly accessible and so what is measured in the experiments are heavy mesons and light particles created from the heavy quarks. This being the current reality, you should add these limits to the study of heavy quarks. The final cross-section σ obtained is therefore defined as the convolution of the different stages of the evolution of the system:

$$E\frac{d^3\sigma}{dp^3} = E_1\frac{d^3\sigma}{dp_i^3} \otimes P(E_1 \to E_f) \otimes P(Q \to H_Q) \otimes P(H_Q \to e^{\pm}), \tag{4.2}$$

in which the initial cross-section of the heavy quark Q is convoluted with the energy loss, the hadronization, and finally the decay into the semi-leptonic channel. This equation assumes the validity of the factorization property of the QCD and allows for a separate study of each aspect of the collision.

To understand how the heavy quarks are created inside the plasma, one of the conditions is that their masses are greater than the QCD scale Λ_{QCD} in the Eq. 1.3. As mentioned earlier the cross-section is calculable as a perturbation series in the QCD running coupling α, evaluated at the mass of the heavy quark m. The Fig. 8 and 9 show schematically the leading order and some of the next-to-leading order Feynman diagrams of heavy flavor production in nucleus+nucleus collisions. For this production process for heavy flavor, there is the inclusion of the gluon fusion, pair annihilation and further corrections such as pair creation with gluon emission.

It is important to note that for this approach the Next-to-leading order calculations (NLO) (102) fail at high p_T,i.e. $p_T >> m$ due to large logarithms of the ratio $\frac{p_T}{m}$. In view of this situation arises all orders in the perturbative expansion. Those logarithms for the inclusive transverse momentum distribution can be classified into $\alpha_s^2[\alpha_s log(p_T/m)]^k$ and $\alpha_s^3[\alpha_s log(p_T/m)]^k$, respectively leading- logarithmic order (LL) and next-to-leading-logarithmic order (NLL). Both approaches have been tested to deal with this problem (103, 104), but both cases led to different problems at different p_T intervals. Subsequently, calculations proposed that the merged both approaches in order to obtain all the terms of order α^2 and α^3 exactly, including mass effects and also all the logarithmic terms (105, 106).

The fixed-order NLO calculation leads to:

$$\frac{d^2\sigma^{NLO}}{dp_T^2} = A(m)\alpha_s^2 + B(m)\alpha_s^3 + \mathcal{O}(\alpha_s^4), \tag{4.3}$$

.

To the NNL calculation is given by:

$$\begin{aligned}\frac{d^2\sigma^{NLL}}{dp_T^2} = \alpha_s^2 \sum_{i=0}^{\infty} a_i(\alpha_s log\frac{\mu}{m})^i + \\ \alpha_s^3 \sum_{i=0}^{\infty} b_i(\alpha_s log\frac{\mu}{m})^i + \\ \mathcal{O}[\alpha_4(\alpha_s log\frac{\mu}{m})^i] + \mathcal{O}(\alpha_s^2 \times PST),\end{aligned} \tag{4.4}$$

in which PST are suppressed terms at high p_T by powers of m/p_T, momentum, the dependency on the collision energy and scale μ have not been made explicitly.

Combine the result of the Eq. 4.3 and 4.4 we will have the following result:

$$\begin{aligned}\frac{d^2\sigma^{NLO}}{dp_T^2} &= A(m)\alpha_s^2 + B(m)\alpha_s^3 + \\ [\alpha_s^2\sum_{i=0}^{\infty} a_i(\alpha_s log\frac{\mu}{m})^i + \alpha_s^3\sum_{i=0}^{\infty} b_i(\alpha_s log\frac{\mu}{m})^i] &\times G(m,p_T) + \\ \mathcal{O}[\alpha_s^4(\alpha_s log\frac{\mu}{m})^i] &+ \mathcal{O}(\alpha_s^4 \times PST),\end{aligned} \tag{4.5}$$

in which $G(m, p_T)$ is an arbitrary function that must approach unity in the limit $m/p_T \to 0$. This term is given by:

$$G(m,p_T) = \frac{p_T^2}{p_T^2 + c^2m^2} \tag{4.6}$$

For evaluate the cross-section of heavy quarks, the fixed-order FO part of the computation needs to have its renormalization scheme changed to the same idea used by the NLL calculations. The result of this step led to an exact match between two coefficients of both terms, up to order α_s^3. These terms follow as:

$$\frac{d^2\sigma^{FOM0}}{dp_T^2} = a_0\alpha_s^2 + (a_1 log\frac{\mu}{m} + b_0)\alpha_s^3 + \mathcal{O}(\alpha_s^2 \times PST). \tag{4.7}$$

After this, FONLL can be written as:

$$FONLL = FO + (NLL - FOM0) \times G(m,p_T). \tag{4.8}$$

There are significant problems for the Eq. 4.8, particularly FOM0, which are corrected by analyzing the transverse mass $m_T = \sqrt{p_T^2 + m^2}$ and mass. You can view the analysis at (105). The $G(m, p_T)$ function has to be chosen to suppress the correction $(NLL - FOM0)$ in that case.

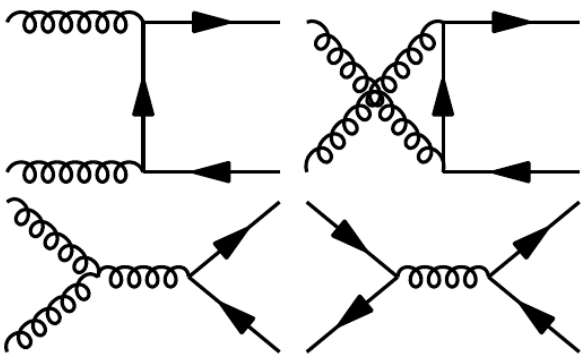

Figure 8 – Leading order Feynman diagrams of heavy flavor production mechanisms in nuclei collisions.

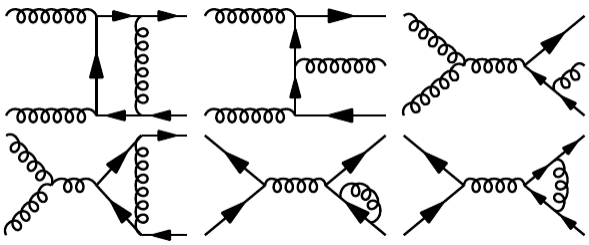

Figure 9 – Example of the Next-to-Leading order Feynman diagrams of heavy flavour production mechanisms in nuclei collisions.

4.2 Energy Loss

There are two main mechanisms of energy loss of heavy quarks in the Plasma of quarks and Gluons and this mechanism can be done by collisions, related to the loss of energy due to quasi-elastic scattering or by radiative loss, being this mechanism due to gluonic radiation (107). Once the two mechanisms have been established in the study of the QGP, the comparison with the data in the intermediate p_T regimes is better represented. It is observed for high p_T the dominance of energy loss by radiation. On the other hand, it is observed the elastic scattering dominance in low p_T and radiative scattering. These types of behaviors can be observed in Fig. 10.

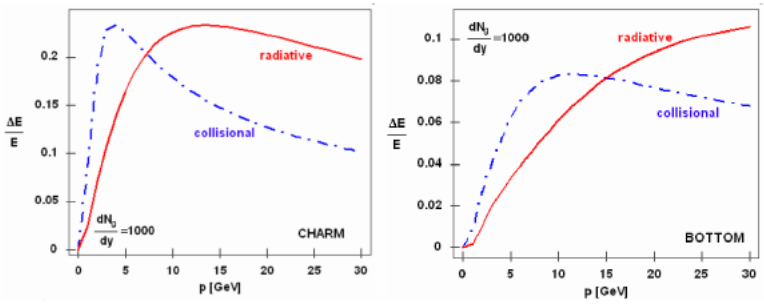

Figure 10 – Comparison between elastic scattering and gluon radiation induced energy loss for heavy quarks charm (left) and bottom (right)(16)

During their propagation through a thermalized QCD matter, heavy quarks lose energy via both quasi-elastic scatterings with light patrons in the medium and gluon radiation induced by multiple scatterings. In this work, we utilize the following modified Langevin equation. We can describe this time evolution of energy and momentum as:

$$\frac{d\vec{p}}{dt} = -\eta_D(p)\vec{p} + \vec{\xi} \tag{4.9}$$

with η_D the momentum drag coefficient and the stochastic term $\xi(t)$ that delivers random momentum "kicks" uncorrelated in time, given by:

$$\langle \xi_i(t)\xi_j(t')\rangle = \kappa\delta_{ij}\delta(t-t'), \tag{4.10}$$

in which 3κ is the mean-squared momentum transfer per unit time (108).

For a thermal heavy quark of mass $m \gg T$ and typical momentum $p \approx \sqrt{mT}$, the stochastic solution of equation **??** leads to:

$$\langle p^2 \rangle = 3mT = \frac{3\kappa}{2\eta_D} \Rightarrow \eta_D = \frac{\kappa}{2mT} \tag{4.11}$$

and the diffusion constant in space is obtained as (108):

$$D = \frac{T}{m\eta_D} = \frac{2T^2}{\kappa} \tag{4.12}$$

subject to the determination of κ. The leading-order calculation can show that the momentum loss per time is very similar to the one obtained with a constant momentum drag coefficient leading to

$$\frac{dp}{dt} \propto p \tag{4.13}$$

Assuming the diffusion coefficients to be isotropic and the momentum space diffusion coefficient k to be independent of the heavy quark momentum p, one can write the relativistic Langevin equation as:

$$dx_i = \frac{p_i}{E} dt \tag{4.14}$$

$$dp_i = -\Gamma(p) p_i dt + \sqrt{dt}\sqrt{k}\rho, \tag{4.15}$$

in which the index $i = x, y$ corresponds to transverse plane coordinates, ρ is the fluctuating force described classically by white noise in a Markovian process, and Γ is the drag coefficient.

For this work, it was necessary to perform Lorentz boosts between the local rest frame of the moving medium (in which the heavy quark interacts) and the global laboratory frame (where it propagates). After the boost of the heavy quark 4−momentum, p_i can be written as:

$$p_i = p'_i - \Gamma(p) p'_i dt + \sqrt{\Delta t'}\sqrt{k}\rho, \tag{4.16}$$

in which the time $\Delta t'$ in the local rest frame of the medium is given by:

$$\Delta t' = \Delta t \frac{p^\mu v_\mu^{flow}}{E} = \Delta t^\gamma [1 - \frac{||p||||v_{flow}||}{E} cos(\varphi_Q - \varphi_{flow})], \tag{4.17}$$

in which $v^{flow} = (\gamma, \gamma \mathbf{v_{flow}})$, δt is associated with the time step in the global frame, and $\gamma = \sqrt{1 - \mathbf{v_{flow}}^2}$ is the Lorentz factor. The boost of the heavy quark 4-momentum back to the global frame and so the propagation is evaluated in the transverse plane via:

$$x_i(t + \Delta t) = x_i(t) + \frac{p_i}{E}\Delta t. \tag{4.18}$$

This operation is repeated until reaching the hadronization temperature.

For this work, we use two diffusion coefficients. The first parameter is denoted by "k_{MT}". This parameter is inspired by Moore e Teaney (109). In this model, the spatial diffusion coefficient is:

$$D = f_{MT}/2\pi T. \tag{4.19}$$

The second parametrization in this work is denoted by GA. This model is based on a running coupling constant and an optimized hard thermal loop correction of the gluon propagator (110). To obtain a tunable parameter we multiply the drag "A_{GA}" by a k_{GA}. The result is:

$$\Gamma_{GA} = k_{GA} \cdot A_{GA} \tag{4.20}$$

We have also in literature other models, like Boltzman equation used by other groups that study hadronization(111). This models, within a common scheme devised for understanding nuclear factor modification, could be a powerful tool to increase the knowledge about the hadronization. The Linear Boltzmann Transport (LBT) model has been developed by the CCNU-LBNL (112), for example. They use this equation:

$$p_1^\mu \partial_\mu f(x_1, p_1) = E_1(C_{el} + C_{inel}), \tag{4.21}$$

in which C_{el} and C_{inel} are collision integrals for elastic and inelastic scatterings.

An interesting conclusion for multiple scatterings in the QGP is that we can describe it as Brownian motion.(113) which will lead to the Fokker-Planck equation:

$$\frac{\partial}{\partial t} = \frac{\partial}{\partial p_i}[\tau^{FP} D] + \tau^{FP} \left(\frac{\partial}{\partial p}\right)^2 D, \tag{4.22}$$

in which D is the distribution due to the motion of the particles , p is the initial momentum of the particle and the transport coefficients are given by:

$$\tau_{FP} = p_i A, \tag{4.23}$$

$$\tau_2^{FP} = B_0, \tag{4.24}$$

The Fokker-Planck equation can be also be obtained from a discretization of the Langevin equation (108).

Langevin approaches for the computation of collisional energy loss of the heavy quarks have successfully described experimental data in a low transverse momentum regime. In this case, the gluon emission is reduced and thus, radiative energy loss becomes useless. Otherwise, it is generally assumed that radiative energy loss will dominate the evolution of the heavy quarks at higher momentum. Moore and Teaney (108) argue that, even then, elastic scattering is the dominant energy loss mechanism. There are many other different models based on the Langevin approach for the collisional energy loss mechanism (114, 115, 116, 117, 118, 119).

One can add a new term to the Langevin equation in order to include radiative energy loss of the heavy quarks. The new Langevin equation can then be written as:

$$\frac{dp_i}{dt} = \xi_i(t) - \eta_D p_i + (f_g), \tag{4.25}$$

in which $f_g = dp_g/d_t$ is the recoil force experienced by the heavy quarks from the medium-induced gluon radiation due to gluon momentum p_g. The p_g term is obtained from a gluon distribution function. This function leads to the probability of gluon radiation from a heavy quark. There is a possible model to this goal given by the higher-twist calculations (72, 120, 121)

$$\frac{dN_g}{dxdk^2dt} = \frac{2\alpha_s P(x)\hat{q}}{\pi k_\perp^4} sin^2(\frac{t-t_i}{2\tau_f})(\frac{k_\perp^2}{k_\perp^2 + x^2m^2}), \tag{4.26}$$

in which $P(x)$ is the gluon splitting function, τ_f is the gluon formation time, m is the heavy quark , x is the fractional energy taken by the emitted gluon from the heavy quark, and the $k_\perp^2$ gluon transverse momentum. Recently in the literature, work was launched in which the comparison of the Langevin energy loss model with Gluon radiation indicates a strong correlation between decoupling temperature (122).

The dead cone effect (123, 124) is based in the last term of the Eq. 4.26.

The gluon transport coefficient $\hat{q}$ in Eq. 4.26 and 4.25 can be obtained from the quark diffusion coefficient (72):

$$\hat{q} = \frac{2\kappa C_A}{C_F} \tag{4.27}$$

4.3 Hadronization and particle decay

Once the quarks are created in the guark-gluon plasma, and the interaction is carried out during the process of hydrodynamic expansion, the medium undergoes a phase transition from the QGP to the hadronic matter. Once there is a need to understand this hadronization process, as the knowledge about such mechanisms remains without complete understanding. The mechanisms that are candidates for this hadronization mechanism are the fragmentation of partons and the coalescence of quarks. The coalescence help to improve low p_T while the fragmentation is the most used at high p_T. In this scenario, a single parton has a given probability of the parton probability of fragmentation or coalescence.

In this work, we implement two methods, the fragmentation and the coalescence. We do not consider the possible interactions between the produced heavy mesons, and the hadronic gas (125).

The approach used is The Peterson fragmentation function (126). This common approach is to parametrize the fragmentation function disregarding the dynamics of the processes. Some of the most common models are Kartvelishvili (127).

To perform the fragmentation the definition of the Peterson function is:

$$f(z) = \frac{1}{z(1 - 1/z - \epsilon_Q/(1-z))^2}, \tag{4.28}$$

in which $\epsilon \approx m_q^2/m_H^2$ is the ratio between the quark mass an the hadron mass. The z is defined as the ratio between the hadron and the originating quark energy and longitudinal moment:

$$z = \frac{E^{meson} + p_l^{meson}}{E^{quark} + p_l^{quark}}, \tag{4.29}$$

in which E is the energy and p the momentum. However, this variable is not experimentally accessible (128) and thus should be converted to:

$$z = x : \frac{\sqrt{x_E^2 - x_{min}^2}}{\sqrt{1 - x_{min}^2}} \tag{4.30}$$

in which $x_{min} = 2m_H/\sqrt{s}$, with $\sqrt{s}$ being the center of mass energy and $x_E := 2E_H/\sqrt{s}$.

In this work, the Peterson function parameters ϵ_c and ϵ_b are chosen such as to reproduce D^0 and B^0 meson FONLL spectra in pp collisions and include the energy loss parametrization between the heavy quark production and hadronization. The heavy mesons decay into the semi-leptonic channels is the final result of the system's evolution that is analyzed.

The next section is the review of the azimuthal anisotropy analysis procedures, which consists of one of the most important tools to the study of the QGP.

4.4 Azimuthal anisotropy

For collision analysis, the azimuthal anisotropy of particles is widely used as a tool to understand the Heavy Ion Collision. Basically, the initial anisotropic spatial distribution of particles that form the QGP, coupled with the nearly perfect liquid behavior of the plasma (medium), creates pressure gradients that transfer this anisotropy to the momentum space in the final state. The existence of this observable means that there is evidence of the behavior of the plasma (129, 130). This observable has a relationship with the contribution of initial state fluctuations. These fluctuations generate all Fourier flow harmonics in each event.

The azimuthal distribution is usually defined as an expansion of a fourier series:

$$E\frac{d^3N}{dp^3} = \frac{1}{2\pi}\frac{d^2N}{p_T dp_T dy}(1 + \sum_{n=1}^{\infty} 2v_n cos[n(\varphi - \Phi_R)]), \tag{4.31}$$

in which φ is the azimuthal angle and Φ_R is defined as the reaction plane angle.

Basically, the azimuthal analysis is the measurement of the values of v_n harmonics coefficients. From the establishment of the collision geometry the symmetry planes will have a direct relationship with the reaction plane by Φ_R, however, with fluctuations in the spatial distribution of the particles, the angle Φ_R can have a different direction that the expected reaction plane. These are called the participant planes and are differently related to each of the Fourier n-harmonics.

There are methods to calculate the participant plane Φ_n. One of the methods that aim at accomplishing that is the event-plane method. The event-plane angle Ψ_n is defined as the angle of symmetry of the particle azimuthal distribution in the transverse plane. One can define as (131, 132, 133, 134):

$$\Psi_n = \frac{1}{n}\arctan\frac{Q_{n,y}}{Q_{n,x}}, \tag{4.32}$$

in which the flow vector in the harmonic n is defined as:

$$Q_n = \begin{pmatrix} |Q_n|cos(n\Psi_n) \\ |Q_n|sin(n\Psi_n) \end{pmatrix} = \frac{1}{N}\sum_{j=1}^{N}\begin{pmatrix} cos(n\varphi_j) \\ sin(n\varphi_j) \end{pmatrix}, \tag{4.33}$$

for each azimuth angle being traversed for N particles added. It is worth noting that it is essentially a one-particle probability distribution analysis. Because of that, the

distribution may differ from the participant plane angle, being highly dependent on the number of particles used to generate the distribution. To obtain the harmonic value v_n using the event plane method, the event plane resolution is used. This approach leads us to (131, 132, 133, 134):

$$v_n = \frac{\langle cos[n(\varphi - \Psi_n)]\rangle}{\langle cos[n(\varphi - \Phi_n)]\rangle}, \tag{4.34}$$

where the denominator represents the resolution correction. This denominator is obtained, for instance, via sub-event method (131).

There is also the scalar product method that weights the event averages using $|Q_n|$ (135):

$$v_n = \frac{\langle |Q_n| cos[n(\varphi - \Psi_n)]\rangle}{\langle cos[n(\varphi - \Phi_n)]\rangle}, \tag{4.35}$$

where the denominator represents the resolution correction. This approach leads to an unambiguous estimation of the flow harmonics:

$$v_n \{SP\} = \sqrt{\langle v_n^2 \rangle}. \tag{4.36}$$

There is also an equivalent method to the scalar product that provides us with an unambiguous estimation of the second moment of the distribution, which is the 2-particle correlation (132). Moreover, by increasing the number of correlated particles (2,4,6,8,..), one can obtain unambiguous measurements of the even moments of the distribution $\sqrt{\langle v_n^{2k} \rangle}$. Let us redefine the flow vector from the Eq. 4.33 as a complex number[2]. Otherwise, the flow vector is like in the Eq. 4.37:

$$Q_n \rightarrow Q_n = e^{in\varphi} \tag{4.37}$$

$$V_n \rightarrow V_n = V_n e^{in\varphi} \tag{4.38}$$

in which φ is the azimuthal angle of a given particle. However, in the hard sector we are considering the particle of interest from separate p_T bins so a p_T dependence appears as (132, 134):

$$V_n(p_T) \rightarrow V_n = V_n(p_T) e^{in\varphi} \tag{4.39}$$

[2] Here we use the same notation as in (132, 134).

This approach leads to a p_T dependent two particle correlation that uses the complex conjugate to produce a real valued result as:

$$ReV_nV_n^*(p_T) = v_n v_n(p_T) cos[n(\psi_n - \psi_n(p_T))]. \tag{4.40}$$

For instance, if we consider the typical 2-particle correlations by taking one hard and one soft particle and the 4-particle correlation by taking 1 hard particle and 3 soft particles that are averaged over events within a fixed centrality window. They are defined by:

$$v_n\{2\}(p_T) = \frac{d_n\{2\}(p_T)}{c_n\{2\}^{1/2}} \tag{4.41}$$

$$v_n\{4\}(p_T) = \frac{d_n\{4\}(p_T)}{-c_n\{4\}^{3/4}} \tag{4.42}$$

in which:

$$d_n\{2\}(p_T) = \langle\langle V_n V_n^*(p_T)\rangle_j\rangle \tag{4.43}$$

$$c_{n,j}\{2\}(p_T) = \langle\langle V_n V_n^*\rangle_j\rangle \tag{4.44}$$

Here, the outer bracket $\langle ...\rangle$ is an artifact of centrality rebinning where in experiments finer centrality bins are taken e.g. 0.5% centralities or other, which we indicate as j, that are then recombined using multiplicity weighing in a wider centrality bin of a width of 10%, for instance. The inner brackets indicate averaging over the events within the j^{th} fine centrality bin.

There exists a couple of methods to calculate cumulants. The direct cumulants (136, 137) leads to non-biased cumulants due to interference between harmonics. The average (m particle) azimuthal correlations for a single event:

$$\langle\langle 2\rangle\rangle := \langle\langle e^{in(\varphi_1-\varphi_2)}\rangle\rangle := \frac{1}{A_{M,2}}{\sum_{i,j}}' e^{in(\varphi_i-\varphi_j)}. \tag{4.45}$$

in which $A_{n,m} = n!/(n-m)!$ and the primed sum symbol indicates that the indexes must all be taken differently.

The m-particle correlator is then defined as the average over all the events of the azimuthal correlations:

$$\langle\langle m\rangle\rangle := \frac{\sum_{ev} W_{\langle\langle m\rangle\rangle}\langle m\rangle}{\sum_{ev} W_{\langle m\rangle}} \tag{4.46}$$

in which the weights $W_{\langle\langle m\rangle\rangle}$ are used to minimize the bias due to multiplicity variations in the set of events used to estimate the m-particle correlations. $W_{\langle\langle m\rangle\rangle}$ is defined as:

$$W_{\langle\langle m\rangle\rangle} = \frac{\sum_{ev} M a_m^p}{\sum_{ev} M}, \tag{4.47}$$

which M is (p-1) and p is the number of events and a_m is related to v_n.

The unbiased coefficients of the m-particle cumulants are written as:

$$c_n\{2\} = \langle\langle 2\rangle\rangle, \tag{4.48}$$

$$c_n\{4\} = \langle\langle 4\rangle\rangle - 2\langle\langle 2\rangle\rangle^2 \tag{4.49}$$

One can define the differential cumulants by changing one of the correlating particles with the particle of interest (138):

$$d_n\{2\} = \langle\langle 2'\rangle\rangle \tag{4.50}$$

$$d_n\{4\} = \langle\langle 4'\rangle\rangle - 2\langle\langle 2\rangle\rangle\langle\langle 2'\rangle\rangle \tag{4.51}$$

in which the primes indicate the substitution. The correlation between two particles leads to the same average result in Eq. 4.45.

For this work, we used the cumulant calculation method to measure contributions from $v_n\{n\}$ and compare them with the data available in the literature.

Chapter

5 Heavy quarks evolution in an event-by-event expanding QGP

After all previous chapters, which were presented theoretical frameworks to study the evolution of quarks inside the quark gluon plasma and study of small systems, (THE-STATE-OF-ART) simulation framework DaBMod (D and B mesons Modular framework) (139, 140, 141). The heavy flavor sector is described using this program. This program has been developed using $C++$ programming language with the aid of ROOT (142) and Pythia8 (143) libraries. DabMod consists of a Monte-Carlo simulation of heavy quarks transversing an expanding hot quark gluon plasma in which they interact through an energy loss model. The final spectra obtained from the simulation is then used to evaluate different observables on an event-by-event approach, such as the nuclear modification factor and the azimuthal anisotropy. The Analysis could be done through the results of the simulation. All the simulation has been built with a modular feature, taking for granted the QCD factorization. The purpose of this method is to enable the easy selection of different models for each stage of the system's evolution, such as the energy loss, medium backgrounds, or hadronization processes, so one can analyze, investigate separately the effects of each one of those stages on the final results. Once the program is executed, the event-by-event analysis is implemented in the code so that each simulated event is chosen independently of another possible event. A High-Performance-Computing(HPC) cluster is then used to simulate all desired events in the code, directly using the parallelization of the program execution. This step generates intermediate results. From the construction of these results is performed analyses in which all events are combined in order to conceive final results. In this work, the SAMPA cluster of the High Energy Physics Instrumentation Center (HEPIC), located in the city of São Paulo, University of São Paulo, was used to perform all the simulations. For these bottom and charm simulations are sampled within a mid-rapidity transverse plane of the QGP medium with an initial time τ_0 with initial momentum given by the calculations provided by pQCD. The hydrodynamic evolution of

the background of the medium is performed independently of the evolution of the heavy quarks, therefore, no effect from probes on the medium are considered. In this structure, each sampled heavy quark travels along the transverse plane with velocity v and a constant direction φ_{quark} and loses energy utilizing some parametrization of dE/dx. Once the heavy quarks reach a certain position (x, y) in which the temperature of the medium is below a chosen decoupling temperature T_d, the quarks undergo a hadronization process leading to heavy mesons B^0 and D^0, which in turn decay into electrons and positrons. Information about this process can be accessed. Heavy quarks positions and p_T spectra are stored in order to obtain the desired observables meant for study. For this process, the execution setup is fixed with some parameters using available data from the Particle Data Group (34). Those parameters are presented in Tab. 2.

Tab. 2 – Constant values used on all executions of the simulation

Name	Symbol	Value
Bottom mass	m_b	$4.18GeV$
B^0	m_B	5.27 GeV
Charm mass	m_c	1.275 GeV
D^0	m_D	1.86 GeV
Electron mass	m_c	5.109 KeV

This chapter presents the details on how each stage of the system's evolutions is evaluated.

5.1 Initial Conditions

The First part of the setup system evolution, the initial conditions have the purpose in the simulation to serve as a starting point for the hydrodynamic evolution of the plasma and also setting up the spatial distribution of the sampled heavy quarks that traverse the medium. DABMOD could be changed for two different initial conditions. In this work the results are collected from the MCKLN (144, 145, 146), based on the CGC formalism and TRENTO (4) initial condition.

In order to run the simulation, the event LHC (PbPb) with energy $\sqrt{s_{NN}} = 5.02$TeV have been selected for centralities in the range of $0 - 50\%$. We will also use Wood-Saxon theories to predict outcomes for the following systems: Ar^{42}, and O^{16}. These systems will be used respectively with $\sqrt{s_{NN}} = 5.85$TeV, and $\sqrt{s_{NN}} = 6.02$TeV. The Xe^{129} with $\sqrt{s_{NN}} = 5.44$TeV system will also be used in this study. The configurations of this system were used based on the work of the ALICE, LHC experiment. The centrality selection has been set up to be selected using the average number of participants for each event $\langle N_{part} \rangle$ and the events have been binned using 1%-wide centrality classes. We will use small bins centralities for our results to perform the event-by-event analyzes with the results of the literature. Since the event profiles are constructed and separated

by centralities, they are selected for the evolution of the system. In order to obtain the results of significant observables for comparison with data in the literature, event-by-event analyzes are necessary for the most accurate measurements possible, however, certain heavy quarks are only produced in a few events. For this analysis to be statistically reasonable for the results, the heavy quarks measurements must be obtained through oversampled. These events (Profiles) can then be classified by geometrical resembling and events in the same class can be treated as the same. Thus, event-by-event in this circumstance should not be regarded as a single real one but rather a grouping of possible distributions. The results obtained from the simulation are then probabilities and the oversampling works like an apparatus in order to evaluate these probabilities. For the results obtained from the simulations of this work, data with 1×10^7 heavy quarks have been sampled for the R_{AA} and the same for the measurements of v_n. The plots in Fig. 11 and 12 show examples of initial conditions energy distributions for Pb+Pb,Xe+Xe,Ar+Ar, and O+O with energies of $\sqrt{s_{NN}} = 5.02$TeV, $\sqrt{s_{NN}} = 5.44$TeV, $\sqrt{s_{NN}} = 5.85$TeV, and $\sqrt{s_{NN}} = 6.02$TeV respectively. They present examples of the starting and ending positions of heavy quarks inside QGP. The parameters of the initial condition are setup with $p = 0$, $k = 1.6$, and $\sigma = 0.51$ according to the Bayesian analysis (147). This method estimate the parameters of computationally intensive models.

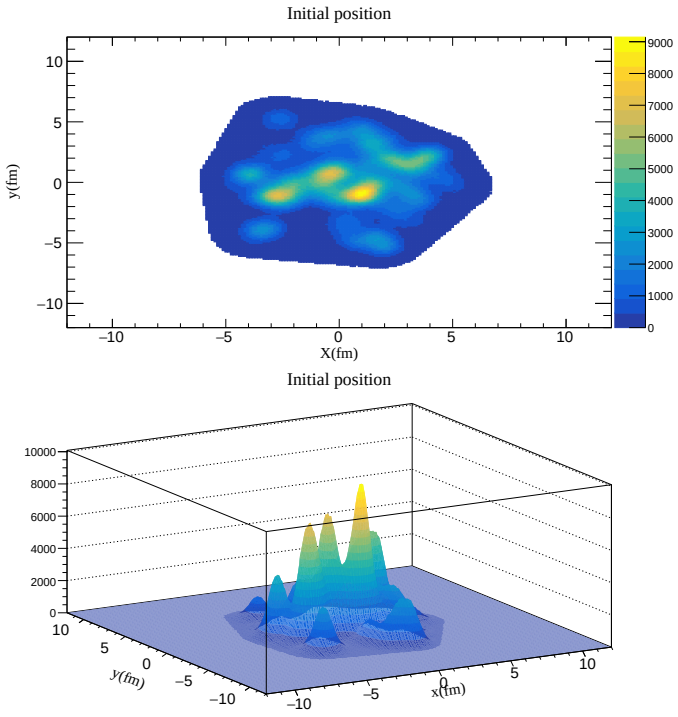

Figure 11 – Profile events showing the initial condition for Pb+Pb collisions (Initial position) in $\sqrt{s_{NN}} = 5.02$TeV. This is one example of this sample. The Initial Condition used is TRENTO. The evolution of the heavy quarks is here obtained via the Langevin equation with the MT parametrization. The z axis use a.u. label

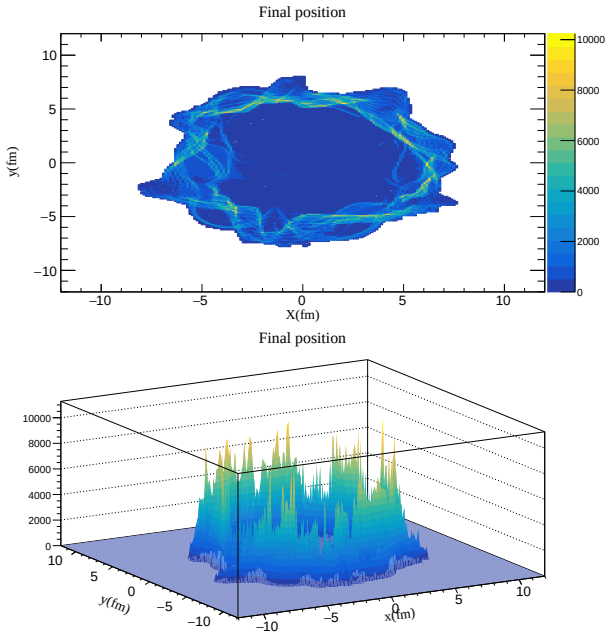

Figure 12 – Profile events showing the initial condition for Pb+Pb collisions (Final position) in $\sqrt{s_{NN}} = 5.02$TeV. This is one example for this sample. The Initial Condition used is TRENTO. The temperature used is $T_d = 160$MeV. The evolution of the heavy quarks is here obtained via the Langevin equation with the MT parametrization. The z axis use a.u. unit.

The construction of the other systems was also carried out using the same Initial Condition.

Once the heavy quarks are sampled within the medium at the initial stage of the simulation they move on to the next stage (evolves) interacting with the hydrodynamical background. We will describe in the next topic how this interaction between the quark and the medium takes place.

5.2 Hydrodynamics

Once the initial condition for studying the QGP is established, we must configure the hydrodynamic stage. In this step, each heavy quark sampled from the initial condition travels along the transverse plane (medium) of an evolving plasma that is obtained from a relativistic hydrodynamic evolution of the initial conditions created by the TRENTO (4) approach, although heavy quark affect the hydrodynamical evolution by medium recoil (148, 149). In this work, the effects associated with medium response are disregarded. The medium acts as a background for the heavy quark probes. The background samples are built on first principles for the heavy quark evolution and are finally stored so that the program simulations can be performed.

The tool used to perform the measurements of the profiles that will be used for

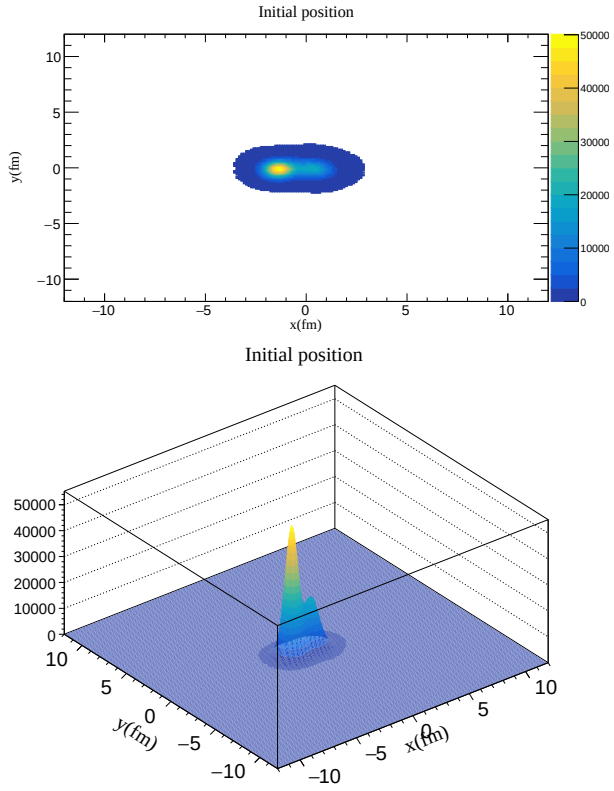

Figure 13 – Profile events showing the initial condition for Ar+Ar collisions in $\sqrt{s_{NN}} = 5.85$TeV. This is one example of this sample. The Initial Condition used is TRENTO. The evolution of the heavy quarks is here obtained via the Langevin equation with the MT parametrization. The z axis use a.u. unit.

the evolution of heavy quarks inside the medium, the event-by-event relativistic viscous hydrodynamical model developed at the University of São Paulo (Viscous Ultrarelativistic Smoothed Particle Hydrodynamics - V-USPHYDRO) (62, 150, 151, 152, 153, 154) is implemented to evolve the TRENTO events and then create the local temperature and medium velocities that are used in the energy loss calculations implemented. This code is implemented using a mesh-free Lagrangian method implementation of the Smoothed Particle Hydrodynamics (SPH) (155, 156, 157, 158, 61, 60) to solve the equations of a 2D+1 relativistic hydrodynamics. This method presents an overall fast computational time compared to different approaches using grid-based computations (159). For this study, it is assumed a boost-invariant longitudinal expansion (160). This means for central rapidity, the system is invariant under Lorentz boosts. The evolution is set up to start at an initial time $\tau_0 = 0.6$fm, with shear viscosity given by $\eta/s = 0.047$. The simulation used the lattice-based equation of state (EOS) s95n-v1 (161) of the Eq. 1.6 and the freeze-out temperature T_{FO} (or just T_d) of the Cooper-Frye (162) was set to vary between $T_d = 150$MeV and $T_d = 160$MeV.

Once the hydrodynamic simulation is finished, this step provides transverse plane profiles over time for the energy density, local temperature, and flow velocity in both $\hat{x}$ and

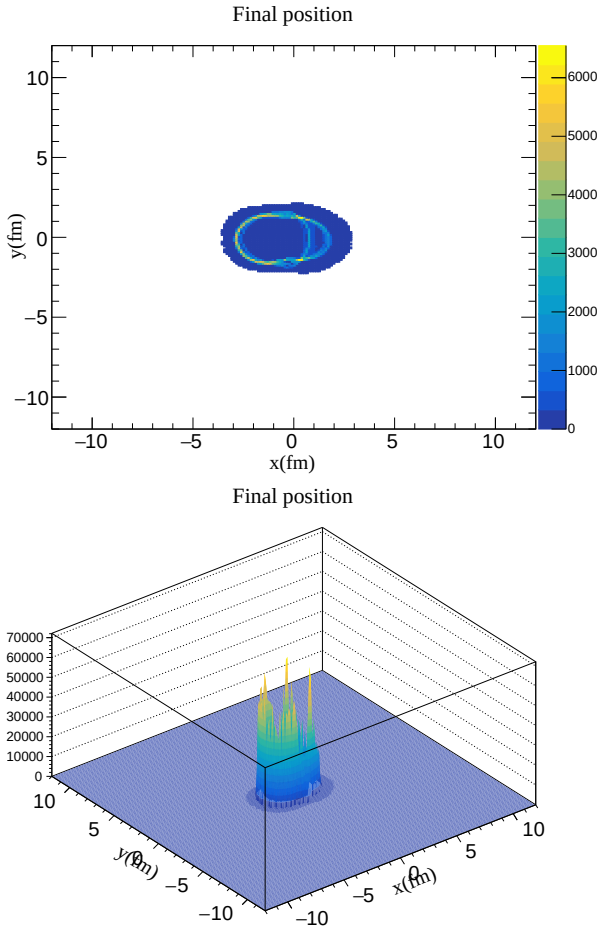

Figure 14 – Profile events showing the initial condition for Ar+Ar collisions in $\sqrt{s_{NN}} =$ 5.85TeV. This is one example for this sample. The Initial Condition used is TRENTO. The temperature used is $T_d = 160$MeV. The evolution of the heavy quarks is here obtained via the Langevin equation with the MT parametrization. The z axis use a.u. unit.

$\hat{y}$ directions. The profiles and quantities are used in DABmod for evaluating the energy loss and making predictions for small systems. Furthermore, from the Cooper-Frye freeze-out, charged soft particle spectra are obtained which are used to obtain the integrated flow harmonic coefficients. Those are later correlated with the heavy flavor sector obtained from DABMOD.

5.3 Heavy quark production (DabMod)

For the representation of the heavy quarks produced at the beginning of collisions in parton scatterings, we chose to work with the description by perturbative QCD (pQCD). In this work, we use to build the initial momentum distribution using First-Order-Next-to-Leading-Logs (FONLL) (105, 106, 163). Currently, this method has improvements for the construction of top quark (164). A momentum probability distribution in the reference

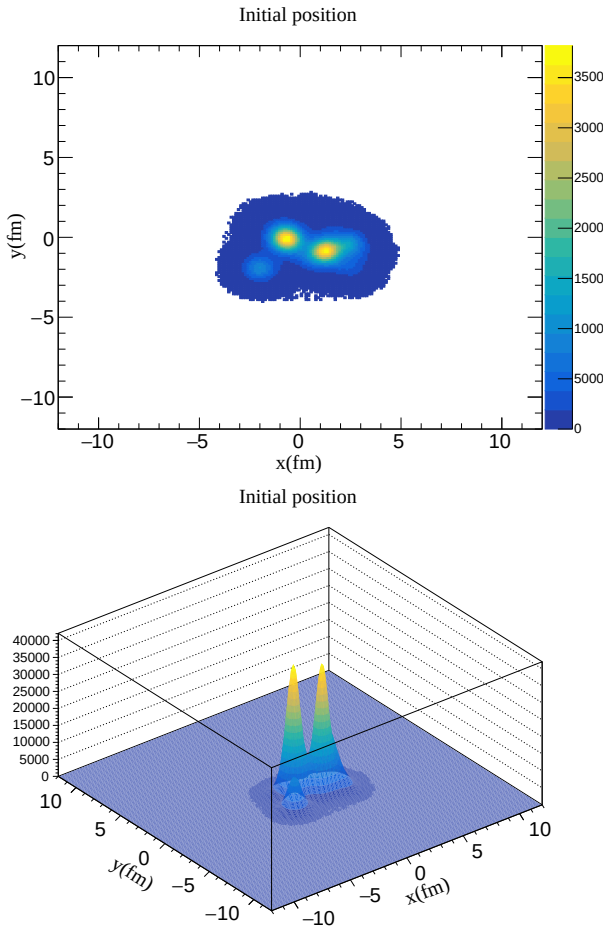

Figure 15 – Profile events showing the initial condition for O+O collisions in $\sqrt{s_{NN}} = 6.02$TeV. This is one example for this sample. The Initial Condition used is TRENTO. The evolution of the heavy quarks is here obtained via the Langevin equation with the MT parametrization. The z axis use a.u. unit.

proton-proton collision is obtained from the cross section, proportional to the invariant yield:

$$E\frac{d^3\sigma}{dp^3} \approx E\frac{d^3N}{dp^3} = E\frac{d^3N}{dp_x p_y p_z}, \tag{5.1}$$

in which E is the energy, p the momentum, and N is the number of partons. The definition of beam axis in the direction $\hat{x}$ and performing a coordinate change of $dp_x = Edy$. For the rapidity y in the same way we can write this way:

$$dp_y dp_z = p_T dp_T d\varphi, \tag{5.2}$$

in which p_T is the transverse momentum and φ is the azimuthal angle, one can rewrite the invariant yield as:

$$E\frac{d^3N}{dp^3} = \frac{d^3N}{p_T dp_T dy d\varphi}. \tag{5.3}$$

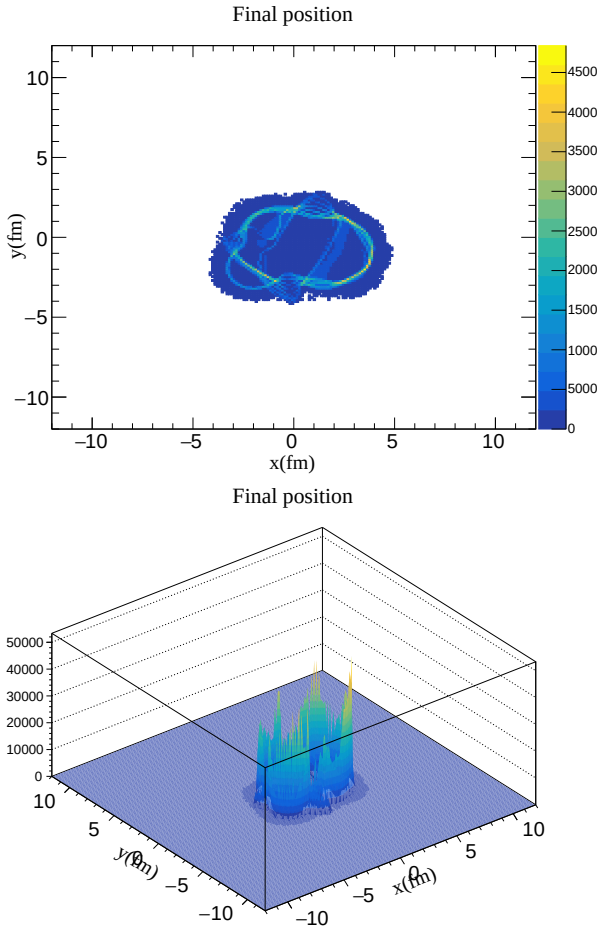

Figure 16 – Profile events showing the initial condition for O+O collisions in $\sqrt{s_{NN}} = 6.02$TeV. This is one example for this sample. The Initial Condition used is TRENTO. The temperature used is $T_d = 160$MeV. The evolution of the heavy quarks is here obtained via the Langevin equation with the MT parametrization. The z axis use a.u. unit.

Moreover, it is assumed isotropic production in the azimuthal direction so the above equation becomes:

$$E\frac{d^3N}{dp^3} = \frac{1}{2\pi}\frac{d^2N}{p_T dp_T dy}. \tag{5.4}$$

The initial azimuthal directions φ of the heavy quark momenta are chosen randomly.

In conclusion, the evolution of the heavy quarks in the simulation is performed in the mid-rapidity regime:

$$E\frac{d^3N}{dp^3} = \frac{1}{2\pi}\frac{d^2N}{p_T dp_T dy}|_{y=0}. \tag{5.5}$$

For this work, this simulation heavy quarks are first set to have initial p_T following a uniform distribution between a defined range$[p_T^{min}, p_T^{max}]$, after this the distribution

histograms are filled using dN/dp_T from Eq. 5.5 as a weighting factor. The motivation for that choice in order to obtain reasonable statistics for the high p_T is necessary for the statistics of some of the observables under study[1]. We largely oversample the number of heavy quarks to $\sim 10^7$ for each hydrodynamic event.

The main motivation for that choice of the proton-proton reference yield is to provide means for evaluating the nuclear modification factor. The definition of R_{AA} in Eq. **??** is a ratio between the differential yields in nucleus-nucleus collisions with respect to proton-proton collisions. This definition is scaled by the nuclear overlap function $\langle T_{AA} \rangle = \frac{\langle N_{col} \rangle}{\sigma^{pp}_{inelastic}}$. Usually, is understood as the R_{AA} the comparison of changes in nuclear collisions with proton-proton collisions. Moreover, the expected value for R_{AA} would equal unity. However, when exploring the overlapping study of events by using FONLL spectra for the heavy quarks the value for R_{AA} can provide valuable information about the QGP. The R_{AA} is evaluated by considering the ratio of spectra after interacting with the medium (Energy loss is the main actor here). This ratio is made concerning the ones without medium interaction. This approach is defined as:

$$R_{AA}(p_T, \varphi) = \frac{(dN((p_T, \varphi)/dp_T))}{dN(p_T)/dp_T}. \tag{5.6}$$

The R_{AA} for both quarks in the simulation is evaluated independently and FONLL distribution itself is used to perform the total contribution by correctly weighting the R_{AA} for each quark, c and b quark.

Once that we include the FONNL in the computations one can not use predictions directly for heavy mesons and electrons come from this process, moreover, these predictions are still used as references for the choice of parameters of the next steps of the simulation. The next text is about hadronization and decay. We will talk about two process main processes involving the Langevin model.

5.4 Hadronization and decay

For the development of the assigned steps to the QGP, it is necessary to establish an uncoupling temperature T_d. When establishing this temperature in the program, The Peterson Fragmentation Function (126) is employed. The low p_T quark coalescence (112, 165, 166) is implemented in the simulation, which is responsible for predictions into the $p_T \leq 10$ GeV range. The Peterson fragmentation function previously defined in 4.3:

$$f(z) = \frac{1}{z(1 - 1/z - \epsilon_Q/(1-z))^2}, \tag{5.7}$$

[1] e.g. multiparticle cumulants.

in which z is defined as the fraction of the heavy quark:

$$z = \frac{E^{meson} + p_l^{meson}}{E^{quark} + p_l^{quark}}, \tag{5.8}$$

For the Eq. 5.8, the `l` indicates the direction of the heavy quark. The p_T can be obtained through:

$$p_T \approx \frac{z^2(E^q + p_T^q)^2 - m^2}{2z(E^q + p_T^q)^2 - m^2} \tag{5.9}$$

The condition established for this approach is the fact that they are both colinear. m is the heavy quark mass. The simulation draws a random value for z assigned to each heavy quark that undergoes fragmentation to perform the Monte Carlo computation of the p_T. In this step, the distributed random value is assigned to The fragmentation and coalescence.

Once the spectra for the heavy mesons have been obtained for heavy quarks, we choose to the mesons are made to decay into the semi-leptonic channels using PYTHIA8 (167) The Pythia implementation is performed after the particle probability results, the heavy mesons, undergo coalescence or fragmentation.

To measure observable values R_{AA}, for instance, two distinct spectra must be evaluated, one which includes the medium interaction and others that the interaction is not present. One is obtained by directly performing the fragmentation on the heavy quarks sampled in the simulation regardless of the local temperature of the medium.

When implementing PYTHIA, an event is associated with the heavy meson with all the kinematical properties obtained from the two hadronization processes. All non-relevant channels are turned off in order to cause all heavy mesons to decay into electrons and positrons. The diagram in Fig. 17 shows the two processes implemented in the simulation in which the values of the heavy quark spectrum are measured to obtain the observables. In this step, the energy loss model interacts with one of these processes. R_{AA} is built for three particles: quarks, mesons, and electrons. This is accomplished through the implementation of energy loss parametrization. To discuss a little about the energy loss model the next section will elucidate the theoretical concepts of this model.

5.5 Energy Loss parametrization

To carry out a study on the dependence of some common variables, we used an energy loss parametrization based on different jet studies (168, 169, 170, 171, 172, 173).

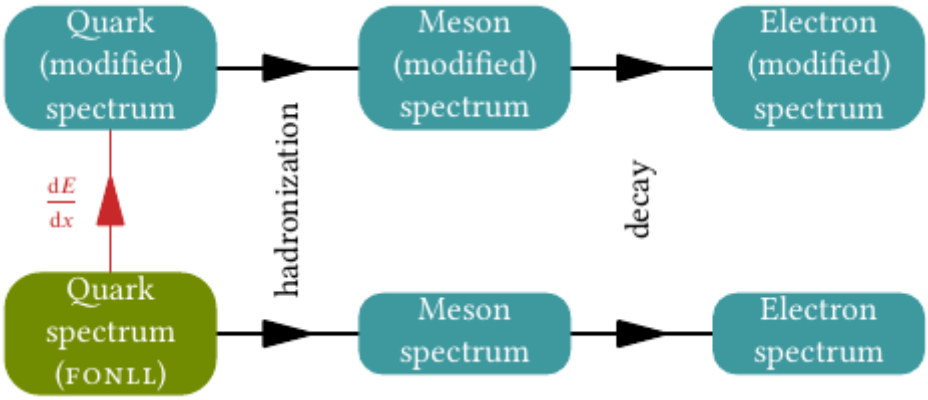

Figure 17 – Map Program flow scheme showing the start point with quark spectrum obtained from FONLL and ramify into two different branches. The lower branch does not include any interaction with the medium and the upper branch includes the energy loss. For evaluate R_{AA} the ratio between the upper and lower branches is computed.

The dE/dx is:

$$\frac{dE}{dx} = -\frac{dP}{d\tau}(x_0, \varphi, \tau) = \kappa(T) P^{\alpha}(\tau) \tau T^{c} \zeta \tag{5.10}$$

in which $\kappa(T)$ and $T[x(\tau), \tau]$ describes the local temperature along the jet path at a local time τ, $P^{\alpha}(\tau)$ describes the dependence on the jet energy and ζ is the term describing the energy loss fluctuations along the path-length. In this work, we use a simple parametric model for the heavy quark energy loss per unit length:

$$\frac{dE}{dx}(T, v_Q) = -f(T, v_Q)\zeta\Gamma_{flow}, \tag{5.11}$$

in which $f(T, v_Q)$ is a function encoding the energy loss parametrization, T is the local medium temperature experienced by the heavy quark, v_Q is the heavy quark velocity in the global laboratory frame, ζ is a random variable related to the energy loss fluctuations, and Γ_{flow} takes into account the boost from the rest frame of the moving medium to the general laboratory frame (174). The Γ is given by:

$$\Gamma_{flow} = \gamma[1 - v_{flow}\cos(\varphi_{quark} - \varphi_{flow})], \tag{5.12}$$

in which $\gamma = 1/\sqrt{1 - v_{flow}^2}$, v_{flow} is the local velocity, φ_{flow} is the azimuthal angle, and φ_Q is the azimuthal angle defined by the propagating heavy quark in the transverse plane. The Eq. 5.12 is interpreted in such a way that heavy quarks propagating with the same direction as the flow will lose less energy than heavy quarks in other directions.

The basis for implementing this approach is realized through the integration of the equation dE/dx by the arbitrary choice of an interval Δx in which the variation is measured by:

$$\Delta E = \frac{dE}{dx} \mid_E \times \Delta x \tag{5.13}$$

The speed of the heavy quark within this displacement is measured to provide a temporal variation comparable to the resolution of hydrodynamic evolution. The position and 4-momentum of the heavy quark are evaluated. The steps of this process are repeated until the medium reaches the temperature of decoupling T_d. From that moment on, coalescence and fragmentation come into play.

For this work, we use a model inspired by conformal ADS/CFT calculations that evaluate the drag force on an external quark moving in a thermal plasma of $N = 4$ super-Yang-Mills theory.

$$f(T, v_{flow}) = \xi T^2 \Gamma \tag{5.14}$$

and we use a constant model that is written as:

$$f(T, v_{flow}) = \alpha \Gamma \tag{5.15}$$

in which ξ, and α are free parameters. T is local temperature.

The free parameters are fitting the R_{AA} results that are obtained from the simulation with available experimental data from CMS and ALICE experiments for each heavy quark. The Data for PbPb collisions at $\sqrt{s_{NN}} = 5.02$ TeV is used for the D^0 meson R_{AA} and sets the parameter for the charm quark simulations. For the bottom, there is data for B^0, moreover, the results are calculated for the whole centrality regime of $0 - 100\%$. Once we have this situation, we use the same parameters for the bottom.

To find the values for each free parameter, finite numbers of those values are chosen. From that are evaluated R_{AA} and then the fit with the data is performed by a least squares algorithm in which bi-linear interpolation is performed in order to obtain the values outside the ${k_{parameter}}^2 \times p_T$ grid.

The configuration of the energy loss is setup for evaluating the R_{AA} for all the events in all centrality classes, which is used to perform event-by-event analysis and leads to v_n estimates for each event. The next section describes the final analysis that is performed from the data obtained from the simulation.

[2] It's a free parameter as α, ξ

5.6 Event-by-event analysis

When obtaining the simulations after performing the steps described so far, an event-by-event analysis is performed. First, the choice of events is made for the analysis. This choice can be made through centrality, integrated v_n in the soft sector, event multiplicity, average number of participants or other physics property for performing event-shape engineering analysis.

The R_{AA} spectra are used to evaluate the differential heavy flavor azimuthal anisotropy from the Fourier harmonics:

$$\frac{R_{AA}(p_T,\varphi)}{R_{AA}(p_T)} = 1 + 2\sum_{n=1}^{\infty} v_n^{heavy}\cos[\varphi - \Psi_n^{heavy}(p_T)], \tag{5.16}$$

in which:

$$v_n^{heavy}(p_T) = \frac{\frac{1}{2\pi}\int_0^{2\pi} d\varphi \cos[\varphi - \Psi_n^{heavy}(p_T)]R_{AA}(p_T,\varphi)}{R_{AA}(p_T)}. \tag{5.17}$$

The event planes angles are defined as:

$$\Psi_n^{heavy} = \frac{1}{n}\arctan\left(\frac{\int_0^{2\pi} d\varphi \sin(n\varphi)R_{AA}(p_T,\varphi)}{\int_0^{2\pi} d\varphi \cos(n\varphi)R_{AA}(p_T,\varphi)}\right) \tag{5.18}$$

The nuclear modification factor $R_{AA}(p_T,\varphi)$ events is the average over all the events selected. The differential azimuthal anisotropy $v_n(p_T,\varphi)$ is computed from the correlation between $v_n^{heavy}(p_T,\varphi)$ in the heavy flavor sector and the integrated v_n^{soft} of all charged particles in the soft sector. This is made through the cumulants method (134, 175, 176). Our approach gives the probability for an event with a certain v_n and Ψ_n in the soft sector to produce the heavy flavor quantities v_n and Ψ_n.

In order to solve problems with events with high multiplicity and as small statistics, refining of results is performed by adding weighting of accumulated records using a multiplicity (177, 175):

$$W_{\langle m\rangle} = \prod_{n=0}^{n=m-1}(M-n), \tag{5.19}$$

in which M is the multiplicity and $\langle m\rangle$ is a single event average particle azimuthal correlations. The above weighting bias can have a non-negligible impact on the final results for the correlations if a wide centrality bin is used. Due to this fact, events are further classified into 1%-wide centrality bins and then averaged into wider bins after the multiplicity weighting is calculated. This has been proven to remove the effect due to the bias (176).

Chapter

6 Results

We will discuss the results obtained from the use of the DAB-MOD program, since we present the theories that were references for the development of the program, along with the configurations defined to obtain the presented results. It is important to highlight the main points of the program and how we can obtain the data presented by manipulating the parameters for the quark c and b coefficients. These energy loss parameters were manipulated for each energy loss model. This coefficient directly affects the results of observables under or overestimating the experimental data, for the case of PbPb, or extravagant results for systems such as Xe-Xe[129], Ar-Ar[42], and O-O[16] mainly. The observables affected in this work are the R_{AA}, v_2, and v_3. Other parameters set in the early parts of the DAB-MOD configuration may affect the final simulation results. In this work, the decoupling temperatures are defined between $T_d = 150MeV$ to $T_d = 160MeV$. The choice of this temperature was determined due to the size of the cross-over transitions from lattice QCD (178, 179). These configurations can be seen as a way to identify the best representation of how the heavy particles lose energy with the QGP. Path-length would be a means commonly attributed to this loss of energy.

As previously mentioned, DAB-MOD is a modular program, that is, it is possible to check each step. Therefore, the stages of analysis are distinctly made, in order to produce more representative results.

The results presented below will cover the following topics: Presentation of the Initial Conditions model compared with experimental data using observables R_{AA}, v_2, and v_3, presentation of the observables of de Xe-Xe compared with the data found in the literature, comparison and presentation of the calculations generated for small systems Ar-Ar, and OO, taking as reference the results of systems like Pb-Pb and Xe-Xe.

6.1 Energy Loss

For each model described above, there is a free parameter, i.e., the coupling factors α and ξ for the chosen energy loss models. There are also the factors $f_M T$ and $f_G A$ for Langevin models, which must be fixed. This step is done by finding the value that gives the best description of differential R_{AA} for $p_T \geq 10$ GeV at LHC energies obtained from the simulation compared to available experimental data for each model, heavy quark type, limiting values of the decoupling temperature vary between 150 MeV and 160 MeV, and also the collision energy. The factors for each model is set up using D^0 meson differential R_{AA} data in one centrality regime. The values for both temperatures were fixed with the same value for all models. The table 3 summarizes the values for each model.

Coupling factors for charm quarks at $T_d = 150 - 160$MeV	LHC PbPb $\sqrt{s_{NN}} = 5.02$TeV
α	1.154
ξ	12.532
k_{MT}	0.41
k_{GA}	0.41

Tab. 3 – Values of the coupling factors for charm quarks determined for each transport model, collision energy, and decoupling temperature. These values are obtained using TRENTO initial conditions.

In this step, in order to obtain the differential nuclear modification factor that is used for comparison with data, events with $0 - 10\%$ centrality are selected and the simulation is performed using the Pb + Pb with system $\sqrt{s_{NN}} = 5.02$ TeV. The program(DaBMod) has been run for about $\sim$ one thousand events in this centrality for each beam energy and the number of heavy quarks.

Comparing the results with the experimental data in Fig. 18 it is possible to notice a big suppression for the models with temperature dependence ξT^2 and the constant model α for the interval varying between 0 GeV $< p_T <$ 3 GeV. Langevin-based models best represent the data presented since all intervals are represented with similar behaviors. For the case of energy loss models α and ξT^2 there is a tendency for there to be a dependency for values of R_{AA} at high transversal momentum. This result bring interesting information about the low p_T. Processes involving a relation between Temperature and a linear can suppress the observable R, indicating that possibly for the moments of interaction of the particles with the bulk there are processes not well understood about the momentum gain process.

The results (Figs.19) for the anisotropy azimuthal contribution is well represented by the energy loss model MT (109) and GA (110). The energy loss models that depend on the temperature and constant value model are highly suppressed. For this plot, it is also possible to perceive a better representation for the temperature $T_d = 150$ MeV for low transverse momentum. The Langevin model hybrid is also suppressed.

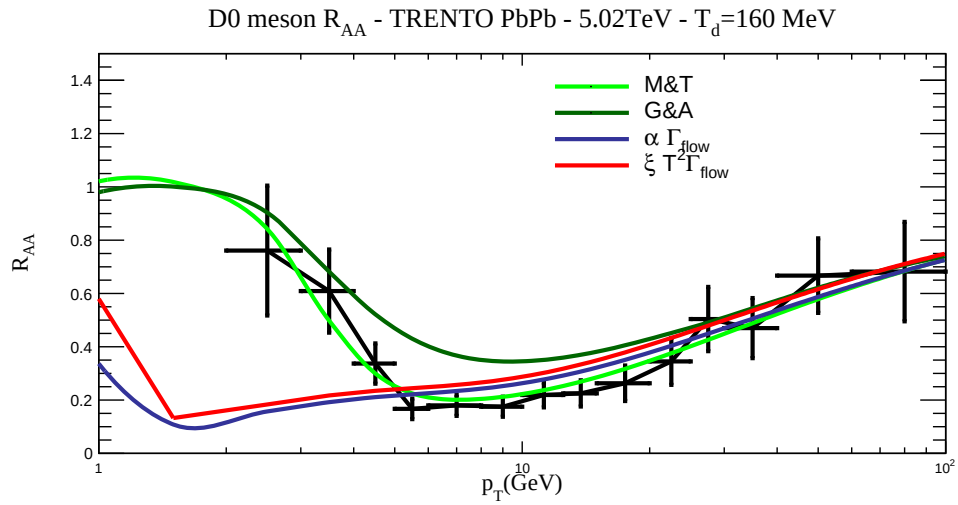

Figure 18 – The Plot of differential R_{AA} for $0-10\%$ centrality for different models of energy loss. The temperature varies between for MT approach. The green line (bright) represents the MT model with MT parameter fixed. The green line (dark) represents the GA model. The red line represents the temperature model previously commented on before. The blue line represents the constant model. This data was taken from collaboration CMS (17).

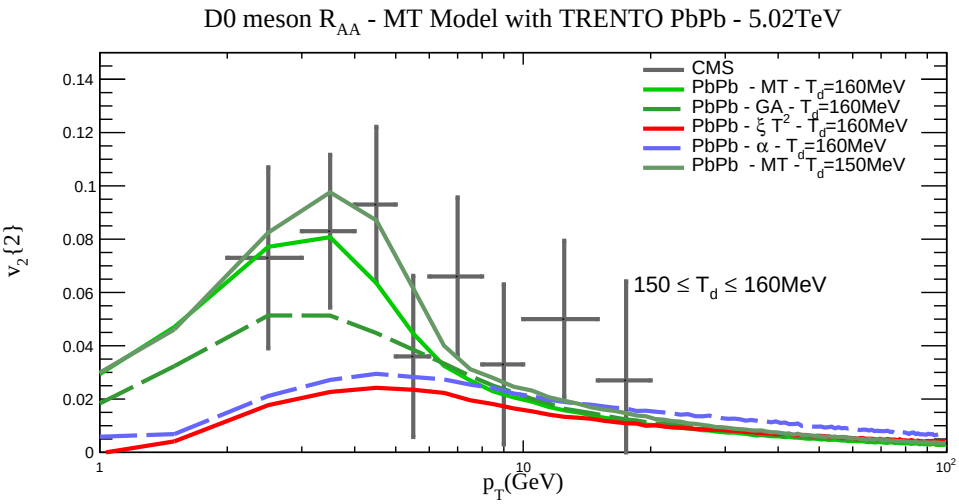

Figure 19 – The Plot of anisotropic azimuthal flow v_2. This data was taken from collaboration CMS (18). The green line (dark) represents MT model with $T_d = 150$MeV. The green line (bright) represents the same model. The green line (dashed) represents the hybrid model. The blue line represents the constant model and finally, the red line represents the ξT^2 model. The $|y| < 1.0$ for the data.

The result presented in Fig. 20 for the contribution of triangular flow also shows a suppression for the values of the models α and ξT^2. The line representing the graph for $T_d = 150$ MeV demonstrates better representing the experimental data (18). In Fig. 20 the representation for high transversal momentum needs more accession in the representation of the data. The deeper analysis of energy loss processes with the environment may be responsible for a better representation of the data.

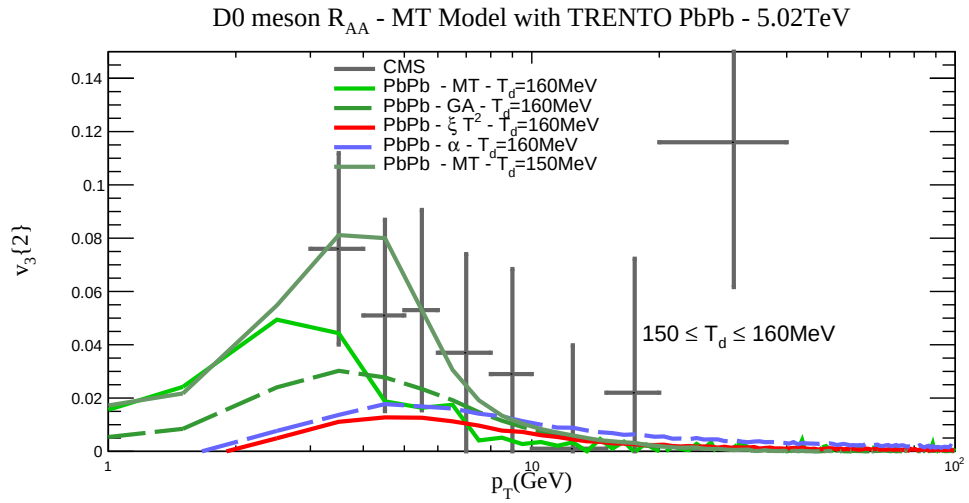

Figure 20 – The Plot of triangular flow v_3. This data was taken from collaboration CMS (18). The green line (dark) represents MT model with $T_d = 150$MeV. The green line (bright) represents the same model. The green line (dashed) represents the hybrid model. The blue line represents the constant model and finally the red line represents the ξT^2 model. The $|y| < 1.0$ for the data.

In Fig. 21 we can see the same behavior for energy loss models even for Langevin models. In this graph, we use only four models of energy loss R_{AA}. We do not use the GA model. In the future, we will run this simulation to consistently supply the analysis described for meson D.

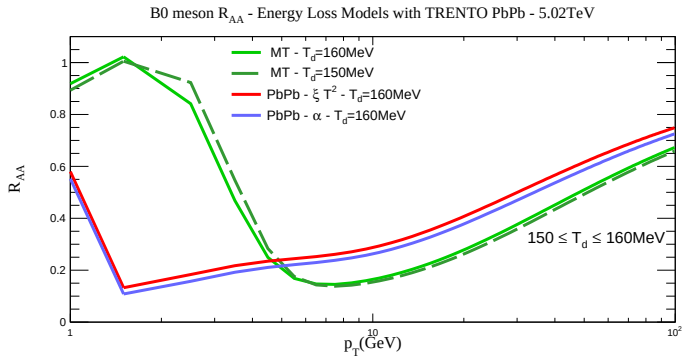

Figure 21 – Graph for Energy Loss Model with B^0 meson. The green line (dashed) is for Moore and Teaney approach with $T_d = 150$ MeV. The green line (solid) is for the same approach, but for $T_d = 160$ MeV. The red line represents the model with dependence on the temperature. The blue line is for the constant model. Both ξ and α models use decoupling temperature $T_d = 160$ MeV

In order to carry out an analysis of the dependence of the transverse moment p_T compared to $v_2\{4\}/v_2\{2\}$. We compared the use of energy loss models with the use of the Langevin model using the coalescence process and another without the use of this process. The use of the coalescence process provides, for high centrality values, an attenuation of the cumulative contribution. This attenuation of the value of this ratio (Fig. 22 upper

plot) is consistent with the coalescence mechanism, since the ratio $v_2\{4\}/v_2\{2\}$ together with the implementation of the coalescence mechanism brings the rise of heavy quarks fluctuations concerning the combination of heavy-light quarks. The addition of coalescence mechanism is observed to generally decrease the low p_T integrated cumulant ratio except in the case of constant energy loss model in most central collisions $0-10\%$. The behavior for the ratio with intervals of the integrated anisotropy values for the constant energy loss model shows great attenuation. The ratio for peripheral collisions is less sensitive.

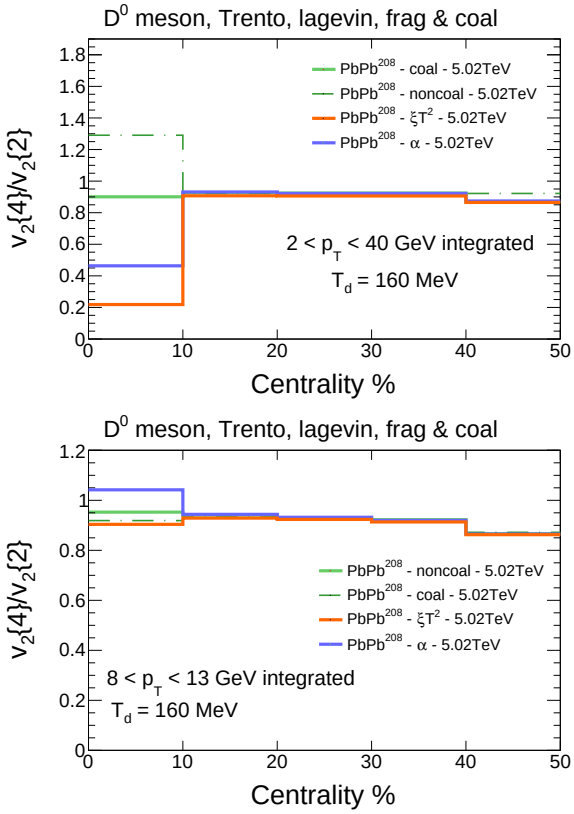

Figure 22 – Centrality dependence of the D^0 meson $v_2\{4\}/v_2\{2\}$ cumulant ratio integrated over two ranges $2 < p_T < 40$ GeV (above) and $8 < p_T < 13$ GeV (down) for $\sqrt{s_{NN}} = 5.02$ TeV PbPb collisions. Here, we use TRENTO initial conditions.

6.2 TRENTO + Coalescence

In the literature, TRENTO (4) is used as one of the main tools for creating the Initial Condition. Therefore, to represent the experimental data using the DABMOD and test how robust the program is, data comparisons were performed using the Initial Condition TRENTO together with the Langevin (4.9) energy loss model. In this simulation, the coalescence process was tested, since previous work on this process was tested using Monte Carlo MCKLN (19). In Fig. 23 we can see the calculations made with DAB-MOD

using the MCKLN and the coalescence process. It is possible to verify that there is enhancement to the representation of the lines compared to the data in the literature.

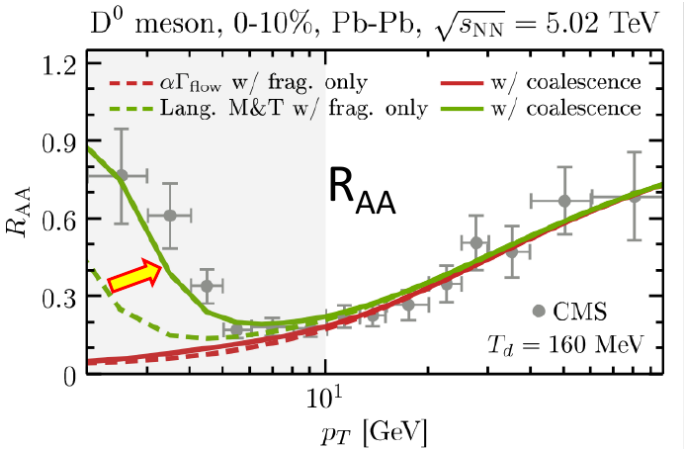

Figure 23 – Graphic of R$_{AA}$ with coalescence in green and simulation without coalescence. The green line (solid) represents enhancement when coalescence process is implemented. This Figure was taken from (19). The data was taken from CMS collaboration for PbPb collisions (17) with $|y| < 1$.

For the plot in Fig. 24, the enhancement can be seen for transversal momentum $(p_T < 8)$GeV. The temperature range $T_d = (150 - 160)$ MeV brought a mapping for the representation of the experimental data and modifications coming from the change of T_d.

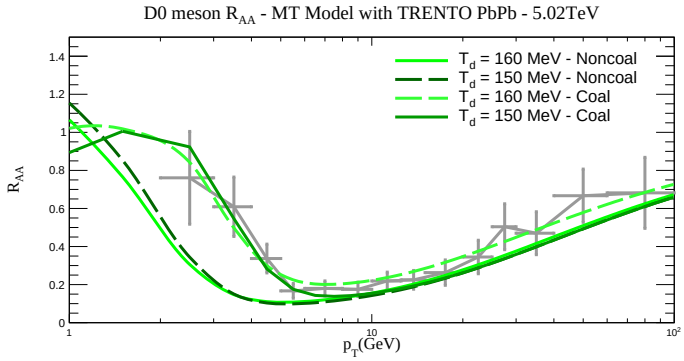

Figure 24 – This graph represents the R_{AA} for high centrality, being $0 - 10\%$. The green line (bright and solid) represents $T_d = 160$MeV with the coalescence process. The green line (dark and dashed) represents $T_d = 150$MeV with the coalescence process while the green line (smoothed and solid) represents $T_d = 160$MeV without the coalescence process. Finally, the green line (smoothed and solid) represents $T_d = 160$MeV without the coalescence process. The data was taken from CMS collaboration for PbPb collisions (17) with $|y| < 1$.

For the plot in Fig. 24, it is worth noting that the changes in R_{AA} due to $T_d = 150$ MeV there is no big difference for representation without the use of the coalescence process for the high transverse momentum.

For the collision interval between $30-50\%$ (Fig. 25), it is noticed that the coupling temperature change for the process without coalescence has a minimal enhancement. By changing T_d to values greater than 150MeV a enhancement in the representation of R_{AA} is noted.

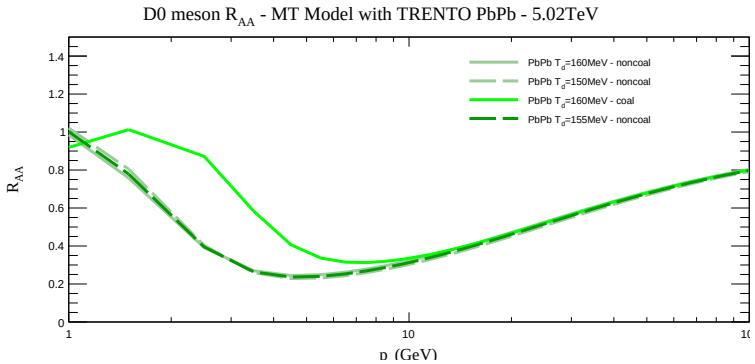

Figure 25 – Graph of the decoupling temperature for nuclear modification factor R_{AA} for the lower transversal momentum p_T. Scan of TRENTO initial condition for $\sqrt{s_{NN}} = 5.02$TeV in $30-50\%$ centrality.

For the values of the triangular flow v_3 it is possible to view the enhancement for the values of low transverse momentum p_T. In Fig. 26 it is possible to see three variations of decoupling temperature T_d in which there is a better representation for the low transversal momentum for v_2 when the coalescence process is used. This enhancement happens for the range of $2 < p_T < 5$ GeV. The same behavior of better representation of the data (17) happens for v_3 for regimes between $2 < p_T < 6$ GeV.

6.3 D meson sensitivity (Size scan)

For these results we investigate how the size of the system changes R_{AA} as we make the system smaller. There are currently indications for studies with ion and proton beams at the LHC in which it is intended to study QCD dynamics from small system (p + p) to large (nucleus + nucleus) systems (180). There are works that explore small systems (p+O, O+O, O+Au, and Be+Au) (77), using the Glauber Model (181) as initial condition. For central collisions, we can observe in Fig. 27 a sensitive behavior. The R_{AA} for Argon system and Oxygen system has a contribution above 0.5. The configuration for the Xe + Xe system used the parameterization $k_M T$ different from the lead-lead system. The value of 0.41 greatly suppressed the value of R_{AA} to the point that there is no tidy difference between the two systems. We use the individual factor $k_{\ M}T = 0.473$ for the Xe + Xe system.

For mid-central collisions there is no visible difference between O+O and Ar+Ar even though their system size is different (7). There is a small difference in low momentum transverse $p_T < 2$GeV.

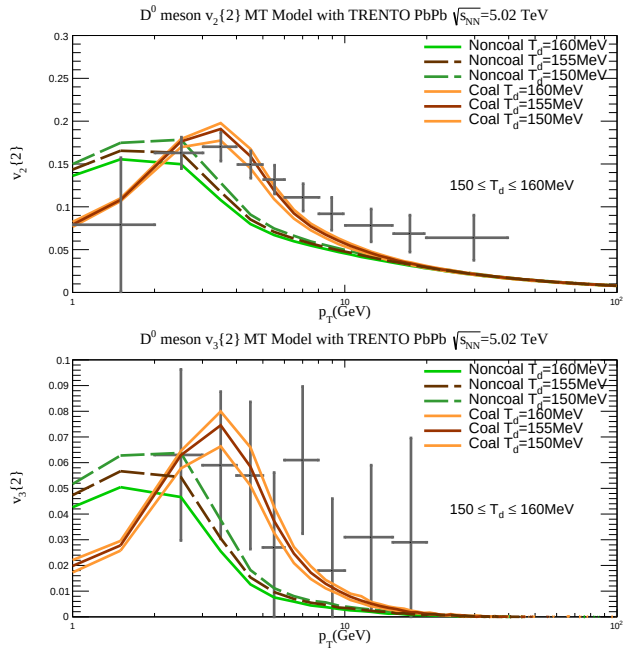

Figure 26 – The first graph (above) represents azimuthal anisotropy v_2 with three different temperatures. In the second plot (down), the graph represents the triangular flow contribution v_3. The range of temperature go to 150MeV until 160MeV. $30-50\%$ The data was taken from the collaboration CMS (17).

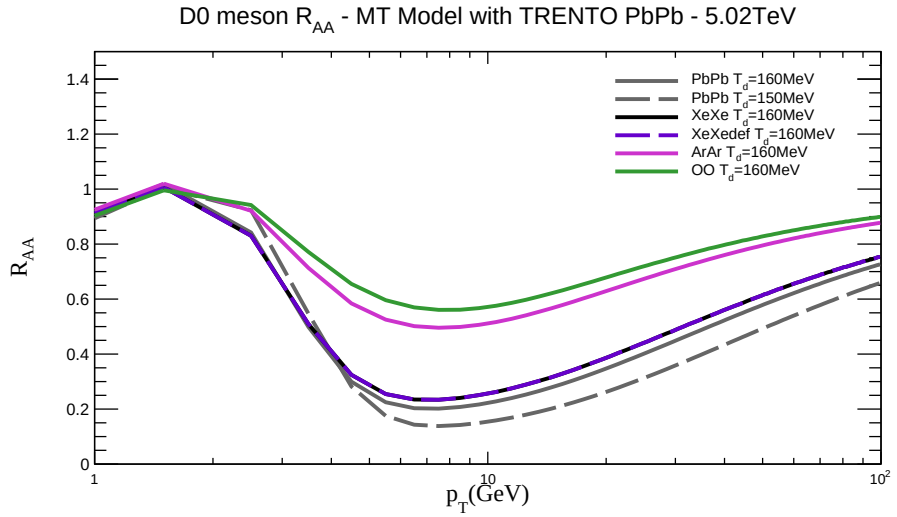

Figure 27 – Direct D^0 meson R_{AA} for O+O in $\sqrt{s_{NN}}$ = 6.02TeV,Ar+Ar in $\sqrt{s_{NN}}$ = 5.85TeV, Xe+Xe $\sqrt{s_{NN}}$ = 5.44TeV, and Pb+Pb collisions in $\sqrt{s_{NN}}$ = 5.02TeV with $0-10\%$ centrality.

Analyzing the Xe + Xe system, we placed two systems, one with deformation and the other completely spherical. This deformation was implemented according to the Wood-Saxon model.

For the azimuthal anisotropies v_n it is possible to perceive in Fig. 29 similarities for the behavior of azimuthal anisotropy, since for the region of low transverse momentum

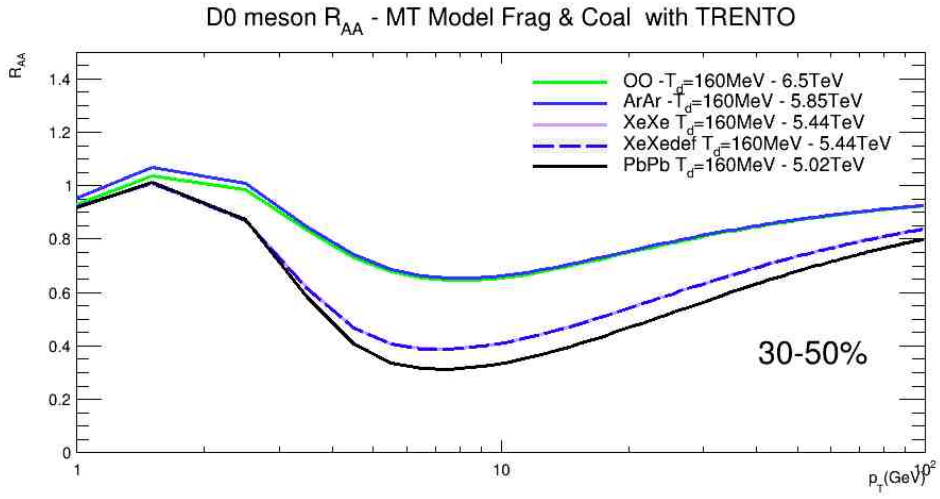

Figure 28 – Direct D^0 meson R_{AA} for O+O,Ar+Ar, Xe+Xe, and Pb+Pb collisions in $30-50\%$ centrality. The purple line (solid and dashed) represents Xe and Xe with deformation. There is no modification of the modification factor for this system.

similar behavior is noted in this scan. It is worth noting that the changes in $T_d = 150$MeV play influence for O+O, Xe+Xe, and Pb+Pb. The $v_2\{2\}$ has more contribution. The $v_3\{2\}$ in Fig. 30 also has a sensitivity for systems to be presented with variations in temperature $T_d = 150$MeV. The size of the system play a significant role for azimuthal anisotropy, which can be described by the typical radius R of the initial conditions.

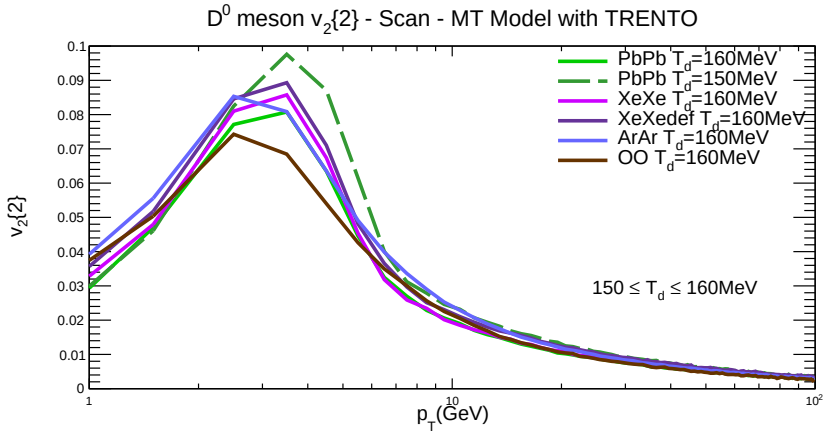

Figure 29 – Direct $v_2\{2\}$ for D^0 meson for O+O,Ar+Ar, Xe+Xe, and Pb+Pb collisions in $0-10\%$ centrality.

For mid-central collisions, the v_2 in Fig. 31 of smaller systems are significantly suppressed across all p_T.

Comparisons with multiparticle cumulants ratio $v_2\{n\}$ in Fig. 33 may show that: $v_2\{4\}/v_2\{2\}$ decreases as the size of the system decreases. We can relate this behavior to the calculations for the eccentricity (7, p 8.) in a qualitative way. In Fig. 33 Ar, Xe, Pb,

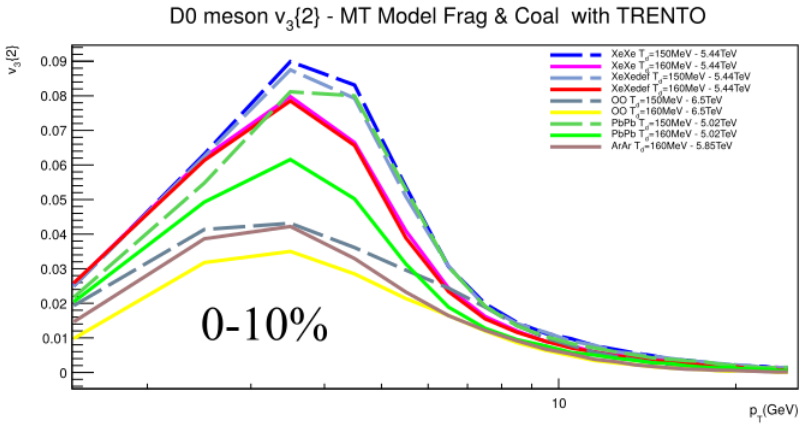

Figure 30 – Direct $v_3\{2\}$ for D^0 meson for O+O,Ar+Ar, Xe+Xe, and Pb+Pb collisions in $0-10\%$ centrality.

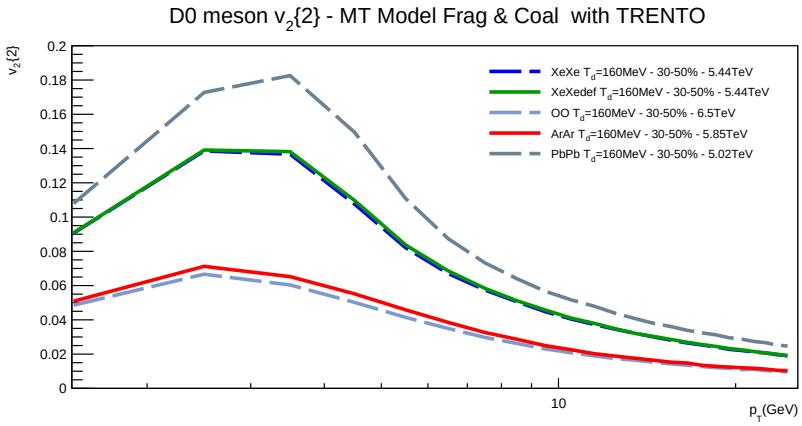

Figure 31 – Direct $v_2\{2\}$ for D^0 meson for O+O,Ar+Ar, Xe+Xe, and Pb+Pb collisions in $30-50\%$ centrality.

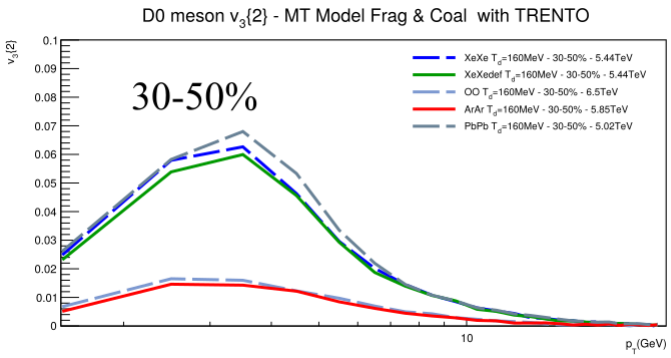

Figure 32 – Direct $v_3\{2\}$ for D^0 meson for O+O,Ar+Ar, Xe+Xe, and Pb+Pb collisions in $30-50\%$ centrality. Th supression for O and Ar is noted.

and O are related so that for the 4-particle cumulant one correlates one heavy particle and three soft ones. These proposals can be seen in (15, 182) and have yet to be measured in the heavy flavor sector. In (19) it was shown this ratio was for the most part dependent on the type of soft initial fluctuations used.

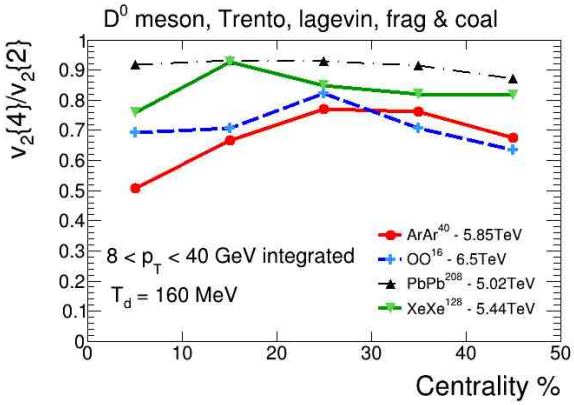

Figure 33 – The multiparticle cumulants ratio $v_2\{4\}$ e $v_2\{2\}$. It was integrated from 8 to 40GeV with $T_d = 160$MeV.

In this same work we performed the comparison of the ALICE collaboration for the values of nuclear modification factor R_{AA}. One can see that the simulation to this system in Fig. 34 suffer for represent the data. Possible factors may have caused this disagreement with the data. Analysis of the parameterization of the coefficients of the energy loss models to the system may be the cause of this disagreement. Further studies must be carried out.

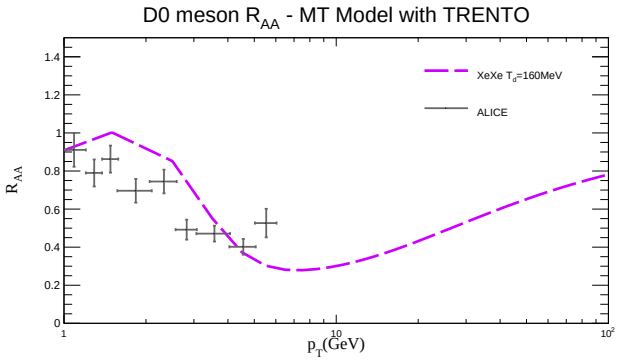

Figure 34 – The plot represents the measurements of open heavy-flavour production in Xe+X collisions by the ALICE (A Large Ion Collider Experiment) collaboration, compared with program DABMOD. The violet line represents the DABMOD simulation. The data was taken from the (20).

6.4 Heavy-soft correlations

Using event-shape engineering heavy-soft correlations in section 5.6, it is possible to relate different ingredients (parameters) used in the simulations and to obtain information on how these ingredients affect the observable of heavy quarks. This work made comparisons with coalescence and two models of energy loss and the ingredients associated with these models that can represent the experimental data. In order to obtain reasonable statistics for the evaluations, 10 million heavy quarks have been sampled from the initial conditions

in the simulation for both bottom and charm quarks. The MT parameter has been fixed as described previously from the $0-10\%$ central events and this parameter has been maintained for the other centrality bins. This choice brings with it changes in the other regions of centrality that will be studied in the future in another work. The integrated p_T regime for all the simulations are set to 8 GeV $\leq p_T \leq$ 13 GeV and 0 GeV $\leq p_T \leq$ 10 GeV. The results in this work are presented for D ^{0} meson.

The first result is shown in Fig. 35. Analyzing the correlations between the heavy quarks v_n^{heavy} for lower transverse momentum in Fig. 35 we can show that when adding the coalescence process we will correlate the heavy quarks and all charged particles elliptic flow v_n^{soft} quarks in proportion to the gain integrated p_T due to coalescence. The first result is shown with solid and dashed colors. The energy loss model MT Langevin model shows a significant increase in p_T between $8-13$ GeV. For the highest centrality interval or mid-centrality, it is possible to perceive an enhancement through the use of the coalescence process.

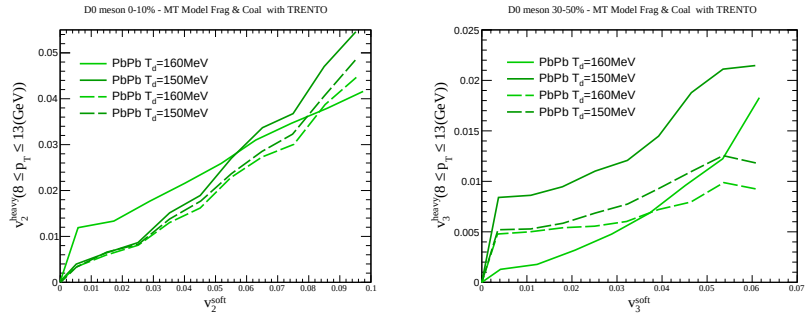

Figure 35 – Correlations between the elliptic anisotropy of D^0 mesons and that all charged particles for $\sqrt{s_{NN}} = 5.02$TeV for PbPb collisions for the transverse momentum range 8-13 GeV comparing two temperatures with and without coalescence. The dashed line represents collisions without coalescence.

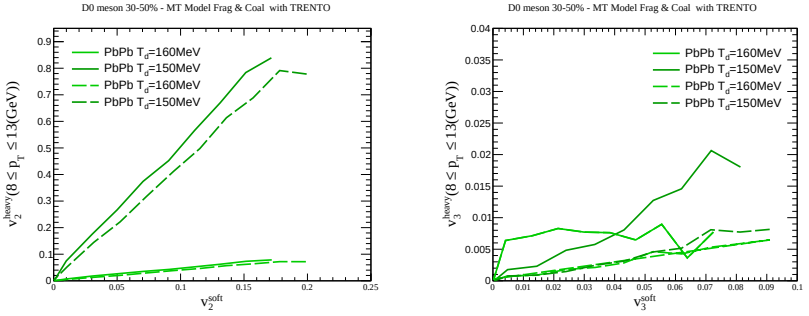

Figure 36 – Correlations between the elliptic anisotropy of D^0 mesons and that all charged particles for $\sqrt{s_{NN}} = 5.02$TeV for PbPb collisions for the transversal momentum range 8-13 GeV comparing two temperatures with and without coalescence. The dashed line represents collisions without coalescence process in $30-50\%$.

The Fig. 35 shows that the implementation of the coalescence process (described by the solid line) directly affects the correlation between heavy mesons anisotropies v_n^{heavy} and all charged particles flow v_n^{soft}. There is a different dependency on temperatures and the implementation of the coalescence process. The observed difference is that when there is an increase in decoupling temperature from 150 MeV to 160 MeV, a significant increase in linear correlation to v_2^{heavy} is observed in the system although for T there is no significant difference compared to the same temperature without the coalescence process. This indicates that elliptic flow is more present than triangular flow in the collision process, as the decoupling temperature is mostly related to the path-length experienced by the heavy quarks, in which the triangular flow is added late in the post-collision process. This behavior is for both cases (with or without coalescence) is more evident for the centrality regime between $30 - 50\%$ in Fig. 36. The temperature change for centrality $30 - 50\%$ provides a great change for the correlation of heavy-light quarks even without the use of the coalescence mechanism. When implementing the coalescence mechanism it is possible to verify a subtle rise compared to the contribution without using this process. The decoupling temperature affect how the particles travel inside the medium, so the anisotropic contribution is affected on peripheral collision. Once the v_n^{heavy} is integrated into a p_T range and the contribution has a enhancement on low p_T the interaction contribution caused by coalescence probably causes this behavior. There is a proportional relation between v_2^{heavy} with v_2^{soft} around 1/2. This can be interpreted as the interaction (probability) between the bulk (the soft sector flow) will correspond to a particular value of v_n^{heavy}.

Conclusion

Studying the properties that can confirm and increase our knowledge about the behavior of quarks and the hot system, with high pressure and extremely dense in which quarks are located, can provide us with valuable information for the development of particle physics and high energy physics. We can list the transport models and the representation of the experimental data (its observables), the understanding of the diffusion coefficient, the understanding of the hadronization mechanism, in addition to others.

In this work, one of the focuses was the analysis of meson D and the observables R_{AA} and v_n added the coalescence process as a possible mechanism in the hadronization stage. In this analysis, the profiles of the events created from the use of the initial condition using the IP-GLASMA (TRENTO) provided important results to ascertain the capabilities of the program and its background to be able to represent the experimental data. These generated profiles were built together with the addition of a relativistic hydrodynamic process, the result of which would be the information (profiles) needed to start the simulations.

The results presented when using the coalescence process demonstrated that the process better represents the experimental data, despite the values obtained indicate that a deeper analysis about the influence of this process and the necessary ingredients for a more accurate representation of the experimental data is necessary observable from meson D for all transverse momentum intervals p_T. The low transverse momentum intervals demonstrate a great improvement with the new thermal-like factors (based on hadron masses) between hadrons of identical quark content. This new factor is only phenomenological. There is no theoretical base to use this model, i.e., to improve the quality of the coalescence probabilities.

In this same work, the analysis of some energy loss models was used with a view to ascertaining the behavior and correlating some quantities related to the physical observables.

The results presented demonstrated a direct relationship between the parameters used and the high transverse momentum interval. However, the energy model that best represents the data is the Langevin model, fulfilling the objective of representing the experimental data well once the model parameterization is performed. This result makes it clear that a more in-depth study about the two models used in this work, namely, a model with temperature dependence and another associated with a constant, can be carried out in the future.

The preparation for the new battery of relativistic collisions in the LHC experiments and the systems proposed for these new collisions made predictions for different systems using AA collisions, together with the use of the collision simulation program (2d + 1) configured with Langevin energy loss models, the initial condition TRENTO, and the fragmentation process plus the coalescence process. These predictions would provide a first model of the experimental data of possible collisions.

The results provided information that led us to conclude that the nuclear modification factor for the mesons D of intermediate systems tends towards the unit while the size of the system decreases. The less central collisions demonstrated that the smaller systems used in this work are less sensitive. The observable $v_2\{2\}$ proved to be an important factor when related to the size of the systems for central collisions, although the eccentricity increases for the small system, it tends to resolve the suppression for the azimuthal anisotropy. The results for the observable v_3 show great suppression for central collisions, although there is a trend while there is a decrease in the size of the system. As for mid-central collisions, an influence for v_3 and the size of the system is perceived. The triangular azimuthal anisotropy is more sensitive to the system size itself.

In that same work, a first comparison of the Xe + Xe system was performed with the data provided in the literature. Although we still do not have more consistent experimental data for different centralities and different mesons, there is a initial representation of the literature data. A more consistent analysis of this system is necessary for future work.

The simulation predicted a linear correlation between the heavy and the soft sector, although the mechanisms responsible for each sector are different. The event shape engineering can lead to useful information on the correlation of the particles which is consistent with similar information obtained from the cumulants method. This method can also provide a novel insight into the mechanisms of heavy flavor coupling with the medium.

The results achieved in this work were presented at the XL National Meeting on Particles Physics and Fields (ENFPC) and XLII Working Meeting on Nuclear Physics in Brazil (RTFNB) - 2019 at Campos do Jordão -São Paulo. Besides, there is the intention to submit the new results presented in this work in some scientific journal in this field or peer reviewed journal.

The program used here is intended to implement different energy loss models in the future and add other collisions of small systems p+Pb and p +. The addition of new ingredients and the implementation in the current code are objectives for accessing the current results. Thus, the prospects for using the program for future studies are promising, since the representation capabilities of the observables compared to the experimental data are significant and within the error bar in most of the momentum transversal intervals p_T.

Reference

1 TANABASHI, M. et al. Review of particle physics. *Phys. Rev. D*, American Physical Society, v. 98, p. 030001, Aug 2018. Disponível em: <https://link.aps.org/doi/10.1103/PhysRevD.98.030001>. Citado 3 vezes nas páginas 11, 3 e 6.

2 COMMITTEE, T. D. N. S. A. *The Frontiers of Nuclear Science, A Long Range Plan.* 2008. Citado 2 vezes nas páginas 11 e 7.

3 QIN, G.-Y. Anisotropic Flow and Jet Quenching in Relativistic Nuclear Collisions. *Int. J. Mod. Phys.*, E24, n. 02, p. 1530001, 2015. Citado 2 vezes nas páginas 11 e 8.

4 MORELAND, J. S.; BERNHARD, J. E.; BASS, S. A. Alternative ansatz to wounded nucleon and binary collision scaling in high-energy nuclear collisions. *Phys. Rev.*, C92, n. 1, p. 011901, 2015. Citado 5 vezes nas páginas 11, 19, 42, 44 e 59.

5 AAMODT, K. et al. Charged-particle multiplicity measurement in proton–proton collisions at $\sqrt{s} = 0.9$ and 2.36 tev with alice at lhc. *The European Physical Journal C*, Springer Science and Business Media LLC, v. 68, n. 1-2, p. 89–108, Jun 2010. ISSN 1434-6052. Disponível em: <http://dx.doi.org/10.1140/epjc/s10052-010-1339-x>. Citado 2 vezes nas páginas 11 e 19.

6 ABELEV, B. et al. Multiparticle azimuthal correlations inp-pb and pb-pb collisions at the cern large hadron collider. *Physical Review C*, American Physical Society (APS), v. 90, n. 5, Nov 2014. ISSN 1089-490X. Disponível em: <http://dx.doi.org/10.1103/PhysRevC.90.054901>. Citado 2 vezes nas páginas 11 e 19.

7 SIEVERT, M. D.; NORONHA-HOSTLER, J. CERN Large Hadron Collider system size scan predictions for PbPb, XeXe, ArAr, and OO with relativistic hydrodynamics. *Phys. Rev.*, C100, n. 2, p. 024904, 2019. Citado 5 vezes nas páginas 11, 24, 25, 61 e 63.

8 BERAUDO, A. et al. Heavy flavors in heavy-ion collisions: quenching, flow and correlations. *The European Physical Journal C*, Springer Science and Business Media LLC, v. 75, n. 3, Mar 2015. ISSN 1434-6052. Disponível em: <http://dx.doi.org/10.1140/epjc/s10052-015-3336-6>. Citado 2 vezes nas páginas 11 e 28.

9 KE, W.; XU, Y.; BASS, S. A. Linearized boltzmann-langevin model for heavy quark transport in hot and dense qcd matter. *Physical Review C*, American Physical Society (APS), v. 98, n. 6, Dec 2018. ISSN 2469-9993. Disponível em: <http://dx.doi.org/10.1103/PhysRevC.98.064901>. Citado 2 vezes nas páginas 11 e 28.

10 NAHRGANG, M. et al. Influence of hadronic bound states abovetcon heavy-quark observables in pb + pb collisions at the cern large hadron collider. *Physical Review C*, American Physical Society (APS), v. 89, n. 1, Jan 2014. ISSN 1089-490X. Disponível em: <http://dx.doi.org/10.1103/physrevc.89.014905>. Citado 2 vezes nas páginas 11 e 28.

11 UPHOFF, J. et al. Elastic and radiative heavy quark interactions in ultra-relativistic heavy-ion collisions. *Journal of Physics G: Nuclear and Particle Physics*, IOP Publishing, v. 42, n. 11, p. 115106, Oct 2015. ISSN 1361-6471. Disponível em: <http://dx.doi.org/10.1088/0954-3899/42/11/115106>. Citado 2 vezes nas páginas 11 e 28.

12 PLUMARI, S. et al. Charmed hadrons from coalescence plus fragmentation in relativistic nucleus-nucleus collisions at rhic and lhc. *The European Physical Journal C*, Springer Science and Business Media LLC, v. 78, n. 4, Apr 2018. ISSN 1434-6052. Disponível em: <http://dx.doi.org/10.1140/epjc/s10052-018-5828-7>. Citado 2 vezes nas páginas 11 e 28.

13 HE, M.; FRIES, R. J.; RAPP, R. Heavy flavor at the large hadron collider in a strong coupling approach. *Physics Letters B*, Elsevier BV, v. 735, p. 445–450, Jul 2014. ISSN 0370-2693. Disponível em: <http://dx.doi.org/10.1016/j.physletb.2014.05.050>. Citado 2 vezes nas páginas 11 e 28.

14 SONG, T. et al. Charm production in pb + pb collisions at energies available at the cern large hadron collider. *Physical Review C*, American Physical Society (APS), v. 93, n. 3, Mar 2016. ISSN 2469-9993. Disponível em: <http://dx.doi.org/10.1103/PhysRevC.93.034906>. Citado 2 vezes nas páginas 11 e 28.

15 PRADO, C. A. G. et al. Event-by-event correlations between soft hadrons and d0 mesons in 5.02 tev pbpb collisions at the cern large hadron collider. *Physical Review C*, American Physical Society (APS), v. 96, n. 6, Dec 2017. ISSN 2469-9993. Disponível em: <http://dx.doi.org/10.1103/PhysRevC.96.064903>. Citado 3 vezes nas páginas 11, 28 e 64.

16 DJORDJEVIC, M. An overview of heavy quark energy loss puzzle at rhic. *Journal of Physics G: Nuclear and Particle Physics*, IOP Publishing, v. 32, n. 12, p. S333–S341, Nov 2006. ISSN 1361-6471. Disponível em: <http://dx.doi.org/10.1088/0954-3899/32/12/S41>. Citado 2 vezes nas páginas 12 e 31.

17 SIRUNYAN, A. et al. Nuclear modification factor of d0 mesons in pbpb collisions at $\sqrt{s_{NN}} = 5.02tev$. *Physics Letters B*, Elsevier BV, v. 782, p. 474–496, Jul 2018. ISSN 0370-2693. Disponível em: <http://dx.doi.org/10.1016/j.physletb.2018.05.074>. Citado 6 vezes nas páginas 13, 14, 57, 60, 61 e 62.

18 SIRUNYAN, A. et al. Measurement of prompt d0 meson azimuthal anisotropy in pb-pb collisions at $\sqrt{s_{NN}} == 5.02$tev. *Physical Review Letters*, American Physical Society (APS), v. 120, n. 20, May 2018. ISSN 1079-7114. Disponível em: <http://dx.doi.org/10.1103/PhysRevLett.120.202301>. Citado 3 vezes nas páginas 13, 57 e 58.

19 KATZ, R. et al. *DAB-MOD sensitivity study of heavy flavor R_{AA} and azimuthal anisotropies based on beam energy, initial conditions, hadronization, and suppression mechanisms*. 2019. Citado 4 vezes nas páginas 13, 59, 60 e 64.

20 WILKINSON, J. Open heavy-flavour production in heavy-ion collisions at the lhc. *Journal of Physics: Conference Series*, IOP Publishing, v. 1137, p. 012032, Jan 2019. ISSN 1742-6596. Disponível em: <http://dx.doi.org/10.1088/1742-6596/1137/1/012032>. Citado 2 vezes nas páginas 14 e 65.

21 COLLINS, J. *Foundations of Perturbative QCD*. [S.l.]: Cambridge University Press, 2011. (Cambridge Monographs on Particle Physics, Nuclear Physics and Cosmology). Citado 3 vezes nas páginas 17, 3 e 4.

22 BERRYMAN, S. Democritus. Metaphysics Research Lab, Stanford University, 2016. Citado na página 1.

23 GREINER WALTER, S. S. S. E. *Quantum chromodynamics*. Springer 2007. [S.l.]: Springer, 2007. Citado 5 vezes nas páginas 1, 2, 3, 4 e 5.

24 GREENBERG, O. W. Spin and unitary-spin independence in a paraquark model of baryons and mesons. *Phys. Rev. Lett.*, American Physical Society, v. 13, p. 598–602, Nov 1964. Disponível em: <https://link.aps.org/doi/10.1103/PhysRevLett.13.598>. Citado 3 vezes nas páginas 1, 2 e 3.

25 QUIGG, C. GAUGE THEORIES OF THE STRONG, WEAK AND ELECTROMAGNETIC INTERACTIONS. *Front. Phys.*, v. 56, p. 1–334, 1983. Citado 3 vezes nas páginas 1, 3 e 4.

26 ZIGIC, D. et al. Dreena-b framework: First predictions of r and v2 within dynamical energy loss formalism in evolving qcd medium. *Physics Letters B*, Elsevier BV, v. 791, p. 236–241, Apr 2019. ISSN 0370-2693. Disponível em: <http://dx.doi.org/10.1016/j.physletb.2019.02.020>. Citado na página 2.

27 NORONHA-HOSTLER, J. et al. *Ultracentral Collisions of Small and Deformed Systems at RHIC: UU, dAu, $^{9}BeAu$, $^{9}Be^{9}Be$, $^{3}He^{3}He$, and $^{3}HeAu$ Collisions*. 2019. Citado 2 vezes nas páginas 2 e 16.

28 BOżEK, P. Collective flow inp-pb andd-pb collisions at tev energies. *Physical Review C*, American Physical Society (APS), v. 85, n. 1, Jan 2012. ISSN 1089-490X. Disponível em: <http://dx.doi.org/10.1103/PhysRevC.85.014911>. Citado na página 2.

29 CHATRCHYAN, S. et al. Multiplicity and transverse momentum dependence of two- and four-particle correlations in ppb and pbpb collisions. *Physics Letters B*, Elsevier BV, v. 724, n. 4-5, p. 213–240, Jul 2013. ISSN 0370-2693. Disponível em: <http://dx.doi.org/10.1016/j.physletb.2013.06.028>. Citado 2 vezes nas páginas 2 e 23.

30 MAJUMDER, A.; LEEUWEN, M. van. The theory and phenomenology of perturbative qcd based jet quenching. *Progress in Particle and Nuclear Physics*, Elsevier BV, v. 66, n. 1, p. 41–92, Jan 2011. ISSN 0146-6410. Disponível em: <http://dx.doi.org/10.1016/j.ppnp.2010.09.001>. Citado na página 2.

31 GELL-MANN, M. A schematic model of baryons and mesons. *Physics Letters*, v. 8, n. 3, p. 214 – 215, 1964. ISSN 0031-9163. Disponível em: <http://www.sciencedirect.com/science/article/pii/S0031916364920013>. Citado na página 2.

32 ZWEIG, G. An su_3 model for strong interaction symmetry and its breaking; version 2. n. CERN-TH-412, p. 80 p, Feb 1964. Disponível em: <http://cds.cern.ch/record/570209>. Citado na página 2.

33 MARTIN, L. *Grupos De Lie*. UNICAMP. ISBN 9788526813564. Disponível em: <https://books.google.com.br/books?id=llKvswEACAAJ>. Citado na página 2.

34 TANABASHI, M. et al. Review of particle physics. *Phys. Rev. D*, American Physical Society, v. 98, p. 030001, Aug 2018. Disponível em: <https://link.aps.org/doi/10.1103/PhysRevD.98.030001>. Citado 2 vezes nas páginas 3 e 42.

35 OKUN, L. *Leptons and Quarks*. Elsevier Science, 2013. (North-Holland Personal Library). ISBN 9780444596215. Disponível em: <https://books.google.com.br/books?id=CFA7Re707KkC>. Citado na página 3.

36 HALZEN, F.; MARTIN, A. *QUARK & LEPTONS: AN INTRODUCTORY COURSE IN MODERN PARTICLE PHYSICS*. Wiley India Pvt. Limited, 2008. ISBN 9788126516568. Disponível em: <https://books.google.com.br/books?id=ITQy9G62H0gC>. Citado 2 vezes nas páginas 3 e 4.

37 Nambu, Y. A systematics of hadrons in subnuclear physics. In: _____. *Preludes in Theoretical Physics in honor of V.F. Weisskopf*. [S.l.: s.n.], 1966. p. 133. Citado na página 4.

38 HAN, M. Y.; NAMBU, Y. Three-triplet model with double SU(3) symmetry. *Phys. Rev.*, American Physical Society, v. 139, p. B1006–B1010, Aug 1965. Disponível em: <https://link.aps.org/doi/10.1103/PhysRev.139.B1006>. Citado na página 4.

39 FRITZSCH, H.; GELL-MANN, M.; LEUTWYLER, H. Advantages of the color octet gluon picture. *Physics Letters B*, v. 47, n. 4, p. 365 – 368, 1973. ISSN 0370-2693. Disponível em: <http://www.sciencedirect.com/science/article/pii/0370269373906254>. Citado na página 4.

40 BLOOM, E. D. et al. High-energy inelastic $e - p$ scattering at 6° and 10°. *Phys. Rev. Lett.*, American Physical Society, v. 23, p. 930–934, Oct 1969. Disponível em: <https://link.aps.org/doi/10.1103/PhysRevLett.23.930>. Citado na página 4.

41 BREIDENBACH, M. et al. Observed behavior of highly inelastic electron-proton scattering. *Phys. Rev. Lett.*, American Physical Society, v. 23, p. 935–939, Oct 1969. Disponível em: <https://link.aps.org/doi/10.1103/PhysRevLett.23.935>. Citado na página 4.

42 BJORKEN, J. D. Asymptotic sum rules at infinite momentum. *Phys. Rev.*, American Physical Society, v. 179, p. 1547–1553, Mar 1969. Disponível em: <https://link.aps.org/doi/10.1103/PhysRev.179.1547>. Citado na página 4.

43 FEYNMAN, R. P. Very high-energy collisions of hadrons. *Phys. Rev. Lett.*, American Physical Society, v. 23, p. 1415–1417, Dec 1969. Disponível em: <https://link.aps.org/doi/10.1103/PhysRevLett.23.1415>. Citado na página 4.

44 YANG, C. N.; MILLS, R. L. Conservation of isotopic spin and isotopic gauge invariance. *Phys. Rev.*, American Physical Society, v. 96, p. 191–195, Oct 1954. Disponível em: <https://link.aps.org/doi/10.1103/PhysRev.96.191>. Citado na página 4.

45 GROSS, D. J.; WILCZEK, F. Ultraviolet behavior of non-abelian gauge theories. *Phys. Rev. Lett.*, American Physical Society, v. 30, p. 1343–1346, Jun 1973. Disponível em: <https://link.aps.org/doi/10.1103/PhysRevLett.30.1343>. Citado na página 5.

46 PESKIN, M.; SCHROEDER, D. *An Introduction To Quantum Field Theory*. Avalon Publishing, 1995. (Frontiers in Physics). ISBN 9780813345437. Disponível em: <https://books.google.com.br/books?id=EVeNNcslvX0C>. Citado na página 5.

47 Clay Mathematics Institute. *Yang–Mills and Mass Gap*. 2019. Acessado em 28 de outubro - 2019. Disponível em: <https://www.claymath.org/millennium-problems/yang%E2%80%93mills-and-mass-gap>. Citado na página 6.

48 SUSSKIND, L. Lattice models of quark confinement at high temperature. *Phys. Rev. D*, American Physical Society, v. 20, p. 2610–2618, Nov 1979. Disponível em: <https://link.aps.org/doi/10.1103/PhysRevD.20.2610>. Citado 2 vezes nas páginas 6 e 17.

49 DING, H.-T.; KARSCH, F.; MUKHERJEE, S. Thermodynamics of strong-interaction matter from lattice qcd. *International Journal of Modern Physics E*, World Scientific Pub Co Pte Lt, v. 24, n. 10, p. 1530007, Oct 2015. ISSN 1793-6608. Disponível em: <http://dx.doi.org/10.1142/s0218301315300076>. Citado 2 vezes nas páginas 6 e 17.

50 ADAMS, J. et al. Experimental and theoretical challenges in the search for the quark–gluon plasma: The star collaboration's critical assessment of the evidence from rhic collisions. *Nuclear Physics A*, Elsevier BV, v. 757, n. 1-2, p. 102–183, Aug 2005. ISSN 0375-9474. Disponível em: <http://dx.doi.org/10.1016/j.nuclphysa.2005.03.085>. Citado 2 vezes nas páginas 7 e 17.

51 ADAMS, J. et al. Experimental and theoretical challenges in the search for the quark–gluon plasma: The star collaboration's critical assessment of the evidence from rhic collisions. *Nuclear Physics A*, Elsevier BV, v. 757, n. 1-2, p. 102–183, Aug 2005. ISSN 0375-9474. Disponível em: <http://dx.doi.org/10.1016/j.nuclphysa.2005.03.085>. Citado na página 7.

52 ECKART, C. The thermodynamics of irreversible processes. iii. relativistic theory of the simple fluid. *Phys. Rev.*, American Physical Society, v. 58, p. 919–924, Nov 1940. Disponível em: <https://link.aps.org/doi/10.1103/PhysRev.58.919>. Citado na página 11.

53 LANDAU, L. D.; LIFSHITZ, E. M. CHAPTER XV - RELATIVISTIC FLUID DYNAMICS. In: LANDAU, L. D.; LIFSHITZ, E. M. (Ed.). *Fluid Mechanics (Second Edition)*. Pergamon. p. 505–514. ISBN 978-0-08-033933-7. ZSCC: NoCitationData[s0]. Disponível em: <http://www.sciencedirect.com/science/article/pii/B9780080339337500234>. Citado na página 11.

54 ISRAEL, W. Nonstationary irreversible thermodynamics: A causal relativistic theory. v. 100, n. 1, p. 310–331. ISSN 0003-4916. ZSCC: 0001038. Disponível em: <http://www.sciencedirect.com/science/article/pii/0003491676900646>. Citado 2 vezes nas páginas 12 e 13.

55 ISRAEL, W.; STEWART, J. M. Transient relativistic thermodynamics and kinetic theory. v. 118, n. 2, p. 341–372. ISSN 0003-4916. ZSCC: 0001295. Disponível em:

<http://www.sciencedirect.com/science/article/pii/0003491679901301>. Citado 2 vezes nas páginas 12 e 13.

56 CHAUDHURI, A. K. Viscous hydrodynamic model for relativistic heavy ion collisions. v. 2013, p. 1–25. ISSN 1687-7357, 1687-7365. ZSCC: 0000014. Disponível em: <http://www.hindawi.com/journals/ahep/2013/693180/>. Citado 4 vezes nas páginas 12, 13, 17 e 18.

57 HISCOCK, W. A.; LINDBLOM, L. Generic instabilities in first-order dissipative relativistic fluid theories. *Phys. Rev. D*, American Physical Society, v. 31, p. 725–733, Feb 1985. Disponível em: <https://link.aps.org/doi/10.1103/PhysRevD.31.725>. Citado na página 14.

58 HISCOCK, W. A.; LINDBLOM, L. Stability and causality in dissipative relativistic fluids. *Annals of Physics*, v. 151, n. 2, p. 466 – 496, 1983. ISSN 0003-4916. Disponível em: <http://www.sciencedirect.com/science/article/pii/0003491683902889>. Citado na página 14.

59 DENICOL, G. S. et al. Stability and causality in relativistic dissipative hydrodynamics. *Journal of Physics G: Nuclear and Particle Physics*, IOP Publishing, v. 35, n. 11, p. 115102, Sep 2008. ISSN 1361-6471. Disponível em: <http://dx.doi.org/10.1088/0954-3899/35/11/115102>. Citado na página 14.

60 AGUIAR, C. E. et al. Smoothed particle hydrodynamics for relativistic heavy ion collisions. *Journal of Physics G: Nuclear and Particle Physics*, IOP Publishing, v. 27, n. 1, p. 75–94, dec 2000. Disponível em: <https://doi.org/10.1088%2F0954-3899%2F27%2F1%2F306>. Citado 3 vezes nas páginas 15, 16 e 45.

61 COSSINS, P. J. *Smoothed Particle Hydrodynamics*. 2010. Citado 2 vezes nas páginas 15 e 45.

62 NORONHA-HOSTLER, J. et al. Bulk viscosity effects in event-by-event relativistic hydrodynamics. *Physical Review C*, American Physical Society (APS), v. 88, n. 4, Oct 2013. ISSN 1089-490X. Disponível em: <http://dx.doi.org/10.1103/PhysRevC.88.044916>. Citado 2 vezes nas páginas 16 e 45.

63 COOPER, F.; FRYE, G. Single-particle distribution in the hydrodynamic and statistical thermodynamic models of multiparticle production. *Phys. Rev. D*, American Physical Society, v. 10, p. 186–189, Jul 1974. Disponível em: <https://link.aps.org/doi/10.1103/PhysRevD.10.186>. Citado na página 17.

64 SHANAHAN, P. E. Chiral effective theory methods and their application to the structure of hadrons from lattice QCD. *Journal of Physics G: Nuclear and Particle Physics*, IOP Publishing, v. 43, n. 12, p. 124001, oct 2016. Disponível em: <https://doi.org/10.1088%2F0954-3899%2F43%2F12%2F124001>. Citado na página 17.

65 AND, Y. I. The tetraquark candidate ${z}_{{c}}(3900)$ from dynamical lattice QCD simulations. *Journal of Physics G: Nuclear and Particle Physics*, IOP Publishing, v. 45, n. 2, p. 024002, jan 2018. Disponível em: <https://doi.org/10.1088%2F1361-6471%2Faa9afd>. Citado na página 17.

66 SCHEE, W. van der; ROMATSCHKE, P.; PRATT, S. Fully dynamical simulation of central nuclear collisions. *Physical Review Letters*, American Physical Society (APS), v. 111, n. 22, Nov 2013. ISSN 1079-7114. Disponível em: <http://dx.doi.org/10.1103/PhysRevLett.111.222302>. Citado na página 18.

67 SCHENKE, B.; TRIBEDY, P.; VENUGOPALAN, R. Fluctuating glasma initial conditions and flow in heavy ion collisions. *Physical Review Letters*, American Physical Society (APS), v. 108, n. 25, Jun 2012. ISSN 1079-7114. Disponível em: <http://dx.doi.org/10.1103/PhysRevLett.108.252301>. Citado na página 18.

68 BERGES, J. et al. Turbulent thermalization process in high-energy heavy-ion collisions. *Nuclear Physics A*, Elsevier BV, v. 931, p. 348–353, Nov 2014. ISSN 0375-9474. Disponível em: <http://dx.doi.org/10.1016/j.nuclphysa.2014.08.103>. Citado na página 18.

69 MCLERRAN, L.; VENUGOPALAN, R. Computing quark and gluon distribution functions for very large nuclei. *Physical Review D*, American Physical Society (APS), v. 49, n. 5, p. 2233–2241, Mar 1994. ISSN 0556-2821. Disponível em: <http://dx.doi.org/10.1103/physrevd.49.2233>. Citado na página 18.

70 SONG, H.; HEINZ, U. Multiplicity scaling in ideal and viscous hydrodynamics. *Physical Review C*, American Physical Society (APS), v. 78, n. 2, Aug 2008. ISSN 1089-490X. Disponível em: <http://dx.doi.org/10.1103/PhysRevC.78.024902>. Citado na página 19.

71 CHOJNACKI, M. et al. Therminator 2: Thermal heavy ion generator 2. *Computer Physics Communications*, Elsevier BV, v. 183, n. 3, p. 746–773, Mar 2012. ISSN 0010-4655. Disponível em: <http://dx.doi.org/10.1016/j.cpc.2011.11.018>. Citado na página 19.

72 CAO, S.; QIN, G.-Y.; BASS, S. A. Energy loss, hadronization, and hadronic interactions of heavy flavors in relativistic heavy-ion collisions. *Physical Review C*, American Physical Society (APS), v. 92, n. 2, Aug 2015. ISSN 1089-490X. Disponível em: <http://dx.doi.org/10.1103/PhysRevC.92.024907>. Citado 2 vezes nas páginas 20 e 34.

73 GRECO, V.; KO, C.; RAPP, R. Quark coalescence for charmed mesons in ultrarelativistic heavy-ion collisions. *Physics Letters B*, Elsevier BV, v. 595, n. 1-4, p. 202–208, Aug 2004. ISSN 0370-2693. Disponível em: <http://dx.doi.org/10.1016/j.physletb.2004.06.064>. Citado na página 20.

74 OH, Y. et al. Ratios of heavy baryons to heavy mesons in relativistic nucleus-nucleus collisions. *Physical Review C*, American Physical Society (APS), v. 79, n. 4, Apr 2009. ISSN 1089-490X. Disponível em: <http://dx.doi.org/10.1103/PhysRevC.79.044905>. Citado 2 vezes nas páginas 20 e 21.

75 ABELEV, B. I. et al. Long range rapidity correlations and jet production in high energy nuclear collisions. *Phys. Rev. C*, American Physical Society, v. 80, p. 064912, Dec 2009. Disponível em: <https://link.aps.org/doi/10.1103/PhysRevC.80.064912>. Citado na página 23.

76 ADARE, A. et al. Measurements of mass-dependent azimuthal anisotropy in central p + au, d+au, and he3+au collisions at s_nn = 200gev. *Physical Review C*, American Physical Society (APS), v. 97, n. 6, Jun 2018. ISSN 2469-9993. Disponível em: <http://dx.doi.org/10.1103/PhysRevC.97.064904>. Citado na página 23.

77 LIM, S. H. et al. Exploring new small system geometries in heavy ion collisions. *Physical Review C*, American Physical Society (APS), v. 99, n. 4, Apr 2019. ISSN 2469-9993. Disponível em: <http://dx.doi.org/10.1103/PhysRevC.99.044904>. Citado 2 vezes nas páginas 23 e 61.

78 WIRINGA, R. B.; STOKS, V. G. J.; SCHIAVILLA, R. Accurate nucleon-nucleon potential with charge-independence breaking. *Physical Review C*, American Physical Society (APS), v. 51, n. 1, p. 38–51, Jan 1995. ISSN 1089-490X. Disponível em: <http://dx.doi.org/10.1103/PhysRevC.51.38>. Citado na página 23.

79 PUDLINER, B. S. et al. Quantum Monte Carlo calculations of nuclei with A <= 7. *Phys. Rev.*, C56, p. 1720–1750, 1997. Citado na página 23.

80 HABICH, M.; NAGLE, J. L.; ROMATSCHKE, P. Particle spectra and hbt radii for simulated central nuclear collisions of c + c, al + al, cu + cu, au + au, and pb + pb from $\sqrt{s}$ = 62.4 s = 62.4 – 2760 2760 gev. *The European Physical Journal C*, Springer Science and Business Media LLC, v. 75, n. 1, Jan 2015. ISSN 1434-6052. Disponível em: <http://dx.doi.org/10.1140/epjc/s10052-014-3206-7>. Citado na página 23.

81 ROMATSCHKE, P. Light-heavy ion collisions: A window into pre-equilibrium qcd dynamics? 2015. Citado na página 23.

82 SNELLINGS, R. Elliptic flow: a brief review. *New Journal of Physics*, IOP Publishing, v. 13, n. 5, p. 055008, May 2011. ISSN 1367-2630. Disponível em: <http://dx.doi.org/10.1088/1367-2630/13/5/055008>. Citado na página 23.

83 KHACHATRYAN, V. et al. Observation of long-range, near-side angular correlations in proton-proton collisions at the lhc. *Journal of High Energy Physics*, Springer Science and Business Media LLC, v. 2010, n. 9, Sep 2010. ISSN 1029-8479. Disponível em: <http://dx.doi.org/10.1007/JHEP09(2010)091>. Citado na página 23.

84 AABOUD, M. et al. Measurement of multi-particle azimuthal correlations in pp, p + pb and low-multiplicity pb + pb collisions with the atlas detector. *The European Physical Journal C*, Springer Science and Business Media LLC, v. 77, n. 6, Jun 2017. ISSN 1434-6052. Disponível em: <http://dx.doi.org/10.1140/epjc/s10052-017-4988-1>. Citado na página 23.

85 AABOUD, M. et al. Measurement of long-range multiparticle azimuthal correlations with the subevent cumulant method in *pp* and *p*+pb collisions with the atlas detector at the cern large hadron collider. *Phys. Rev. C*, American Physical Society, v. 97, p. 024904, Feb 2018. Disponível em: <https://link.aps.org/doi/10.1103/PhysRevC.97.024904>. Citado na página 23.

86 AAD, G. n. o. Measurement with the ATLAS detector of multi-particle azimuthal correlations in p+Pb collisions at $\sqrt{s_{NN}}$ =5.02 TeV. *Phys. Lett.*, B725, p. 60–78, 2013. Citado na página 23.

87 SIRUNYAN, A. M. e. a. Elliptic flow of charm and strange hadrons in high-multiplicity $p + pb$ collisions at $\sqrt{s_{NN}} = 8.16tev$. *Phys. Rev. Lett.*, American Physical Society, v. 121, p. 082301, Aug 2018. Disponível em: <https://link.aps.org/doi/10.1103/PhysRevLett.121.082301>. Citado na página 23.

88 ADARE, A. et al. Quadrupole anisotropy in dihadron azimuthal correlations in central $d + au$ collisions at $\sqrt{s_{NN}} = 200gev$. *Phys. Rev. Lett.*, American Physical Society, v. 111, p. 212301, Nov 2013. Disponível em: <https://link.aps.org/doi/10.1103/PhysRevLett.111.212301>. Citado na página 24.

89 ADARE, A. e. a. Measurement of long-range angular correlation and quadrupole anisotropy of pions and (anti)protons in central d + Au collisions at $\sqrt{s_{NN}} = 200$ gev. *Phys. Rev. Lett.*, American Physical Society, v. 114, p. 192301, May 2015. Disponível em: <https://link.aps.org/doi/10.1103/PhysRevLett.114.192301>. Citado na página 24.

90 MäNTYSAARI, H. et al. Imprints of fluctuating proton shapes on flow in proton-lead collisions at the LHC. *Physics Letters B*, 772, p. 681 – 686, 2017. ISSN 0370-2693. Disponível em: <http://www.sciencedirect.com/science/article/pii/S0370269317305944>. Citado na página 24.

91 GIACALONE, G. et al. Hydrodynamic predictions for 5.44 tev xe+xe collisions. *Phys. Rev. C*, American Physical Society, v. 97, p. 034904, Mar 2018. Disponível em: <https://link.aps.org/doi/10.1103/PhysRevC.97.034904>. Citado na página 24.

92 ACHARYA, S. et al. Anisotropic flow in Xe–Xe collisions at sNN=5.44 TeV. *Physics Letters B*, v. 784, p. 82 – 95, 2018. ISSN 0370-2693. Disponível em: <http://www.sciencedirect.com/science/article/pii/S037026931830515X>. Citado na página 24.

93 ACHARYA, S. et al. Transverse momentum spectra and nuclear modification factors of charged particles in xe–xe collisions at snn=5.44tev. *Physics Letters B*, Elsevier BV, v. 788, p. 166–179, Jan 2019. ISSN 0370-2693. Disponível em: <http://dx.doi.org/10.1016/j.physletb.2018.10.052>. Citado na página 24.

94 GIACALONE, G. et al. Confronting hydrodynamic predictions with xe-xe data. *Nuclear Physics A*, v. 982, p. 371 – 374, 2019. ISSN 0375-9474. The 27th International Conference on Ultrarelativistic Nucleus-Nucleus Collisions: Quark Matter 2018. Disponível em: <http://www.sciencedirect.com/science/article/pii/S0375947418302537>. Citado na página 24.

95 ESKOLA, K. J. et al. Predictions for multiplicities and flow harmonics in 5.44 tev xe+xe collisions at the cern large hadron collider. *Phys. Rev. C*, American Physical Society, v. 97, p. 034911, Mar 2018. Disponível em: <https://link.aps.org/doi/10.1103/PhysRevC.97.034911>. Citado na página 24.

96 PRADO, C. A. et al. Event-by-event vn correlations of soft hadrons and heavy mesons in heavy ion collisions. *Nuclear Physics A*, v. 967, p. 664 – 667, 2017. ISSN 0375-9474. The 26th International Conference on Ultra-relativistic Nucleus-Nucleus Collisions: Quark Matter 2017. Disponível em: <http://www.sciencedirect.com/science/article/pii/S0375947417301604>. Citado na página 24.

97 MILLER, M. L. et al. Glauber modeling in high energy nuclear collisions. v. 57, n. 1, p. 205–243. ISSN 0163-8998, 1545-4134. ZSCC: 0001795. Disponível em: <http://arxiv.org/abs/nucl-ex/0701025>. Citado na página 27.

98 NORONHA-HOSTLER, J. et al. Event-by-eventhydrodynamics+jetenergy loss: A solution to theraa⊗v2puzzle. *Physical Review Letters*, American Physical

Society (APS), v. 116, n. 25, Jun 2016. ISSN 1079-7114. Disponível em: <http://dx.doi.org/10.1103/PhysRevLett.116.252301>. Nenhuma citação no texto.

99 DAS, S. K. et al. Toward a simultaneous description of raaand v2for heavy quarks. *Journal of Physics: Conference Series*, IOP Publishing, v. 668, p. 012051, Jan 2016. ISSN 1742-6596. Disponível em: <http://dx.doi.org/10.1088/1742-6596/668/1/012051>. Nenhuma citação no texto.

100 NORONHA-HOSTLER, J. *Resolving the R_{AA} to v_n puzzle*. 2016. Citado na página 28.

101 DAS, S. K. et al. Toward a solution to the r aa and v 2 puzzle for heavy quarks. *Physics Letters B*, Elsevier BV, v. 747, p. 260–264, Jul 2015. ISSN 0370-2693. Disponível em: <http://dx.doi.org/10.1016/j.physletb.2015.06.003>. Citado na página 28.

102 NASON, P.; DAWSON, S.; ELLIS, R. The total cross section for the production of heavy quarks in hadronic collisions. *Nuclear Physics B*, v. 303, n. 4, p. 607 – 633, 1988. ISSN 0550-3213. Disponível em: <http://www.sciencedirect.com/science/article/pii/0550321388904221>. Citado na página 29.

103 CACCIARI, M.; GRECO, M. Large-p_t hadroproduction of heavy quarks. *Nuclear Physics B*, Elsevier BV, v. 421, n. 3, p. 530–544, Jun 1994. ISSN 0550-3213. Disponível em: <http://dx.doi.org/10.1016/0550-3213(94)90515-0>. Citado na página 29.

104 NASON, P.; DAWSON, S.; ELLIS, R. K. The one particle inclusive differential cross-section for heavy quark production in hadronic collisions. *Nucl. Phys.*, B327, p. 49–92, 1989. [Erratum: Nucl. Phys.B335,260(1990)]. Citado na página 29.

105 CACCIARI, M.; GRECO, M.; NASON, P. The pt spectrum in heavy-flavour hadroproduction. *Journal of High Energy Physics*, Springer Science and Business Media LLC, v. 1998, n. 05, p. 007–007, May 1998. ISSN 1029-8479. Disponível em: <http://dx.doi.org/10.1088/1126-6708/1998/05/007>. Citado 3 vezes nas páginas 29, 30 e 46.

106 CACCIARI, M.; FRIXIONE, S.; NASON, P. The pt spectrum in heavy-flavour photoproduction. *Journal of High Energy Physics*, Springer Science and Business Media LLC, v. 2001, n. 03, p. 006–006, Mar 2001. ISSN 1029-8479. Disponível em: <http://dx.doi.org/10.1088/1126-6708/2001/03/006>. Citado 2 vezes nas páginas 29 e 46.

107 DJORDJEVIC, M. An overview of heavy quark energy loss puzzle at RHIC. v. 32, n. 12, p. S333–S341. ISSN 0954-3899, 1361-6471. ZSCC: 0000030. Disponível em: <http://arxiv.org/abs/nucl-th/0610054>. Citado na página 31.

108 MOORE, G. D.; TEANEY, D. How much do heavy quarks thermalize in a heavy ion collision? v. 71, n. 6, p. 064904. ISSN 0556-2813, 1089-490X. ZSCC: 0000655. Disponível em: <http://arxiv.org/abs/hep-ph/0412346>. Citado 2 vezes nas páginas 32 e 34.

109 MOORE, G. D.; TEANEY, D. How much do heavy quarks thermalize in a heavy ion collision? *Physical Review C*, American Physical Society (APS), v. 71, n. 6, Jun 2005. ISSN 1089-490X. Disponível em: <http://dx.doi.org/10.1103/physrevc.71.064904>. Citado 2 vezes nas páginas 33 e 56.

110 GOSSIAUX, P.; AICHELIN, J. Energy loss of heavy quarks in a qgp with a running coupling constant approach. *Nuclear Physics A*, Elsevier BV, v. 830, n. 1-4, p. 203c–206c, Nov 2009. ISSN 0375-9474. Disponível em: <http://dx.doi.org/10.1016/j.nuclphysa.2009.10.015>. Citado 2 vezes nas páginas 33 e 56.

111 CAO, S. et al. Towards the determination of heavy-quark transport coefficients in quark-gluon plasma. v. 99, n. 5, p. 054907. ISSN 2469-9985, 2469-9993. Disponível em: <http://arxiv.org/abs/1809.07894>. Citado na página 33.

112 CAO, S. et al. Linearized boltzmann transport model for jet propagation in the quark-gluon plasma: Heavy quark evolution. *Physical Review C*, American Physical Society (APS), v. 94, n. 1, Jul 2016. ISSN 2469-9993. Disponível em: <http://dx.doi.org/10.1103/PhysRevC.94.014909>. Citado 2 vezes nas páginas 33 e 49.

113 MUSTAFA, M. G. Energy loss of charm quarks in the quark-gluon plasma: Collisional vs radiative. v. 72, n. 1, p. 014905. ISSN 0556-2813, 1089-490X. ZSCC: 0000260. Disponível em: <http://arxiv.org/abs/hep-ph/0412402>. Citado na página 33.

114 HE, M.; FRIES, R. J.; RAPP, R. Heavy-quark diffusion and hadronization in quark-gluon plasma. *Phys. Rev. C*, American Physical Society, v. 86, p. 014903, Jul 2012. Disponível em: <https://link.aps.org/doi/10.1103/PhysRevC.86.014903>. Citado na página 34.

115 SVETITSKY, B. Diffusion of charmed quarks in the quark-gluon plasma. *Phys. Rev. D*, American Physical Society, v. 37, p. 2484–2491, May 1988. Disponível em: <https://link.aps.org/doi/10.1103/PhysRevD.37.2484>. Citado na página 34.

116 AKAMATSU, Y.; HATSUDA, T.; HIRANO, T. Heavy quark diffusion with relativistic langevin dynamics in the quark-gluon fluid. *Physical Review C*, American Physical Society (APS), v. 79, n. 5, May 2009. ISSN 1089-490X. Disponível em: <http://dx.doi.org/10.1103/physrevc.79.054907>. Citado na página 34.

117 YOUNG, C. et al. Martini event generator for heavy quarks: Initialization, parton evolution, and hadronization. *Physical Review C*, American Physical Society (APS), v. 86, n. 3, Sep 2012. ISSN 1089-490X. Disponível em: <http://dx.doi.org/10.1103/PhysRevC.86.034905>. Citado na página 34.

118 LANG, T. et al. Heavy quark transport in heavy ion collisions at energies available at the bnl relativistic heavy ion collider and at the cern large hadron collider within the urqmd hybrid model. *Physical Review C*, American Physical Society (APS), v. 93, n. 1, Jan 2016. ISSN 2469-9993. Disponível em: <http://dx.doi.org/10.1103/physrevc.93.014901>. Citado na página 34.

119 CAO, S.; QIN, G.-Y.; BASS, S. A. Model and parameter dependence of heavy quark energy loss in a hot and dense medium. *Journal of Physics G: Nuclear and Particle Physics*, IOP Publishing, v. 40, n. 8, p. 085103, Jun 2013. ISSN 1361-6471. Disponível em: <http://dx.doi.org/10.1088/0954-3899/40/8/085103>. Citado na página 34.

120 MAJUMDER, A. Hard collinear gluon radiation and multiple scattering in a medium. *Phys. Rev. D*, American Physical Society, v. 85, p. 014023, Jan 2012. Disponível em: <https://link.aps.org/doi/10.1103/PhysRevD.85.014023>. Citado na página 34.

121 ZHANG, B.-W.; WANG, E.; WANG, X.-N. Heavy quark energy loss in a nuclear medium. *Physical Review Letters*, American Physical Society (APS), v. 93, n. 7, Aug 2004. ISSN 1079-7114. Disponível em: <http://dx.doi.org/10.1103/PhysRevLett.93.072301>. Citado na página 34.

122 LI, S.; LIAO, J. *Data-driven extraction of heavy quark diffusion in quark-gluon plasma*. 2019. Citado na página 34.

123 DOKSHITZER, Y. L.; KHOZE, V. A.; TROYAN, S. I. On specific qcd properties of heavy quark fragmentation dead cone. *Journal of Physics G: Nuclear and Particle Physics*, IOP Publishing, v. 17, n. 10, p. 1602–1604, oct 1991. Disponível em: <https://doi.org/10.1088%2F0954-3899%2F17%2F10%2F023>. Citado na página 34.

124 DOKSHITZER, Y.; KHARZEEV, D. Heavy-quark colorimetry of qcd matter. *Physics Letters B*, Elsevier BV, v. 519, n. 3-4, p. 199–206, Nov 2001. ISSN 0370-2693. Disponível em: <http://dx.doi.org/10.1016/s0370-2693(01)01130-3>. Citado na página 34.

125 TORRES-RINCON, J. M. et al. Heavy mesons in a hadronic medium: interaction and transport coefficients. *Journal of Physics: Conference Series*, IOP Publishing, v. 668, p. 012091, Jan 2016. ISSN 1742-6596. Disponível em: <http://dx.doi.org/10.1088/1742-6596/668/1/012091>. Citado na página 35.

126 PETERSON, C. et al. Scaling violations in inclusive e^+e^- annihilation spectra. *Phys. Rev. D*, American Physical Society, v. 27, p. 105–111, Jan 1983. Disponível em: <https://link.aps.org/doi/10.1103/PhysRevD.27.105>. Citado 2 vezes nas páginas 35 e 49.

127 KARTVELISHVILI, V.; LIKHODED, A.; PETROV, V. On the fragmentation functions of heavy quarks into hadrons. *Physics Letters B*, v. 78, n. 5, p. 615 – 617, 1978. ISSN 0370-2693. Disponível em: <http://www.sciencedirect.com/science/article/pii/0370269378906536>. Citado na página 35.

128 BEN-HAIM, E. et al. Extraction of the x-dependence of the non-perturbative qcd b-quark fragmentation distribution component. *Physics Letters B*, Elsevier BV, v. 580, n. 3-4, p. 108–118, Feb 2004. ISSN 0370-2693. Disponível em: <http://dx.doi.org/10.1016/j.physletb.2003.11.041>. Citado na página 35.

129 BILANDZIC, A.; SNELLINGS, R.; VOLOSHIN, S. Flow analysis with cumulants: Direct calculations. *Physical Review C*, American Physical Society (APS), v. 83, n. 4, Apr 2011. ISSN 1089-490X. Disponível em: <http://dx.doi.org/10.1103/PhysRevC.83.044913>. Citado na página 36.

130 TEANEY, D. A. Viscous hydrodynamics and the quark gluon plasma. *Quark-Gluon Plasma 4*, WORLD SCIENTIFIC, p. 207–266, Feb 2010. Disponível em: <http://dx.doi.org/10.1142/9789814293297_0004>. Citado na página 36.

131 POSKANZER, A. M.; VOLOSHIN, S. A. Methods for analyzing anisotropic flow in relativistic nuclear collisions. *Physical Review C*, American Physical Society (APS), v. 58, n. 3, p. 1671–1678, Sep 1998. ISSN 1089-490X. Disponível em: <http://dx.doi.org/10.1103/PhysRevC.58.1671>. Citado 2 vezes nas páginas 36 e 37.

132 LUZUM, M. Flow fluctuations and long-range correlations: elliptic flow and beyond. *Journal of Physics G: Nuclear and Particle Physics*, IOP Publishing, v. 38, n. 12, p. 124026, Nov 2011. ISSN 1361-6471. Disponível em: <http://dx.doi.org/10.1088/0954-3899/38/12/124026>. Citado 2 vezes nas páginas 36 e 37.

133 DANIELEWICZ, P.; ODYNIEC, G. Transverse momentum analysis of collective motion in relativistic nuclear collisions. *Physics Letters B*, v. 157, n. 2, p. 146 – 150, 1985. ISSN 0370-2693. Disponível em: <http://www.sciencedirect.com/science/article/pii/0370269385915357>. Citado 2 vezes nas páginas 36 e 37.

134 LUZUM, M.; OLLITRAULT, J.-Y. Eliminating experimental bias in anisotropic-flow measurements of high-energy nuclear collisions. *Physical Review C*, American Physical Society (APS), v. 87, n. 4, Apr 2013. ISSN 1089-490X. Disponível em: <http://dx.doi.org/10.1103/PhysRevC.87.044907>. Citado 3 vezes nas páginas 36, 37 e 53.

135 SELYUZHENKOV, I.; VOLOSHIN, S. Effects of nonuniform acceptance in anisotropic flow measurements. *Physical Review C*, American Physical Society (APS), v. 77, n. 3, Mar 2008. ISSN 1089-490X. Disponível em: <http://dx.doi.org/10.1103/PhysRevC.77.034904>. Citado na página 37.

136 BILANDZIC, A. et al. Generic framework for anisotropic flow analyses with multiparticle azimuthal correlations. *Physical Review C*, American Physical Society (APS), v. 89, n. 6, Jun 2014. ISSN 1089-490X. Disponível em: <http://dx.doi.org/10.1103/PhysRevC.89.064904>. Citado na página 38.

137 BORGHINI, N.; DINH, P. M.; OLLITRAULT, J.-Y. New method for measuring azimuthal distributions in nucleus-nucleus collisions. *Physical Review C*, American Physical Society (APS), v. 63, n. 5, Apr 2001. ISSN 1089-490X. Disponível em: <http://dx.doi.org/10.1103/PhysRevC.63.054906>. Citado na página 38.

138 COMMISSIONING of the Particle-Flow reconstruction in Minimum-Bias and Jet Events from pp Collisions at 7TeV. In: . Geneva: [s.n.], 2010. Disponível em: <https://cds.cern.ch/record/1279341>. Citado na página 39.

139 PRADO, C. A. et al. Event-by-event vn correlations of soft hadrons and heavy mesons in heavy ion collisions. *Nuclear Physics A*, v. 967, p. 664 – 667, 2017. ISSN 0375-9474. The 26th International Conference on Ultra-relativistic Nucleus-Nucleus Collisions: Quark Matter 2017. Disponível em: <http://www.sciencedirect.com/science/article/pii/S0375947417301604>. Citado na página 41.

140 PRADO, C. A. et al. Heavy meson flow harmonics in event-by-event viscous relativistic hydrodynamics. *Nuclear and Particle Physics Proceedings*, v. 289-290, p. 221 – 224, 2017. ISSN 2405-6014. 8th International Conference on Hard and Electromagnetic Probes of High Energy Nuclear Collisions. Disponível em: <http://www.sciencedirect.com/science/article/pii/S2405601417302407>. Citado na página 41.

141 PRADO, C. A. G. et al. Event-by-event v_n correlations of soft hadrons and heavy mesons in heavy ion collisions. *Nucl. Phys.*, A967, p. 664–667, 2017. Citado na página 41.

142 ANTCHEVA, I. et al. Root — a c++ framework for petabyte data storage, statistical analysis and visualization. *Computer Physics Communications*, Elsevier BV, v. 180, n. 12, p. 2499–2512, Dec 2009. ISSN 0010-4655. Disponível em: <http://dx.doi.org/10.1016/j.cpc.2009.08.005>. Citado na página 41.

143 SJöSTRAND, T.; MRENNA, S.; SKANDS, P. A brief introduction to pythia 8.1. *Computer Physics Communications*, Elsevier BV, v. 178, n. 11, p. 852–867, Jun 2008. ISSN 0010-4655. Disponível em: <http://dx.doi.org/10.1016/j.cpc.2008.01.036>. Citado na página 41.

144 BRONIOWSKI, W.; BOżEK, P.; RYBCZYńSKI, M. Fluctuating initial conditions in heavy ion collisions from the glauber approach. *Physical Review C*, American Physical Society (APS), v. 76, n. 5, Nov 2007. ISSN 1089-490X. Disponível em: <http://dx.doi.org/10.1103/PhysRevC.76.054905>. Citado na página 42.

145 DRESCHER, H.-J.; NARA, Y. Effects of fluctuations on the initial eccentricity from the color glass condensate in heavy ion collisions. *Physical Review C*, American Physical Society (APS), v. 75, n. 3, Mar 2007. ISSN 1089-490X. Disponível em: <http://dx.doi.org/10.1103/PhysRevC.75.034905>. Citado na página 42.

146 KHARZEEV, D.; LEVIN, E.; NARDI, M. Color glass condensate at the lhc: hadron multiplicities in pp, pa and aa collisions. *Nuclear Physics A*, Elsevier BV, v. 747, n. 2-4, p. 609–629, Jan 2005. ISSN 0375-9474. Disponível em: <http://dx.doi.org/10.1016/j.nuclphysa.2004.10.018>. Citado na página 42.

147 BERNHARD, J. E. et al. Applying bayesian parameter estimation to relativistic heavy-ion collisions: Simultaneous characterization of the initial state and quark-gluon plasma medium. *Physical Review C*, American Physical Society (APS), v. 94, n. 2, Aug 2016. ISSN 2469-9993. Disponível em: <http://dx.doi.org/10.1103/PhysRevC.94.024907>. Citado na página 43.

148 TACHIBANA, Y.; CHANG, N.-B.; QIN, G.-Y. Full jet in quark-gluon plasma with hydrodynamic medium response. *Physical Review C*, American Physical Society (APS), v. 95, n. 4, Apr 2017. ISSN 2469-9993. Disponível em: <http://dx.doi.org/10.1103/PhysRevC.95.044909>. Citado na página 44.

149 TACHIBANA, Y. Medium response to jet-induced excitation: theory overview. *Nuclear Physics A*, v. 982, p. 156 – 162, 2019. ISSN 0375-9474. The 27th International Conference on Ultrarelativistic Nucleus-Nucleus Collisions: Quark Matter 2018. Disponível em: <http://www.sciencedirect.com/science/article/pii/S0375947418303555>. Citado na página 44.

150 NORONHA-HOSTLER, J. et al. Event-by-eventhydrodynamics+jetenergy loss: A solution to theraa*otimes*v2puzzle. *Physical Review Letters*, American Physical Society (APS), v. 116, n. 25, Jun 2016. ISSN 1079-7114. Disponível em: <http://dx.doi.org/10.1103/PhysRevLett.116.252301>. Citado na página 45.

151 NORONHA-HOSTLER, J.; NORONHA, J.; GYULASSY, M. Sensitivity of flow harmonics to subnucleon scale fluctuations in heavy ion collisions. *Physical Review C*, American Physical Society (APS), v. 93, n. 2, Feb 2016. ISSN 2469-9993. Disponível em: <http://dx.doi.org/10.1103/PhysRevC.93.024909>. Citado na página 45.

152 SIEVERT, M.; NORONHA-HOSTLER, J. Cern large hadron collider system size scan predictions for pbpb, xexe, arar, and oo with relativistic hydrodynamics. *Physical Review C*, American Physical Society (APS), v. 100, n. 2, Aug 2019. ISSN 2469-9993. Disponível em: <http://dx.doi.org/10.1103/PhysRevC.100.024904>. Citado na página 45.

153 KATZ, R. et al. *Heavy-flavor dynamics in event-by-event viscous hydrodynamic backgrounds*. 2018. Citado na página 45.

154 NORONHA-HOSTLER, J.; NORONHA, J.; GRASSI, F. Bulk viscosity-driven suppression of shear viscosity effects on the flow harmonics at energies available at the bnl relativistic heavy ion collider. *Phys. Rev. C*, American Physical Society, v. 90, p. 034907, Sep 2014. Disponível em: <https://link.aps.org/doi/10.1103/PhysRevC.90.034907>. Citado na página 45.

155 LIU, G.; LIU, M. *Smoothed Particle Hydrodynamics: A Meshfree Particle Method*. World Scientific, 2003. ISBN 9789812564405. Disponível em: <https://books.google.com.br/books?id=_cwFMmEQvZQC>. Citado na página 45.

156 CHOW, E.; MONAGHAN, J. Ultrarelativistic sph. *Journal of Computational Physics*, v. 134, n. 2, p. 296 – 305, 1997. ISSN 0021-9991. Disponível em: <http://www.sciencedirect.com/science/article/pii/S0021999197957089>. Citado na página 45.

157 KHEYFETS, A.; MILLER, W. A.; ZUREK, W. H. Covariant smoothed particle hydrodynamics on a curved background. *Phys. Rev. D*, American Physical Society, v. 41, p. 451–454, Jan 1990. Disponível em: <https://link.aps.org/doi/10.1103/PhysRevD.41.451>. Citado na página 45.

158 THACKER, R. J. et al. Smoothed particle hydrodynamics in cosmology: a comparative study of implementations. *Monthly Notices of the Royal Astronomical Society*, Oxford University Press (OUP), v. 319, n. 2, p. 619–648, Dec 2000. ISSN 1365-2966. Disponível em: <http://dx.doi.org/10.1111/j.1365-8711.2000.03927.x>. Citado na página 45.

159 MARROCHIO, H. et al. Solutions of conformal israel-stewart relativistic viscous fluid dynamics. *Physical Review C*, American Physical Society (APS), v. 91, n. 1, Jan 2015. ISSN 1089-490X. Disponível em: <http://dx.doi.org/10.1103/PhysRevC.91.014903>. Citado na página 45.

160 BJORKEN, J. D. Highly relativistic nucleus-nucleus collisions: The central rapidity region. *Phys. Rev. D*, American Physical Society, v. 27, p. 140–151, Jan 1983. Disponível em: <https://link.aps.org/doi/10.1103/PhysRevD.27.140>. Citado na página 45.

161 HUOVINEN, P.; PETRECZKY, P. Qcd equation of state and hadron resonance gas. *Nuclear Physics A*, Elsevier BV, v. 837, n. 1-2, p. 26–53, Jun 2010. ISSN 0375-9474. Disponível em: <http://dx.doi.org/10.1016/j.nuclphysa.2010.02.015>. Citado na página 45.

162 COOPER, F.; FRYE, G. Single-particle distribution in the hydrodynamic and statistical thermodynamic models of multiparticle production. *Phys. Rev. D*, American Physical Society, v. 10, p. 186–189, Jul 1974. Disponível em: <https://link.aps.org/doi/10.1103/PhysRevD.10.186>. Citado na página 45.

163 CACCIARI, M. et al. Theoretical predictions for charm and bottom production at the lhc. *Journal of High Energy Physics*, Springer Science and Business Media LLC, v. 2012, n. 10, Oct 2012. ISSN 1029-8479. Disponível em: <http://dx.doi.org/10.1007/jhep10(2012)137>. Citado na página 46.

164 CACCIARI, M. Large transverse momentum top production at nlo+nll accuracy. *Proceedings of XXVI International Workshop on Deep-Inelastic Scattering and Related Subjects — PoS(DIS2018)*, Sissa Medialab, Sep 2018. Disponível em: <http://dx.doi.org/10.22323/1.316.0133>. Citado na página 46.

165 NAHRGANG, M. et al. Elliptic and triangular flow of heavy flavor in heavy-ion collisions. *Physical Review C*, American Physical Society (APS), v. 91, n. 1, Jan 2015. ISSN 1089-490X. Disponível em: <http://dx.doi.org/10.1103/physrevc.91.014904>. Citado na página 49.

166 GRECO, V.; KO, C. M.; LéVAI, P. Parton coalescence and the *antiproton/pion* anomaly at rhic. *Physical Review Letters*, American Physical Society (APS), v. 90, n. 20, May 2003. ISSN 1079-7114. Disponível em: <http://dx.doi.org/10.1103/PhysRevLett.90.202302>. Citado na página 49.

167 SJöSTRAND, T.; MRENNA, S.; SKANDS, P. A brief introduction to pythia 8.1. *Computer Physics Communications*, Elsevier BV, v. 178, n. 11, p. 852–867, Jun 2008. ISSN 0010-4655. Disponível em: <http://dx.doi.org/10.1016/j.cpc.2008.01.036>. Citado na página 50.

168 BETZ, B.; GYULASSY, M. Constraints on the path-length dependence of jet quenching in nuclear collisions at rhic and lhc. *Journal of High Energy Physics*, Springer Science and Business Media LLC, v. 2014, n. 8, Aug 2014. ISSN 1029-8479. Disponível em: <http://dx.doi.org/10.1007/jhep08(2014)090>. Citado na página 50.

169 BETZ, B.; GYULASSY, M. *Azimuthal Jet Tomography of Quark Gluon Plasmas at RHIC and LHC*. 2013. Citado na página 50.

170 BETZ, B.; GYULASSY, M.; TORRIERI, G. Fourier harmonics of high-ptparticles probing the fluctuating initial condition geometries in heavy-ion collisions. *Physical Review C*, American Physical Society (APS), v. 84, n. 2, Aug 2011. ISSN 1089-490X. Disponível em: <http://dx.doi.org/10.1103/PhysRevC.84.024913>. Citado na página 50.

171 HOROWITZ, W.; GYULASSY, M. The surprisingly transparent sqgp at lhc. *Nuclear Physics A*, Elsevier BV, v. 872, n. 1, p. 265–285, Dec 2011. ISSN 0375-9474. Disponível em: <http://dx.doi.org/10.1016/j.nuclphysa.2011.09.018>. Citado na página 50.

172 HOROWITZ, W. A.; GYULASSY, M. Quenching and tomography from the rhic to the lhc. *Journal of Physics G: Nuclear and Particle Physics*, IOP Publishing, v. 38, n. 12, p. 124114, Nov 2011. ISSN 1361-6471. Disponível em: <http://dx.doi.org/10.1088/0954-3899/38/12/124114>. Citado na página 50.

173 HOROWITZ, W. A. Testing pqcd and ads/cft energy loss at rhic and lhc. AIP, 2012. Disponível em: <http://dx.doi.org/10.1063/1.3700710>. Citado na página 50.

174 BAIER, R.; MUELLER, A.; SCHIFF, D. How does transverse (hydrodynamic) flow affect jet-broadening and jet-quenching? *Physics Letters B*, Elsevier BV,

v. 649, n. 2-3, p. 147–151, May 2007. ISSN 0370-2693. Disponível em: <http://dx.doi.org/10.1016/j.physletb.2007.03.048>. Citado na página 51.

175 NORONHA-HOSTLER, J. et al. Cumulants and nonlinear response of high p_T harmonic flow at $\sqrt{s_{NN}} = 5.02$ tev. *Phys. Rev. C*, American Physical Society, v. 95, p. 044901, Apr 2017. Disponível em: <https://link.aps.org/doi/10.1103/PhysRevC.95.044901>. Citado na página 53.

176 GARDIM, F. G. et al. Hydrodynamic predictions for mixed harmonic correlations in 200 gev au+au collisions. *Physical Review C*, American Physical Society (APS), v. 95, n. 3, Mar 2017. ISSN 2469-9993. Disponível em: <http://dx.doi.org/10.1103/PhysRevC.95.034901>. Citado na página 53.

177 GARDIM, F. G. et al. Hydrodynamic predictions for mixed harmonic correlations in 200 gev au+au collisions. *Phys. Rev. C*, American Physical Society, v. 95, p. 034901, Mar 2017. Disponível em: <https://link.aps.org/doi/10.1103/PhysRevC.95.034901>. Citado na página 53.

178 BECATTINI, F. et al. Hadron formation in relativistic nuclear collisions and the qcd phase diagram. *Physical Review Letters*, American Physical Society (APS), v. 111, n. 8, Aug 2013. ISSN 1079-7114. Disponível em: <http://dx.doi.org/10.1103/PhysRevLett.111.082302>. Citado na página 55.

179 BAZAVOV, A. et al. Chiral crossover in qcd at zero and non-zero chemical potentials. *Physics Letters B*, v. 795, p. 15 – 21, 2019. ISSN 0370-2693. Disponível em: <http://www.sciencedirect.com/science/article/pii/S0370269319303223>. Citado na página 55.

180 CITRON, E. Z. et al. Future physics opportunities for high-density qcd at the lhc with heavy-ion and proton beams. *CERN Yellow Reports: Monographs*, v. 7, n. 0, p. 1159, 2019. ISSN 2519-8076. Disponível em: <https://e-publishing.cern.ch/index.php/CYRM/article/view/955>. Citado na página 61.

181 MILLER, M. L. et al. Glauber modeling in high-energy nuclear collisions. *Annual Review of Nuclear and Particle Science*, Annual Reviews, v. 57, n. 1, p. 205–243, Nov 2007. ISSN 1545-4134. Disponível em: <http://dx.doi.org/10.1146/annurev.nucl.57.090506.123020>. Citado na página 61.

182 NORONHA-HOSTLER, J. et al. Cumulants and nonlinear response of high pt harmonic flow at snn=5.02 tev. *Physical Review C*, American Physical Society (APS), v. 95, n. 4, Apr 2017. ISSN 2469-9993. Disponível em: <http://dx.doi.org/10.1103/PhysRevC.95.044901>. Citado na página 64.

A.1

We known,

$$E = m_b \cosh y,$$

$$p_z = m_T \sinh y$$

and

$$m_T^2 = m^2 + \mathbf{p}_T^2.$$

For the beam particles,

$$p_T = 0.$$

Thus,

$$E = m_b \cosh y_b$$

and

$$p_z = m_b \sinh y_b$$

, which m_b and y_b are the rest mass and rapidity of the beam particles.